6-1-2014

Stress Corrosion Cracking in Polymer Matrix Glass Fiber Composites

Jonathan Kosak
University of Denver

Stress Corrosion Cracking in Polymer Matrix Glass Fiber Composites

_____

A Thesis

Presented to

the Faculty of the Daniel Felix Richie School of Engineering and Computer Science

University of Denver

_____

In Partial Fulfillment

of the Requirements for the Degree

Masters of Science

_____

by

Jonathan Kosak

June 2014

Advisor: Dr. Maciej Kumosa

Author: Jonathan Kosak
Title: Stress Corrosion Cracking in Polymer Matrix Glass Fiber Composites
Advisor: Dr. Maciej Kumosa
Degree Date: June 2014

ABSTRACT

With the use of Polymer Matrix Glass Fiber Composites ever expanding, understanding conditions that lead to failure before expected service life is of increasing importance. Stress Corrosion Cracking (SCC) has proven to be one such example of conditions found in use in high voltage transmission line applications that leads to brittle fracture of polymer matrix composites.

SCC has been proven to be the result of acid buildup on the lines due to corona discharges and water buildup. This acid leaches minerals from the fibers, leading to fracture at low loads and service life. In order to combat this problem, efforts are being made to determine which composites have greater resistance to SCC. This study was used to create a methodology to monitor for damage during SCC and classify damage by mechanism type (matrix cracking and fiber breaking) by using 4-point SCC bend testing, 3-point bend testing, a forward predictive model, unique post processing techniques, and microscopy. This would allow a classification in composite resistance to SCC as well as create a methodology for future research in this field.

Concluding this study, only matrix cracking was able to be fully classified, however, a methodology was developed for future experimentation.

ACKNOWLEDGEMENTS

This thesis could not have happened without contributions from many people. I would like to thank the following specifically for their contributions:

Dr. Maciej Kumosa, John Evans professor at DU and my academic supervisor for hand picking me as an undergraduate to be a member of his research group. His faith in me and financial backing were instrumental in my participation as a graduate student at the University of Denver.

MacLean Power Systems, for providing the funding and project for my graduate program as well as positive feedback throughout the process.

Dr. Brian Burks, my technical advisor for always answering my questions and providing useful guidance. Without his seemingly infinite knowledge, my research would not have been nearly as complete as it finished being.

Dr. Euripides Solis, Research Scientist at DU for his tireless microscopy work and ever present participation in this project. His skill and effort have yielded excellent material for the core principals of this research.

James Middleton, my office mate for his help with ancillary computer problems and odd questions. His ability to put up with my personal music choice and playful self-loathing is second to none.

My group, for listening to my presentations, providing feedback and sympathizing.

My family, for always supporting me and for convincing me that I could achieve as much as I choose to.

And anyone else I might have missed.

TABLE OF CONTENTS

LIST OF TABLES

LIST OF FIGURES

1. INTRODUCTION

The electrical grid for the United States and many other countries around the world is the lifeblood of the nation. Without power, everything shuts down. Our ever growing digital world is more dependent on electricity than ever before and consumption only increases every year. This increased demand, coupled with aging infrastructure has caused the power industry to re-evaluate their technology and methods.

While new conductors are in the process of being evaluated, so are new insulators. Previous insulator designs were ceramic, which is fairly expensive and prone to vandalism and contamination. (Gorur 1991) The newest concept is to use Polymer Matrix Composites (PMC) as insulator material with glass fibers. These materials are desirable due to their low cost and track record in other applications, however, with new application come concerns of reliability and durability. (W. Jones 2006) (Sause, Simulation of Lamb Wave Excitation for Different Elastic Properties and Acoustic Emission Source Geometries 2010)

With new materials and implementation come new challenges. These new composites were found to have issues with Stress Corrosion Cracking (SCC) which caused brittle fractures on in service PMC insulators. (Megel 2001) This SCC damage was causing lines to fail very early in service life and costing power companies money to fix. This scared a lot of companies off because the mechanism was not understood and composites in this form were relatively new.

This study has been requested by the sponsoring power utility MacLean Power Systems (MPS) because of the concern of SCC damage in these new materials. Of particular concern is ranking a list of potential replacement materials, determining the level of SCC damage to the PMCs, and classifying this damage.

The goal of this study is to use a combination of Modal Acoustic Emission (MAE), four point bend testing, Microscopy and Finite Element Modeling to determine specific damage mechanisms caused by SCC, primarily fiber fracture, matrix cracking and fiber matrix debonding. (Qiu 1997)

Live monitoring of damage is accomplished via broadband AE sensors, which have shown to be useful for this purpose in previous experiments. (W. H. Prosser 1995) (M. Hamstad 1995) (Sause, Simulation of Lamb Wave Excitation for Different Elastic Properties and Acoustic Emission Source Geometries 2010) This study will provide advanced methods of classification of spectral content contained within the waveforms of acoustic emissions to identify fiber fracture and matrix cracking. It will be shown that the frequency content of the acoustic emissions is most strongly affected by the source mechanism. This supposition was confirmed through forward predictive modeling of the acoustic emission detection process (i.e., transient source, wave propagation through the structure, and sensing of the wave motion), controlled experiments intended to cause specific damage mechanisms, and microscopic observation. This unique contribution will allow a more reliable classification of material groups for their resistance to SCC.

The study was performed at the University of Denver over the period 2012-2014.

1.1 Insulator History and Failures by Brittle Fracture

Insulators are necessary with the current construction of overhead high voltage power lines carrying 69-735 kV to safely ground power being driven through lines to the poles that support them.

Originally, porcelain and glass were the most widely used materials for insulator design. (Gorur 1991) These designs were efficient and cost effective, however, subject to frequent vandalism, mainly destruction by civilians for their explosive reaction when damaged. The advent and subsequent improvement in quality of PMCs lead to their introduction in insulator lines as early as the mid-1960s. This design was a PMC rod with rubber weather-sheds. This design involves one end connecting to the line (hot end) while the other connects to the tower or ground source (cold end). The composite was oriented with fibers in the axial direction for strength. Weathersheds were implemented to protect the composite rod while increasing the leakage distance and allow for an interrupted path for water drainage. (Sharma 2001) Most modern designs made only small changes to this primary design (see Figure 1).

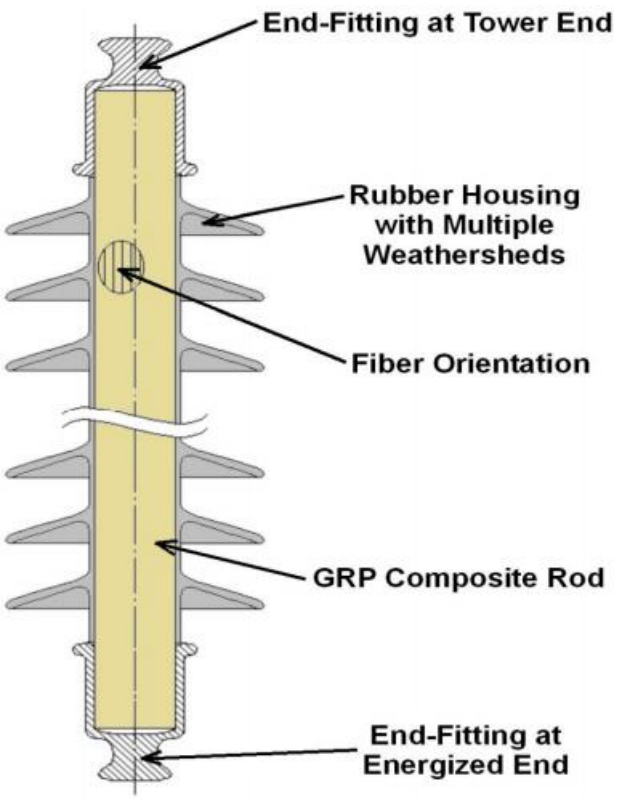

Figure 1: Modern Insulator Line

Source: (M. D. Kumosa 2011)

Material selection for these rods was crucial to their succession of the ceramic models previously used. E-glass fibers were chosen for their cost, relative strength, light weight and electrical insulation properties. ECR glass fibers are also used for their increased corrosion resistance and similar properties to E-glass; however, they tend to be more expensive. These composites are typically pultruded, with anywhere from 60%-80% fiber fractions, and then coated with a polymer matrix. Polymers used for the matrix material of these composites are usually polymers, epoxies and esters. The main concern with material selection for the matrix is electrical insulation, degradation, ability to process, and cost. These designs were an improvement on the previous models for their

weight to strength ratio, impact resistance, contamination performance and increased resistance to vandalism. These newer PMCs were met with great success even as far back as the late 1980's, with only 4% being deemed poor performers. (Schneider 1989)

These lines are subject to mechanical, electrical, and environmental conditions, all of which affect the service life of insulators. All of these conditions can be exacerbated by improper installation techniques, the most common of which is over crimping. This over crimping leads to premature failure, primarily due to damaging of the conductor and increased mechanical loads. (M. K. Kumosa 2005)

Mechanical failures of these rods began to appear in the form of brittle fracture (see Figure 2). Brittle fracture occurs when there is very little plastic deformation, but rapid crack growth. This failure can occur with little or no warning, and is usually catastrophic in nature. Cracks run close to perpendicular to the applied stress, with relatively flat surface at the break. The reason for these fractures at the time was unknown and warranted extensive testing.

Figure 2: Brittle Fracture of a 500 kV Composite Insulator

Source: (Megel 2001)

Since brittle fracture was not expected for these materials, the cause was most likely an outside interaction. These materials were deemed acceptable for long term use but some were found to be failing at relatively low loads and as very short service lives. (Schmuck 2003) It was found that the cause of these failures was attributed to SCC. (Noble 1983) Additionally it was later narrowed primarily to Nitric acid created from Corona discharges on the lines in combination with water. (L. A. Kumosa 2001)

1.2 Stress Corrosion Cracking

In order to investigate the cause of SCC, the differences between E-glass fibers with high boron content and those with little to no boron or ECR glass were examined. Specifically Acid corrosion and stress corrosion characteristics using 1N H_2SO_4 acid at 96°C and room temperature were studied. Stress corrosion testing was done on both sample types. (H. G. Li 2012)

ECR and E-glass fiber are the most common form of reinforcement for PMC's. In recent studies of boron containing E-glass in acid at room temperature significant losses of Al and Ca were found. Limited acid corrosion studies focused on boron-free fibers show no significant composition difference and do not have the same ion-exchange mechanism as boron E-Glass.

Composite rods for this study were fabricated with a bisphenol-A epoxy vinyl ester resin. E-glass fiber direct roving strands of 0, 1.3, and 5.5% B_2O_3 were tested where the samples with 50% glass content by weight were chosen for consistency. Prior to the tests the average ultimate tensile strength values were done to determine the effect of acid on the samples.

Of the samples tested it became immediately apparent that higher levels of boron in the fiber increase corrosion and weight loss (see Figure 3). This corrosion is most likely controlled by surface reaction for a short period of time and by diffusion for longer periods of time. Fibers reached a saturation level after 2 hours in the acid. In the acid the study showed that fibers with higher boron content lost strength rather quickly, 1.3% B_2O_3 outperforms 5.5% B_2O_3 by an order of magnitude. The degradation is taking place

for Si, Ca, and Al in acid where the boron-free glass fibers hydrolysis of the Si-O-Si network prevents degradation.

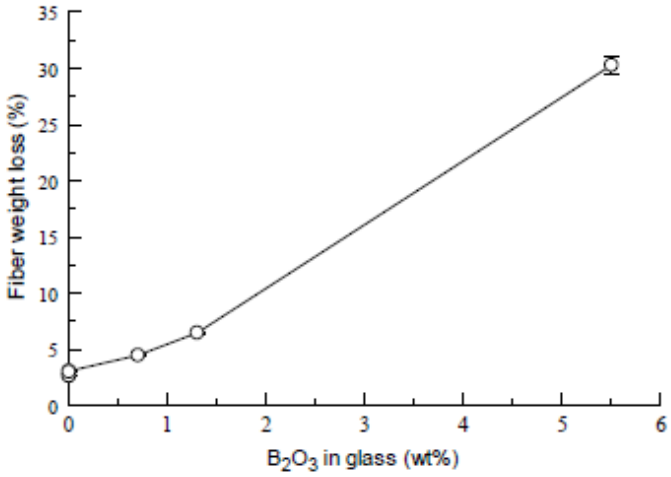

Figure 3: Weight Loss by Boron Content

Source: (H. G. Li 2012)

These results proposed that in the high boron fibers a majority of Ca and Al are separated from the silicate network. This leads to the mass loss in the high boron content fibers whereas the boron free fibers do not react in this manner. This means that the resistance to SCC of boron containing fibers is substantially lower than the boron free fibers.

Additionally, fibers were exposed to Oxalic, hydrochloric, nitric and sulfuric acids with the intent to understand the reaction to different types of acid on glass fiber strands that were sized with a silane agent. (Qiu 1997)

The test was performed with E-glass fibers with average diameters of 13µm sized with a silane agent and cut from a fiber strand with each fiber being about 10 cm in length in a strand of approximately 2500 fibers. These fibers were immersed in nitric,

oxalic, sulfuric and hydrochloric acids, each diluted with deionized water into four solutions of pH1, pH2, pH3, and pH4. This was done in Teflon bottles for a period of 2 weeks after which samples were removed, rinsed with deionized water and air dried.

Fiber weight loss was estimated by comparing weight before and after acid immersion. Loss was strongly dependent on acid type and concentration but more influenced by the former. Oxalic acid created the highest weight loss in all four concentrations. Nitric and hydrochloric acids were similar to one another but much less effective at weight loss than oxalic. The trend for all acids was weight loss became more severe as acid concentration increased (pH decreased).

Calcium and aluminum ion contents in the resultant solutions after acid immersion were analyzed using atomic absorption and colorimetric spectrophotometry. The results of this immersion showed calcium and aluminum depletion from the fibers during acid immersion, as before. The leachables were much higher in oxalic and sulfuric acids than in nitric and hydrochloric acids with calcium depletion appearing more severe than aluminum depletion.

This research showed that acid corrosion of E-glass fibers is primarily attributed to calcium and aluminum depletion, the severity depending on the acid type and concentration. Oxalic and sulfuric acids were much more corrosive than nitric and hydrochloric acids. This leaching is controlled by acid concentration for hydrochloric and nitric acids but for oxalic and sulfuric acids are dominated by the formation of insoluble salts or complex ions. Spiral and axial crack were observed from acid immersion. Ion-depletion-depth is established to explain fiber cracking due to internal stresses as was confirmed. (M. Megel 2001) (L. A. Kumosa 2001) Axial crack formation

is associated with ion-depletion depth relative to spiral crack formation. Fiber surface cracking in acids suggests post-failure damage in E-glass fibers which is much less prevalent in nitric and hydrochloric acids than in sulfuric and oxalic acids.

After the mechanisms behind SCC were understood, it was necessary to test three unidirectional pultruded E-glass/polymer composites with modified polyester, epoxy and vinyl ester resins for their resistance to SCC. (Megel 2001)These specimens were tested due to the common occurrence of brittle fracture during their use as suspension insulators for overhead transmission. These rods are the principle load bearing components and their brittle fractures result from SCC. This cracking is a result of chemical attacks on fibers in conjunction with tensile stresses applied along the rod axis. This acid forms as a result of moisture and corona discharges and penetrates the end fittings to reach the rod. They were tested using nitric acid with a pH of 1.2 in a uniquely designed four point bend fixture (see Figure 4).

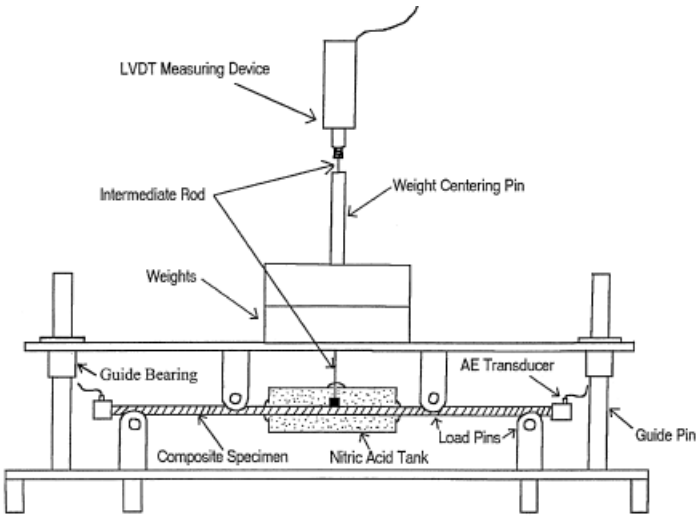

Figure 4: Four Point Bend Fixture

Source: (Megel 2001)

This fixture has four contact points which are labeled load pins. The two outermost pins are allowed to roll but not slip while the two innermost pins apply the load from perfectly centered weights placed on the table above. These pins are spaced far enough from the gage section to allow no shear stress and no local stress concentrations from the pins to affect the test section (see Figure 5). The weights are centered with a weight centering pin which has an LVDT measuring device to monitor displacement. The fixture has guide pins to ensure vertical loading but are spaced far enough apart to allow for acoustic emission sensors to be placed on the end of the specimen. Centered on the specimen is a nitric acid tank which exposes the as received samples to acid while the sample is under load. This tank is made from poly methyl methacralate and sealed with silicone rubber.

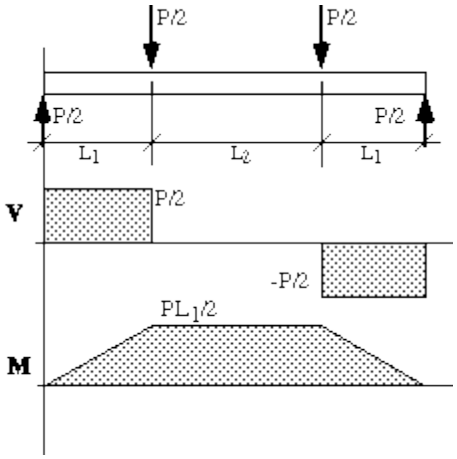

Figure 5: Shear Moment Diagram, 4-point Bend Test

Source: (Rusmee 2005)

Final dimensions of 3.2mmx12.7mmx304.8mm were selected based on a parametric study of stresses and displacements by the ability to have specimens respond linearly to load, simulate tensile stress in the gauge equivalent to in-service conditions,

and geometry allows for AE analysis. Finite element models and numerical modeling were used to in addition to experimental data to validate the test. Only one FEA model was used due to the similarity in the 3 composites. This model was a simplified 4 point bend setup to prove loading conditions matched experimental results (see Figure 6). The test sections were tested in the apparatus up to 110 N where the test data was in good agreement with numerical and analytical results (see Figure 7).

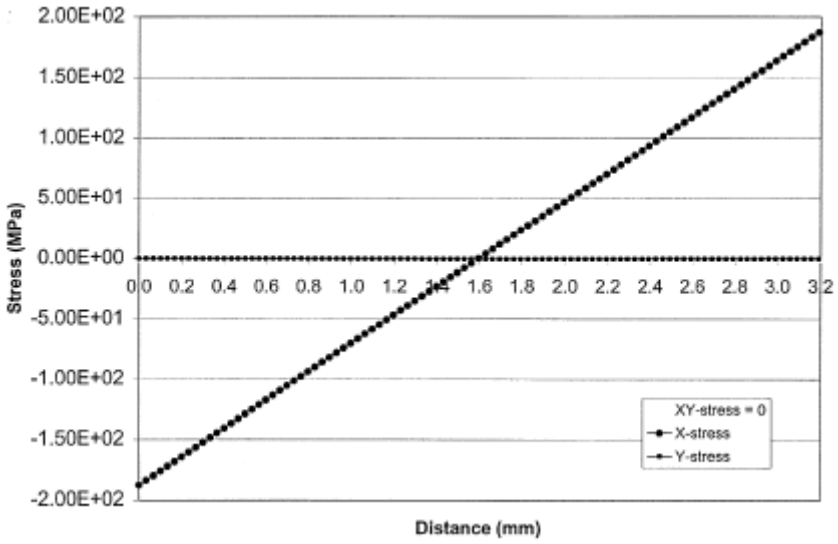

Figure 6: 4-Point Bend Test, FEA

Source: (M. Megel 2001)

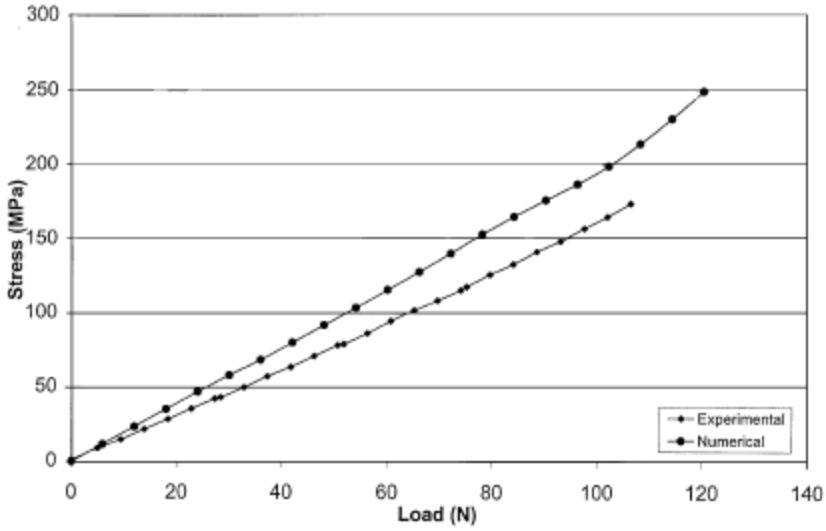

Figure 7: 4-Point Bend Test, FEA, Verification

Source: (M. Megel 2001)

In order to test for stress corrosion the plates were placed in the apparatus with jelly placed on the 3 machined surfaces to ensure the acid only affected the as received surface (which was to be put into tension during four point bending). Each specimen was loaded with a constant load of 83.97 N which generates an equivalent tensile stress on the free surface of 26.7 kN load applied to a composite insulator in-service with a rod diameter of 16mm. After testing the samples were cleaned and prepared for SEM analysis.

SCC experiments have to be performed as a function of time. This opens up the possibility that displacements, stresses and strains could be time dependent with significant creep for long tests. To examine the possibility of creep, two tests under the constant load of 83.97N were performed. One of these tests was dry while the other had the acid tank filled with water. Third order polynomials were fit to this data but it was

more or less the same due to the composites inability to absorb very much moisture (see Figure 8).

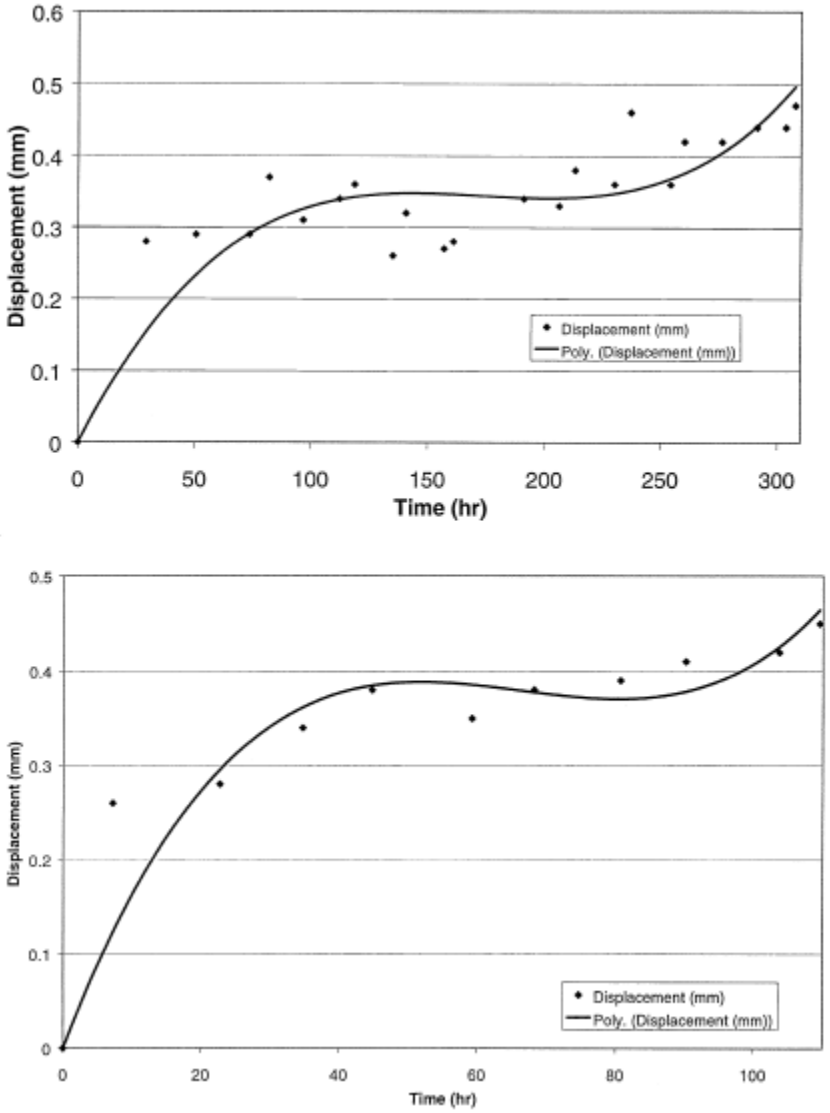

Figure 8: Displacement vs. Time, Dry and Wet

Source: (M. Megel 2001)

SEM testing was also done on each sample to view the overall surface conditions and morphology of SCC damage evaluation. Each composite material had various

amounts of exposed fiber with E-glass/modified polyester having the most. Misalignment of surface fibers existed and varied from sample to sample in amount. Specimens showed signs of mechanical damage such as surface holes and scratches which varied from sample to sample and were likely byproducts of the pultrution process. These are expected to contribute to the SCC process.

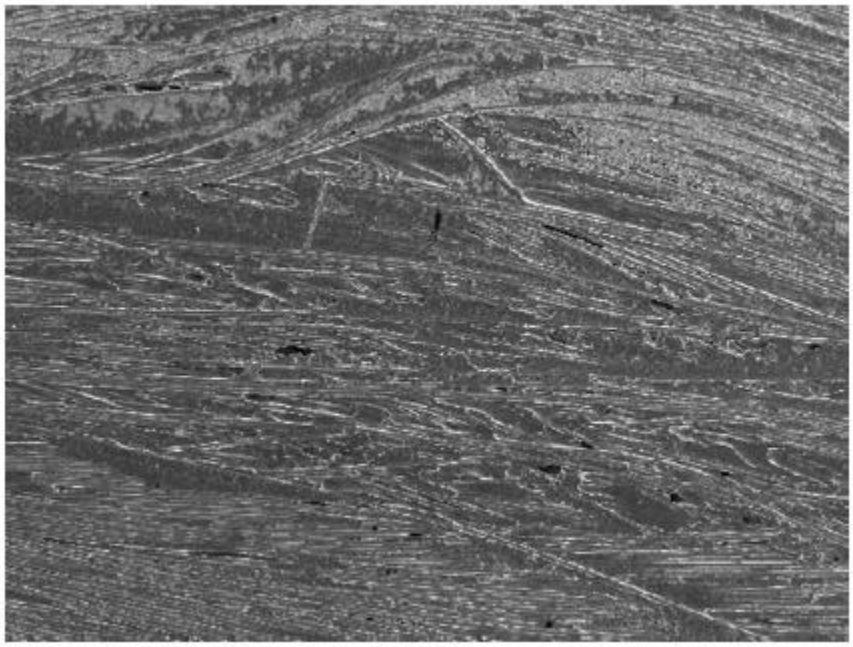

Figure 9: Surface Morphology, As Received, E-glass Epoxy

Source: (M. Megel 2001)

Cracks varied with samples as well. The SCC surface damage in the E-glass/vinyl ester specimens had several cracks on the surfaces of exposed fibers which were located in individual fibers without crack extensions to neighboring fibers. The other two composites had the least amount of SCC damage on the surfaces. The E-glass/modified polyester consisted of numerous cracks on exposed individual fibers, cracks extending to neighboring fibers and a few straight long cracks extending through

multiple fibers and a few long irregular cracks. All surface cracking initiated on the surfaces of exposed fibers but in a few cases it was noticed that cracks initiated from surface imperfections. In one case this lead to total failure of the sample. The cracks formed on the surfaces for all loads but single-fiber cracks were also observed in the specimen with no loading.

The results of this testing showed that the results indicate SCC damage is strongly dependent on the type of polymer resin used. The stress corrosion process has 3 stages: crack initiation, sub-critical crack growth and stable propagation. The initiation stage and sub-critical crack extension stage are random but identifiable using acoustic emission/time curves. The numbers of these signals generated in the first 2 phases are linear functions of time and can be used to determine SCC properties in these composites. The SCC process in these composites, when subjected to nitric acid and tensile stresses, initiate on the surface of exposed glass fibers. The amount of exposed surface area of the fibers alters the amount of SCC surface damage on the samples. The materials resistance to the initiation of stress-corrosion cracking is as follows: E-Glass/vinyl ester is 10 times better than E-glass/epoxy whereas the E-glass/modified Polyester is 5 times worse than the E-glass/epoxy system. Sub-critical crack extension process resistance ranks as follows: E-glass/epoxy is 5 times more resistant than E-glass/modified polyester system.

These samples reacted differently depending on the existence of surface flaws and holes and the manufacturing process. Some samples had SCC without the presence of loading conditions. Samples had contributing factors for initiation of fiber cracking from the following: total surface area exposed, applied and residual stresses, deterioration of

the polymer from acid attack, diffusion of acid through the polymer matrix and interfaces, and fiber sizing.

Further research was conducted as continuation upon the work of Megel as it relates to nitric acids involvement in Stress-Corrosion Cracking on three unidirectional pultruded E-glass/polymer composites with modified polyester, epoxy and vinyl ester resins. The same resins were tested due to their use in high voltage insulators on overhead transmission lines brittle failure from SCC. This work in particular was done to establish critical surface conditions that lead to the initiation of SCC on the surface of these as-supplied resins. This study, in contrast to the Megel research, was done without the presence of mechanical loading. (L. A. Kumosa 2001)

SCC from nitric acid is primarily attributed to calcium and aluminum ion depletion where the leachability of these metallic ions is determined by hydrogen ion concentration and strongly affected by the anions in the acid. The acid corrosion may generate axial and spiral cracks on the surface depending on the acid used.

For this experiment, 15 small samples, 5 of each type from each of the three materials of interest- E-glass/modified polyester, E-glass/epoxy and E-glass/vinylester, were cut using a diamond saw. These samples were wrapped in small aluminum coupons and sputter-coated with gold. The aluminum was then removed to expose a region of 2mmx2mm region not coated in gold. The purpose of this was to aid in the location of the same region multiple times for SEM work. These samples were viewed in the SEM and then placed into nitric acid and left for 24 hours. They were then removed, washed in alcohol and allowed to air dry for 15 minutes. Then the samples were viewed again. This process was repeated with exposure times being 0,24,48,72,144,214,336 hours to the

acid between viewings. The samples were measured for percentage of exposed surface fibers using UTHSCSA Imagetool 2.0. This was determined to have too much error do to the differences in contrast. The SEM was also used to determine surface damage in the form of SCC.

Each resin exhibited different amounts of exposed fibers on as-received samples, with E-glass/epoxy having the most, E-glass/Vinyl ester having the least and E-glass/modified polyester having somewhere in-between. These samples had a few fiber cracks but the morphology of these fiber cracks were entirely different than those resulting from acid attack. Three types of cracking that formed during exposure to nitric acid were: fiber center cracks (straight fiber on the composite surface), fiber end cracking (submerged below the surface), and fiber bend crack (exposed fibers). The third crack was largely absent from these samples.

It can be seen that crack initiation rates in the three composites are significantly different. The majority of all crack growth occurs in the first 48-72 hours after which rates or crack initiation slowed and after 2 weeks essentially stopped. The total number of cracks in the five E-glass/epoxy, five E-glass/modified polyester and five E-glass/vinyl ester specimens were 56, 24, and 2 respectively. This data has a direct correlation between to the total surface area of fibers exposed with a larger area denoting more SCC. The E-glass/vinyl ester ranged between 2-7% surface area exposed while the E-glass/epoxy specimens had 30-45% and the E-glass/modified polyester between 7-20% total surface area exposed.

The cracking of the fibers from the nitric acid appears to be a result of residual manufacturing stresses instead of the actual wearing-away of fibers from nitric acid. This

was confirmed when pure fibers were exposed to nitric acid and no cracking was formed. There was a slight contradiction between this study and Megel regarding the resistance to SCC of the same kinds of samples. It was shown by Megel that E-glass/vinyl ester is 10 times better than E-glass/epoxy and that E-glass/modified polyester exhibits 5 times worse resistance to SCC than E-glass/epoxy. Megel showed as well that SCC in vinyl ester composites in comparison with the other two were quite similar but the presence of mechanical loading could be responsible for this difference. The properties of this composite are superior to the other two if it is determined regardless of mechanical loading.

The results of this test show that SCC is initiated in the samples, even without mechanical loading and that the number of cracks is largely dependent on the volume of exposed fibers on the composites surface. Of the three types tested, the highest rates of SCC and largest total surface areas of exposed fibers were found in the E-glass/epoxy system. The externally applied stresses are not necessary for SCC on the as-supplied surfaces of the composites and SCC can develop in the fibers embedded in the polymer resins due to residual stresses. These initiation rates go to zero if loads are not applied.

1.3 Modal Acoustic Emission

The main purpose for MAE testing is as an effective nondestructive evaluation technique. MAE allows for real time monitoring of events in mechanical testing that are not be visible to the human eye. Modal acoustic emission is a branch of acoustic emission that utilizes broadband transducers and the waveforms resulting from events to enable the categorizing and locating of signals through analysis. Signals themselves are the result of stress-wave propagations due to microstructural changes from localized strain-energy releases. For composites the energy release comes from matrix cracking, fiber matrix interface debonding, fiber fracture and delamination. Despite this useful analysis technique, it must be understood the challenges that come with it. MAE sensors are placed on the surface of the material and at some standoff distance from the signal origin. This means accounting for wave propagation, attenuation, signal leakage and boundary surface interactions.

Certain complications arrive when investigating wave propagation, particularly in plates. While both primary low plate modes are generated, there is discrepancy between the flexural wave velocities and theory. (Gorman, Plate Wave Acoustic Emission 1991) It was noted that flexural waves being predominantly lower frequency than extensional modes, would attenuate more rapidly. Also of note is that source changing from the face of the plate to the edge almost entirely eliminated flexural mode. Modeling has been previously investigated for MAE in plates by use of Mindlin-Medick plate theory as well as dynamic finite element plate method. (W. H. Prosser 1999) From this research it was shown that both models predict flexural mode in agreement with experimental modes, but only the dynamic finite element plate method would be more accurate overall. This is

due to its flexible nature to be able to model different source configurations and geometries. Discrepancies also arose for long times due to contributions from reflections on plate edges, further exacerbated in the Mindlin-Medick plate theory model. It should be noted that Mindlin-Medick plate theory models have trouble with matrix cracking when the source is symmetric with respect to the midplane. This dynamic finite element plate method will be expanded upon in the next section.

AE signals also become much more complex when laminated anisotropic plates are considered. Accuracy when using exact elastic theories proved to have limited accuracy in predicting elastodynamic fields, being dependent on plate thickness, pulse width of the forcing function and source distance. (Lih 1995) These differences are even greater when an approximate method is used. Transfer Matrix method was also used to account for anisotropy, by satisfying continuity conditions at interlayer interfaces. (Nayfeh 1991) This method relates displacements and stresses from one side of the composite to the other, which solves for the propagation of free waves on the plate by understanding the periodic repetition of the plate.

The complex nature of wave propagation in anisotropic plates is further compounded in composites as the frequency content of the signal will experience different amounts of attenuation depending on the location of sensors with regard to fiber orientation. (B. H. Burks, On the Anisotropic Attenuation Behavior of the Flexure Mode of Carbon Fiber Composites 2013)

In order to understand how AE works in composites, it must first be understood how it works in simpler structures, mainly thin metal plates. Waves have classically, and for the purposes of investigation, been investigated by conducting a lead break on the

plates surface and monitoring the signals on AE sensors. (Gorman, Plate Wave Acoustic Emission 1991) (Gary 1994) These lead breaks excite classic low order modes; extensional (S_0) and flexural (A_0) (see Figure 10 and Figure 11).

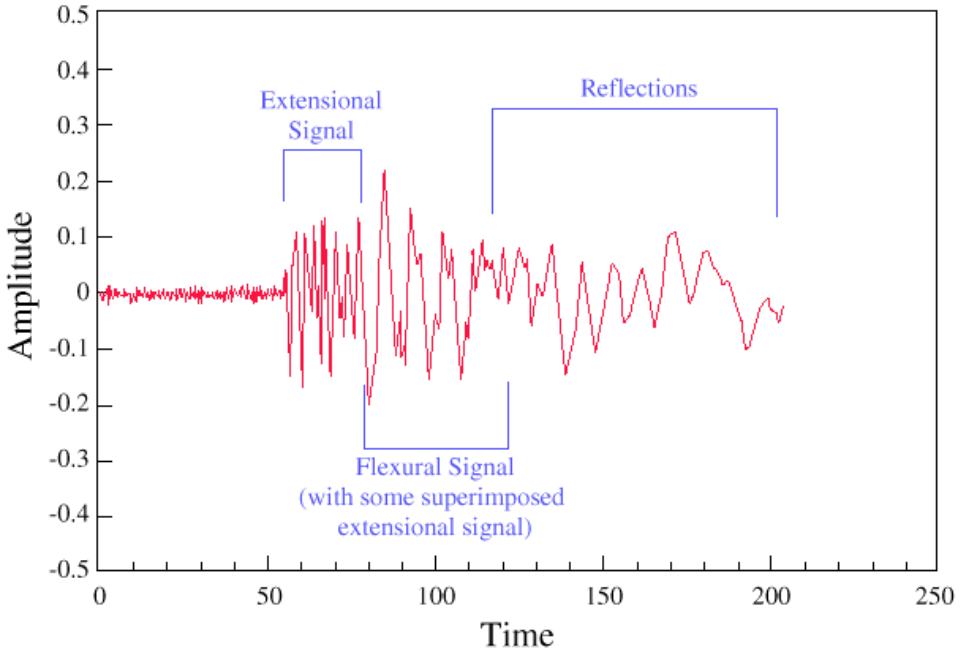

Figure 10: Mode Example, Time Domain

Source: (Huang 1998)

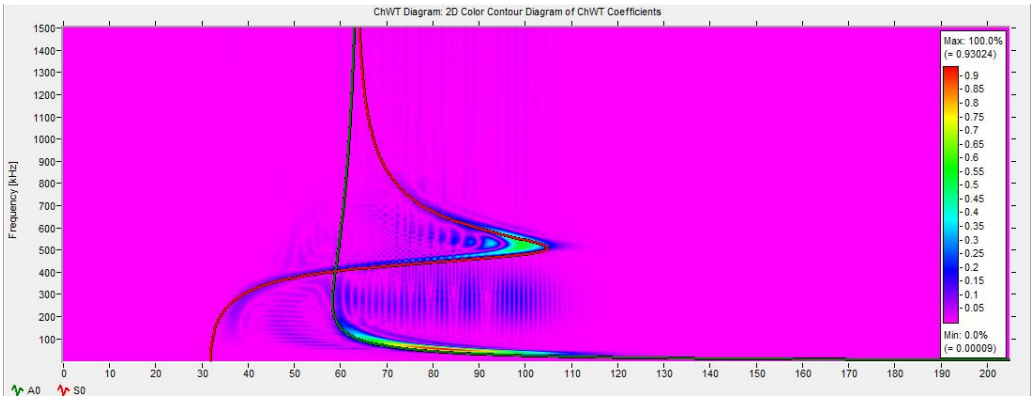

Figure 11: Mode Example, Group Velocity Curves Overlay

Pencil lead breaks are ideal for their repeatability and availability, however, it can only be applied to the outer surface of a test sample and can only be easily applied as an out-of-plane source (In-plane sources are also quite common, depending on accessibility) as well as having a limited range of source rise times and dimensions. Pencil lead breaks were compared to calculated values as well as the effect of rise time and geometric size on far-field displacements. (Gary 1994)

Measurements were conducted on an aluminum alloy plate 31.mm thick with lateral dimensions of 1.5m by 1.2m. A 0.3 mm mechanical pencil lead break was applied at the center of the top surface and measured at a distance of 0.254 m. Computer simulations were done by using a temporal variation of normal stress calculated from a previous study (see Figure 12). (Breckenridge 1990) This is coupled with a change in rise time, which is the time required to achieve maximum stress, which is chosen so that the total force reached 1 N. This matches the force in experiments and the output is measured 0.254 m from the source.

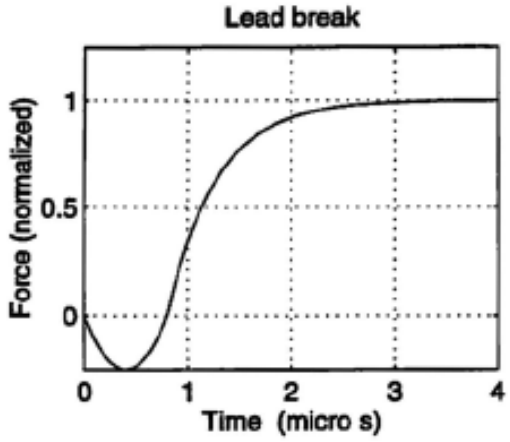

Figure 12: Simulated Lead Break

Source: (Gary 1994)

Experimental data was then compared to computer generated data, paying special attention to the wave between 40 and 90μs. This was done to show agreement between the values calculated and experimental. They both show radial component of the portion of the wave between 60 and 70μs and constant in the z direction and the vertical component nearly linearly anti-symmetric. Almost the entire captured wave is shown to be anti-symmetric as all of the energy at 140μs is in this mode (see Figure 13).

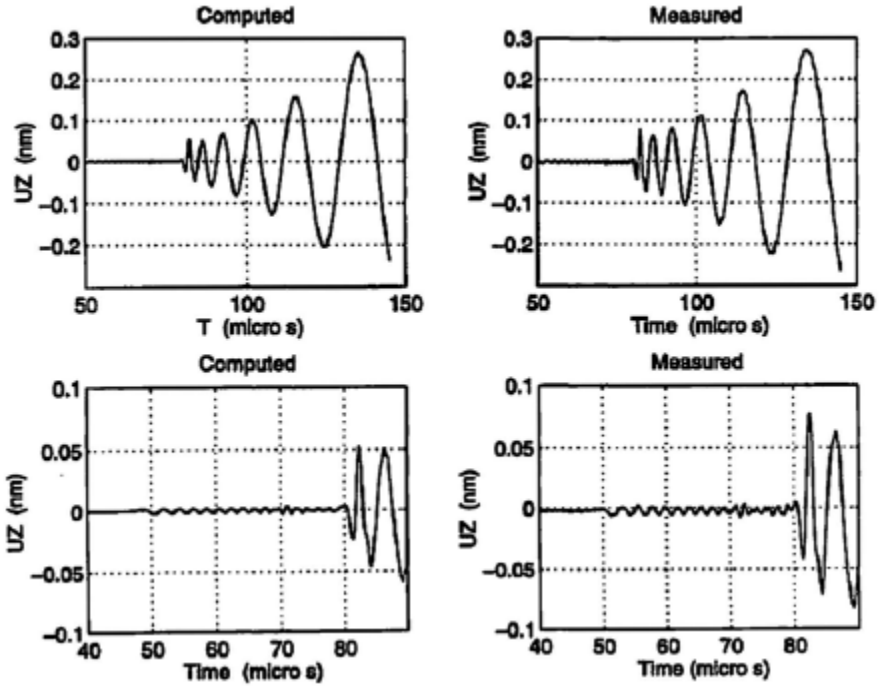

Figure 13: Out-of-Plane displacement (UZ) at Sensor

Source: (Gary 1994)

Sensor diameter is also important to understanding signal analysis; this is known as the aperture effect. (Miller 2005) As the diameter of the sensor is increased to become comparable to the wavelength, phase cancellation occurs. For this sensor distance setup, the displacement was integrated over a circular disk. Severe distortion was seen before

signal filtering as the diameter sufficiently increased, yielding a maximum diameter of 6.35mm for this waveform (see Figure 14). At the time this was not understood, but by integrating over a line in an axi-symmetric model the sensor was not being replicated, but rather a large annular disc.

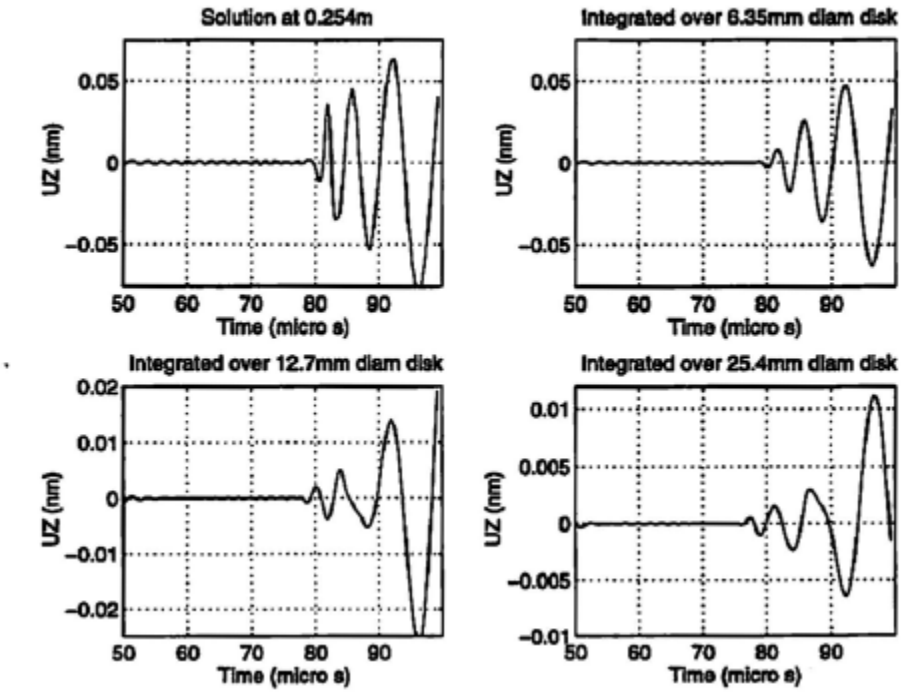

Figure 14: Response as a Function of Sensor Diameter

Source: (Gary 1994)

Key to understanding source location is the effect of Rise Time. Rise time can effectively be seen as the amount of time it takes from beginning to end of an event, in this case, the lead break. As rise time slows, there is observed a significant loss of amplitude, while shape is largely the same (see Figure 15).

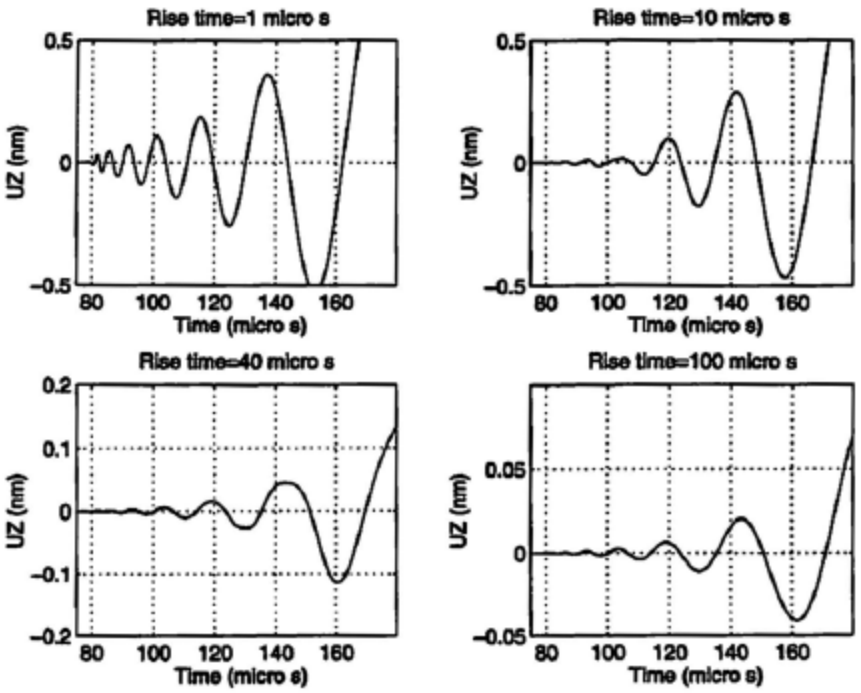

Figure 15: Response as a Function of Rise Time

Source: (Gary 1994)

These factors show the importance and dramatic effect rise time has on source detection. Sources with rise times up to 40μs require an MAE system with good response to relatively low frequencies. In addition, sensor diameters above 6mm do not preserve fidelity of measured waves.

Investigation into classifying damage mechanisms in glass fiber reinforced polyester in tensile tests using acoustic emissions was done, with data from the acoustic emission sensors used as inputs into a Kohonen self-organizing map, which separates signals and allows for a correlation with failure modes. (Huguet 2002)

Several other researchers have experimented with AE in composites and found several results. Some have found specific AE amplitude ranges for damage mechanisms

in their composites. (Barre 1994) Others have showed that fiber breaks and longitudinal splitting occurs in the same location for their unidirectional graphite/epoxy specimens with stronger signals resulting from fiber breakage and weaker ones from longitudinal splits. (Ely 1995) However single damage mechanisms such as matrix cracking can produce a wide range of AE signal parameters. Due to this fact, pattern recognition and multi-parameter analysis is necessary to determine the cause of signals. This is accomplished with supervised pattern recognition in experiments where the number of damage mechanisms is known in advance. Clustering algorithms were used to organize feature vectors into clusters so that points within a cluster are more similar to each other than vectors from other clusters. This was done with the self-organizing neural network from Kohonen's self-organizing map technique. This technique organizes the output layer as a map where similar shapes are detected and categorized.

Tension tests were carried out on rectangular plates of unidirectional glass/polyester composite materials. The composite was a laminate with 12 layers and the test was done at room temperature. Samples were cut using a diamond wheel saw which was found to give a suitably smooth surface finish with minimum sub-surface damage. Tests were done on plates of pure resin, 45° and 90° off-axis. These orientations were chosen due to the expectation of damage modes during tests. Pure resin was expected to have matrix fracture with 90° off axis expected to have mainly matrix fracture with come decohesion and 45° was expected to have mainly decohesions with some matrix fracture. Micro-80 PAC Sensors (not broadband) were used with a sampling rate of 8 MHz and a 40 dB pre-amplification. A total amplification of 80 dB was used

with a filtering threshold of 32dB and a nominal distance of 70 mm between sensors was used.

Tensile tests on pure resin generated little MAE activity. The waves that were detected could all be grouped by burst type indicating that the waves were generated during dynamic and discontinuous micro-fracture. After reaching 2% strain two phases can be considered: micro-crack formation and dynamic breaking. Between 2% strain and final rupture the signals have a typical distribution with values in the 55-70 dB with slow rising waveforms and short duration. These signals cannot be associated with anything but nucleation and vacuoles growth in the resin, i.e. matrix micro-crack formation. The second phase occurs at very high amplitude and high energies from rupture. These signals occur with dynamic breaking and thus are not retained as they cannot be attributed to damaging material response under load.

Tests on the 90° off axis samples showed MAE activities with a noticeable increase in activity around 0.4% strain. After an initiation period the number of MAE counts increased linearly with strain at stresses higher than 3MPa. The activity begins early in loading indicating an early onset of damage. Signals originated from sources randomly distributed within gauge length and their amplitudes fell into two zones. A-type signals were similar waveforms as the resin test (50-70dB range) while B-type amplitudes which are higher but have shorter decay time and higher energies (70-90 dB range). B-type has sharp rising and decaying in a short duration while A-type has slowly rising waveforms with a longer decaying. A-type is again identified as matrix cracking due to its similarity to the resin signals while B-type are identified as Matrix decohesion. This was again confirmed as classification of A-type and B-type signals in the 45° test.

These results can be seen in Figure 1 which shows Activation of the Kohonen's map for the three tensile tests.

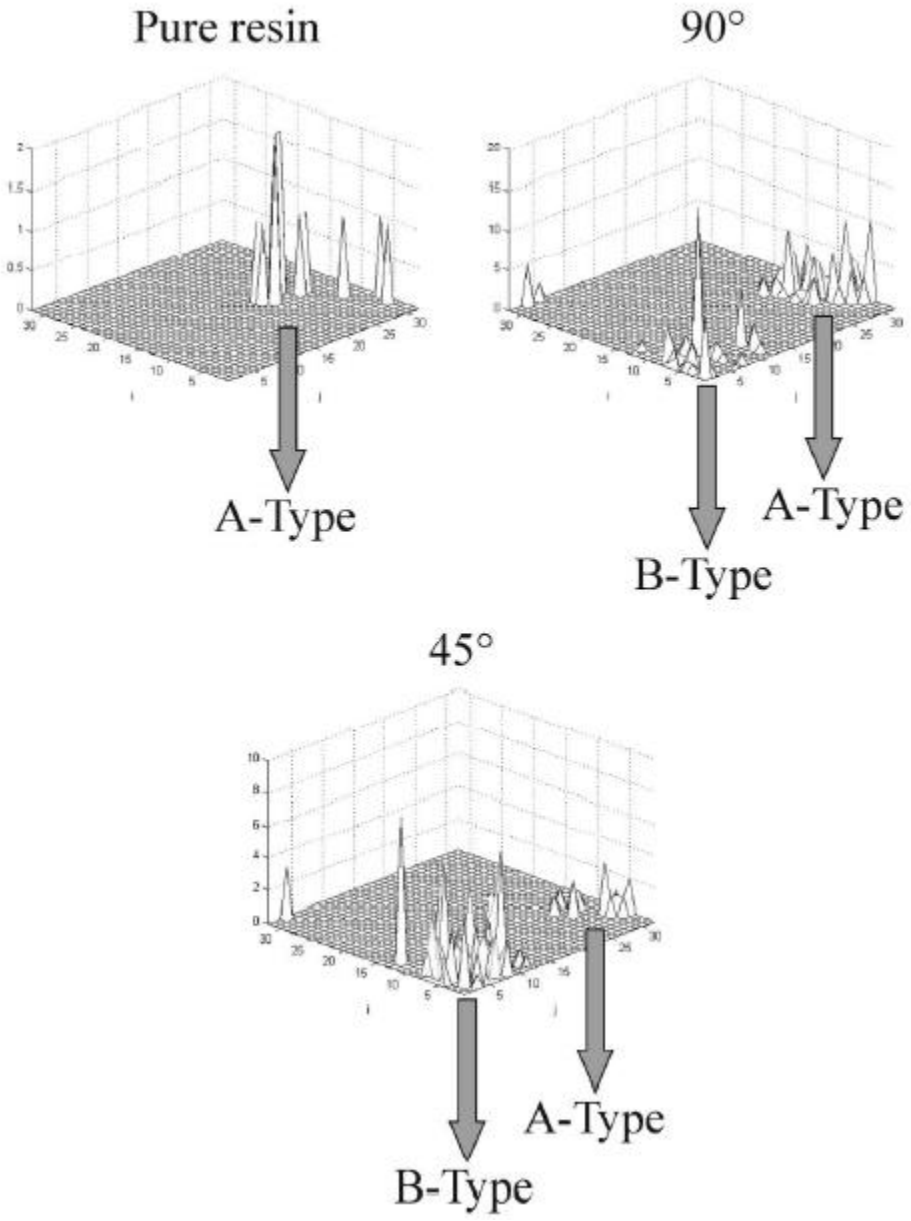

Figure 16: Activation of the Kohonen's Map for the Three Types of Tensile Tests

Source: (Huguet 2002)

This method is not without controversy, as growing support mounts within the AE community that amplitude is irrelevant and that mechanisms are distinguishable by their mode and frequency content rather than time domain structure.

Source location and real world application testing are also important towards establishing validity for MAE testing, prompting MAE testing on a spherical graphite/epoxy pressure vessel. (M. Hamstad 1995) The reasoning for testing this structure was to draw results on the implications for MAE monitoring and future MAE studies of large fiber/polymer composite structures and increase the ability for source location in conjunction with a model for localized failure of large aerospace type fiber/polymer composites. Previous studies had used MAE for source location but were on small samples with small standoff distances between sensor and source (approximately 60mm). This study also sought to answer three questions associated with MAE signals: significance, location and source type.

The study was done on an aerospace-type graphite/epoxy pressure vessel (see Figure 17: Test specimen and sensor location. Location of sensors was chosen based on the expected source of failure being at the poles and there were 16 in total. Sources were placed in two concentric rings around the poles with the same orientation at each pole. The sensors used were wideband non-resonant with a fairly flat displacement response. The PZT sensor outputs were bandpass filtered with -3dB points at 85 and 325KHz. The response was compared to the NIST standards with a pencil lead break.

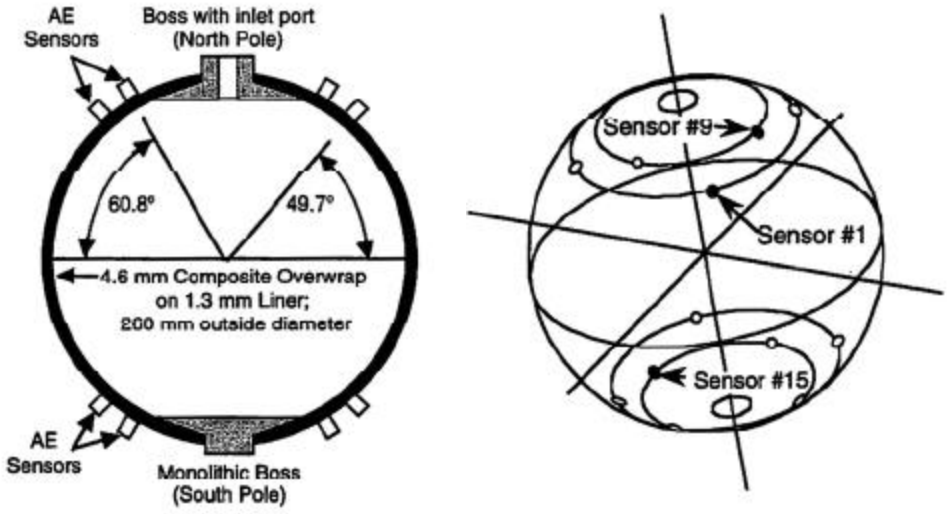

Figure 17: Test specimen and sensor location

Source: (M. Hamstad 1995)

Each pair of waveforms from this study was from a single MAE source event. This was proven from several observations. Waveform pairs were recorded almost exclusively during Felicity ratio loading or well into constant pressure holds where event rates were very low. Also time periods between events and hits from one event were typically observed to be of different orders of magnitude when the hit listings of the results from all sixteen sensors were studied. In addition each waveform was recorded with a window of only 800μs with the trigger set at the central portion of the window. All of these factors allowed for pairs of waveforms to be from only a single event to be able to study the effects of distance from the source to sensor to be studied.

After some testing some observations were made about a single event detected by two sensors. In one case a signal from one event believed to be at the South Pole was detected by sensor #9 and sensor #15. What made the sensor hits interesting were the

large difference in the peak amplitudes of the two sensor hits from the same event. The peak amplitude drops from 484mV for sensor #15 to 73 mV for sensor #9, a drop of about a factor of 5. Also the character of the waveform at the second sensor hit, #9, has the form that is observed with wideband, flat with frequency sensors on a thin plate, i.e. low amplitude extensional wave packet followed by a flexural wave packet with a slower group velocity. This signal is not present in the data collected from sensor #15. Also the rise time and hit duration are much longer for the hit on sensor #9 as well as the energy in the waveform for that sensor shows that it is down by an order of magnitude from the energy at sensor #15. Fast Fourier Transform spectral content shows a significant difference between sensors as well where sensor #9 has a shifted frequency much more towards the lower portion of the frequency band. These differences show strong evidence that the small-specimen database might be inappropriate for far-field, large composite structures for assessing damage level via peak amplitudes or to distinguish source mechanisms.

In another case involving the same sensors rise time, peak amplitude, duration, energy, spectral content are all very similar from one event. In this case the MAE source was located approximately equidistant from each of the two sensors as is evidenced by the nearly equal arrival times and almost identical time-lengths for the extensional portions of the waveforms. This test does verify that for a given event all sensors behaved in the same fashion.

For the case in which an MAE event occurs very near one sensor several observations can be made. Spectral content for the first sensor hit displays a range of frequencies and has a fairly high average frequency (greater than 200KHz). If the second

hit sensor is in the near field the shorter propagation distance results in a spectral content for the second hit sensor that is similar in range and distribution to that for the first hit sensor but with amplitudes reduced. Lastly if the second hit sensor is in the far-field the greater propagation distance causes the higher frequency content of its spectrum to be dramatically reduced, causing a lower average frequency (less than 200KHz) and a spectral distribution which is very different from the first hit sensor.

For the case in which an MAE event occurred in the far-field but equidistant from each sensors observations can be made. Spectral content of the first hit sensor matches that of the spectral content of the second hit sensor with respect to amplitudes, distribution, range and frequency. Also the average frequency is low (less than 200KHz).

Geometric spreading is present for all MAE sources which accounts for the large loss in amplitudes for short propagation distances when one sensor is near the source. This has two components: 1/r losses which govern propagation when spherical waves spread through structure thickness and $1/\sqrt{r}$ losses which govern wave propagation when circular wave fronts spread over the surface area. For thin walled structures only the latter is relevant and as the circular spreading continues it becomes less relevant than the material attenuation which will continue to cause losses in amplitude. For these longer distances the characteristic waveforms are those to be expected from Lamb waves, with the two primary modes being extensional waves with a higher group velocity and flexural waves of a lower group velocity and higher amplitudes. This explains why differences in behavior when an event happened near one sensor but the second sensor hit is far enough away for full development of the Lamb waves. Lastly Lamb waves are dispersive meaning they group velocity depends on frequency. The time difference between the

initial arrival of the extensional wave packet and the subsequent arrival of the flexural wave packet increases with greater propagation distances.

For large composite structures with a plate or shell type geometries there are several implications of this research. First, data and numerical models need to be developed to characterize dependence of MAE hit characteristics on the distance of propagation for different bandpasses and various thicknesses of fiber/polymer composites which would determine sensor distance. Due to cost concerns, sensors must be lower in bandpass to monitor lower frequencies experiencing a lesser degree of material attenuation and take advantage of higher amplitudes which are present in the flexural mode at lower frequencies as well as lower thresholds. Also, an approach needs to be developed to flag MAE hits for which the event characteristics were determined in the near field where event characteristics are changing at a very high rate. There must also be a way to determine source distance by individual sensors.

In order to model stress-induced damage for these kind of composites the following must be accounted for: micro-damage beings at low percentages of failure level, composite structures loaded in biaxial stress increases in stress result in uniformly distributed characteristic damage state, failure of a composites is not determined by the characteristic damage state but rather by the result of a higher concentration of damage accumulation in a localized zone, in a composite the localized zone of concentrated damage often occurs at stress concentrations, and the number of MAE events resulting from the characteristic damage state is orders of magnitude greater than the number of events coming from the zone of localized, concentrated damage. Based on that model it does not make sense to attempt MAE relating to failure strength of a composite unless

accurate track is kept of the source locations. If one is ignored then MAE from the generation of characteristic damage state will confuse the data analysis due mostly to numerical superiority. The same thing applies to MAE from different zones of concentrated damage distinction.

1.4 Finite Element Modeling

Initially, the development of a model for MAE was desired. For the purposes of this research, modeling MAE waves in plates is the most important preliminary modeling.

Early AE modeling was applied using seismology modeling, which has been applied to model propagation of bulk and surface waves. This model works well for infinite dimensions, however in plate geometry only for short propagation distances of less than ten plate thicknesses. (W. H. Prosser 1999) For testing purposes, thin plates are desired, and for these geometries the wave propagation is dominated by guided modes. These modes are more affected by reflections by pate edges. AE signals with very low frequencies, such as flexural, tend to agree experimentally better than other high order modes. For the purposes of advancing AE modeling, the Mindlin Plate Theory (MPT) and Dynamic Finite Element Method (DFEM) were tested to evaluate both thin plate modeling as well as anisotropic conditions. (W. H. Prosser 1999)

For the purposes of investigating thin plates, an aluminum plate with a density of 2770 kg/m^3, Young's modulus of 73 GPa, length of 0.508m, width of 0.381, and plate thickness of 3.175mm was examined. Source was positioned centered on the sample both length and width wise with sensors along the central length line with distances varying from 7.62cm to 17.78 cm. This model used a hexagonal mesh with 40 elements through the thickness. Only asymmetric Lamb modes could be obtained based on conditions simulated. Amplitude of the monopole source force function was 1N. A comparison of results was examined for the two methods at 7.62cm, 12.7cm, and 17.78cm source distance, which showed good comparison but had some discrepancy at higher frequencies (see Figure 18).

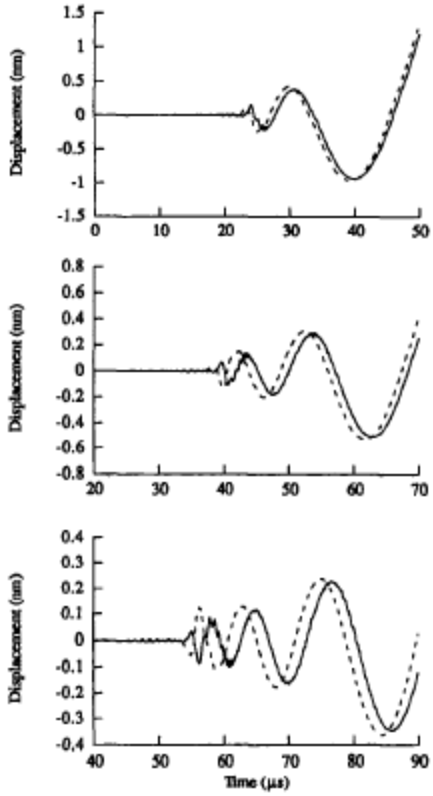

Figure 18: DFEM (solid) and MPT (dashed) Comparison

Source: (W. H. Prosser 1999)

This discrepancy is thought to be due to the approximate nature of MPT. DFEM is based on exact linear elasticity and had been confirmed experimentally. The DFEM method accounts for displacements from all modes, symmetric and anti-symmetric while the MPT only for symmetric modes. Other plate theories can calculate extensional modes, but do not agree well experimentally.

The influence of microscopic elastic properties and the geometry of the MAE source are important to investigate by finite element analysis (FEA). This will be done by investigating the formation process of lamb waves by simulation of five different MAE configurations. (Sause, Simulation of Lamb Wave Excitation for Different Elastic

Properties and Acoustic Emission Source Geometries 2010) A comparison will be made between isotropic and anisotropic materials of aluminum and fiber reinforced materials respectively. Through this work it will be determined if the microscopic elastic properties of the MAE source have significant influence on the excitation of distinct Lamb wave modes which can be used to identify failure mechanisms.

Analytical descriptions of MAE sources from crack formation and propagation are well documented and linked to macroscopic displacement by Green's functions, they are much more difficult for complex geometries. FEA is deemed as the solution to this problem for plate specimens due to its computational capacities and ability to model and simulate MAE. This modeling can be done for the source mechanism, signal propagation and signal detection. For the purposes of this research a source model with a finite dimension of the crack model and the geometry and elastic properties in the vicinity of the crack model was used.

After the signal excitation, the elastic wave propagates into the solid and is reflected at the respective boundaries of the geometry. For the FEA simulation the propagation of such signals is modeled based on time dependent solutions of differential equations of the equilibrium states. Different source radiation directions can excite different ratios of symmetric and anti-symmetric Lamb wave modes. This can lead to different frequency compositions of the detected MAE signals. Signal propagation in previously used specimen types suffered drastically from boundary reflections since interference of signals with their boundary reflections makes identification of distinct Lamb wave modes more difficult. This is extended to larger specimen geometries and for isotropic media is treated as a reference. Most importantly, the detection process of

MAE signals will be detected by the simulation of surface displacements at distinct positions.

Simulations were performed for rectangular plate specimens utilizing symmetric boundary conditions at the yz and xz plane (see Figure 19). The MAE source is located at the medial plane where (x,y,z) = (0,0,0)mm. This model was used in 5 different configurations: Isotropic aluminum with homogeneous source, anisotropic CFRP plate with homogeneous source, Anisotropic with inhomogeneous source (resin properties), Anisotropic CFRP with inhomogeneous source (carbon fiber properties) and point force couple.

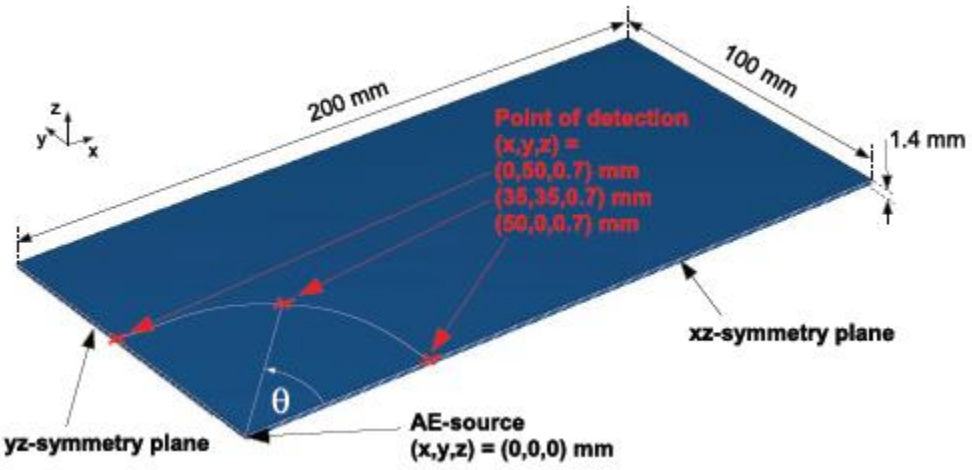

Figure 19: FEA model

Source: (Sause, Simulation of Lamb Wave Excitation for Different Elastic Properties and Acoustic Emission Source Geometries 2010)

The first configuration has a crack that is modeled as a three-axes cross, which is cut out of the homogeneous medium around the sources. For this configuration all domains were assigned elastic properties of aluminum. For the second configuration the

same configuration was used although all domains were now assigned homogeneous, anisotropic elastic properties of T800/913. The third configuration has microscopic elastic properties of a cube with the properties of the HexPly 913 resin and the elastic properties of the macroscopic plate made of T800/913. While the dimensions of the crack model and domains were comparable to previous configurations, now a smooth transition between microscopic and macroscopic elastic properties is achieved utilizing a cube which encloses the resin cube. This causes a gradual change in elastic properties of the enclosed medium to those of the surrounding medium along with gradual material density change.

In order to excite an MAE signal a linear source-time function was used to deflect the respective crack surface. After the excitation time, the boundaries of the source model are free of constraints. For better comparison of the obtained results the magnitude and excitation time was kept constant for all models at 100nm and 100ns respectively. Refinement of the FEA mesh was gradual from 2.0 mm to 0.01 mm when approaching the model source. The higher resolution close to the source is necessary to resolve the geometric details of the source model, while the coarse macroscopic resolution is sufficient enough to describe signal propagation within the plate specimen. As a result of the break of symmetry with respect to the xy-plane Lamb wave modes can occur with the sensitivity of the Lamb wave formation based on this effect. With reasonable steps of refinement of the mesh density around the source model the excitation of anti-symmetric Lamb waves could not be prevented. This setup ensures a more realistic model as opposed to perfect symmetric mesh conditions. All simulations were done on identical meshes.

Signals of both homogenous, isotropic medium models are dominated by the contributions of the S_o Lamb wave mode with an excitation of the A_o Lamb wave mode. This contribution is hardly visible in the Choi Williams Distribution (CWD)-diagram since the magnitude of the coefficients is dominated by the intensity of the S_o Lamb wave mode. CWDs allow for the visualization of a signal in the time domain, but with frequency visible. This is valuable because it allows for the visualization of wave content as it arrives at the sensor, and an easy classification of mode (see Figure 11). Since the source model configuration A uses an axially oriented surface displacement, a dependency on the orientation of the source relative to the sensor can be expected. Surface displacement signals were detected at three distinct points, reflecting three different source-sensor angles of 0, 45, and 90 degrees respectively between the crack surface normal (x-axis) and the investigated propagation direction.

Inhomogeneous, anisotropic medium models modeling matrix cracking, the signals are dominated by the A_o mode for all source-sensor angles. Only minor contributions of the S_o Lamb wave modes are observed. This configuration for the fiber breakage model has a strong contribution of the S_o Lamb wave mode for propagation direction parallel to the crack surface normal. Increasing source-sensor angle decreases S_o mode contribution. The same source excitation time was used in this simulation for both source model configurations. Source excitation time of fiber breakage is expected to be shorter than for resin fracture which results in a stronger contribution of the intensity of the S_o mode for the case of fiber breakage and emphasizes the characteristic difference between the associated source mechanisms further.

As increased understanding of anisotropic, thin-plate modeling of MAE was understood, models could grow in accuracy to represent more experimentally accurate representations of damage mechanisms in fiber/polymer composites. Explicit dynamic finite element methodology was determined the most ideal due to its explicit time integration scheme, computational efficiency, as well as ability to account for complex geometry, anisotropy, wave reflections and increase in model size. (B. K. Burks 2013)

In order to advance modeling capabilities, research was done to investigate a unidirectional hybrid polymer matrix composite, with carbon and glass reinforcing fibers in a high temperature epoxy matrix (see Figure 20). This model was took advantage of symmetry by modeling ¼ of the cross section, and used fracture mechanics to set damage mechanisms in proper directions, which will be discussed later in more detail. This model was meshed with hexahedral elements and converged at 147 μm element length.

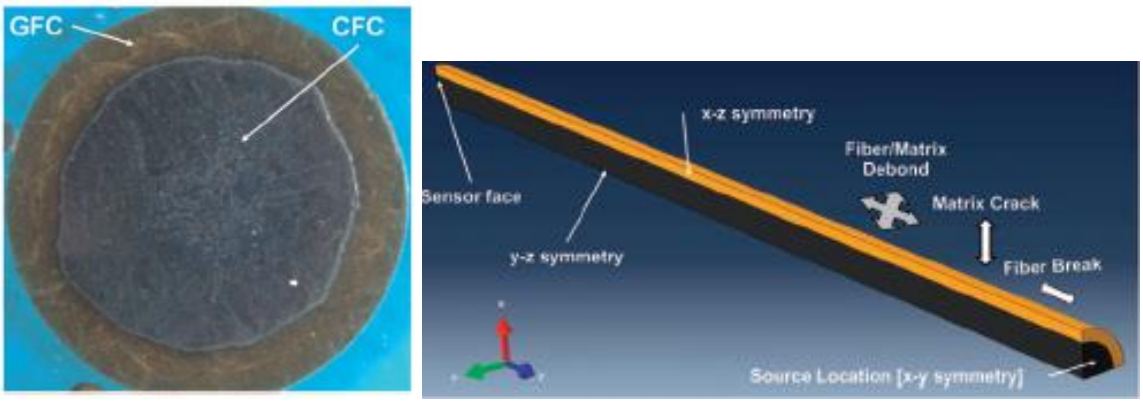

Figure 20: High Voltage Composite, Cross Sectional and FEA view

Source: (B. K. Burks 2013)

This methodology involved a 4 point bend test, with loading pins separated by 202.8mm and 101.4mm for outer and inner pins respectively. AE waves were

experimentally acquired with broadband sensors were placed on the ends of the rod, and signals acquired at a rate of 25MHz, with 2048 points captured and 256 pre-trigger points. Only signals within the inner span were examined, which was identified by examining arrival times. Experimental signals were recorded and examined (see Figure 21 and Figure 22).

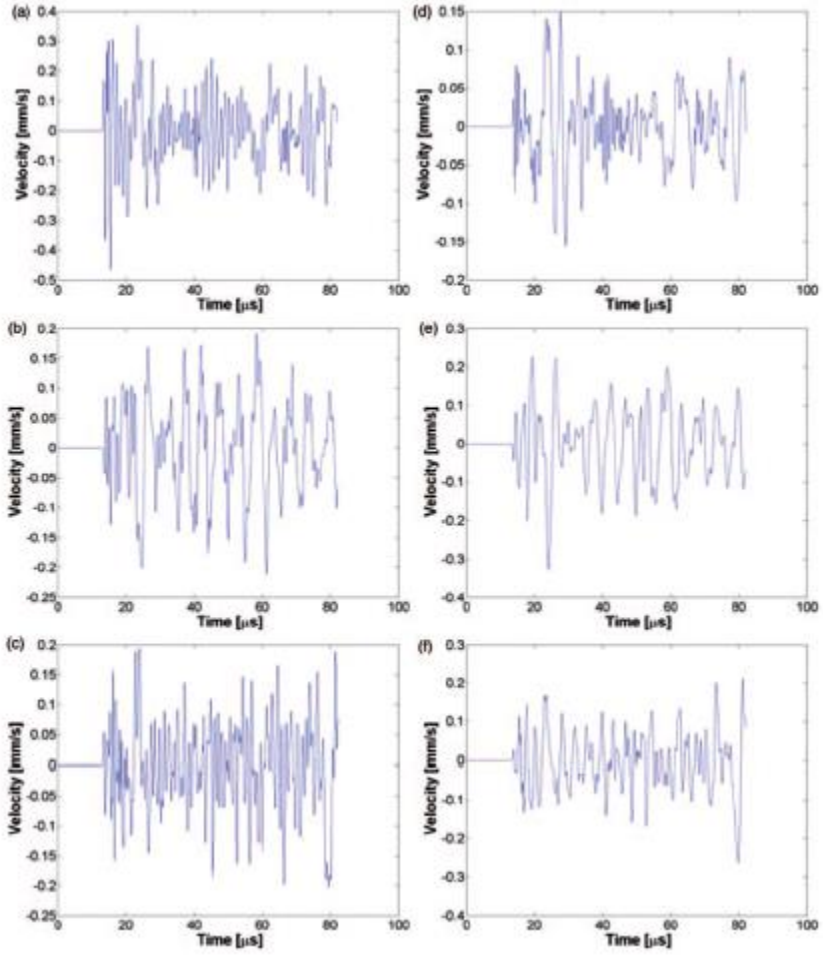

Figure 21: Fiber Fracture (a,d), Matrix Cracking (b,e), Fiber Matrix Debonding (c,f)

Source: (B. K. Burks 2013)

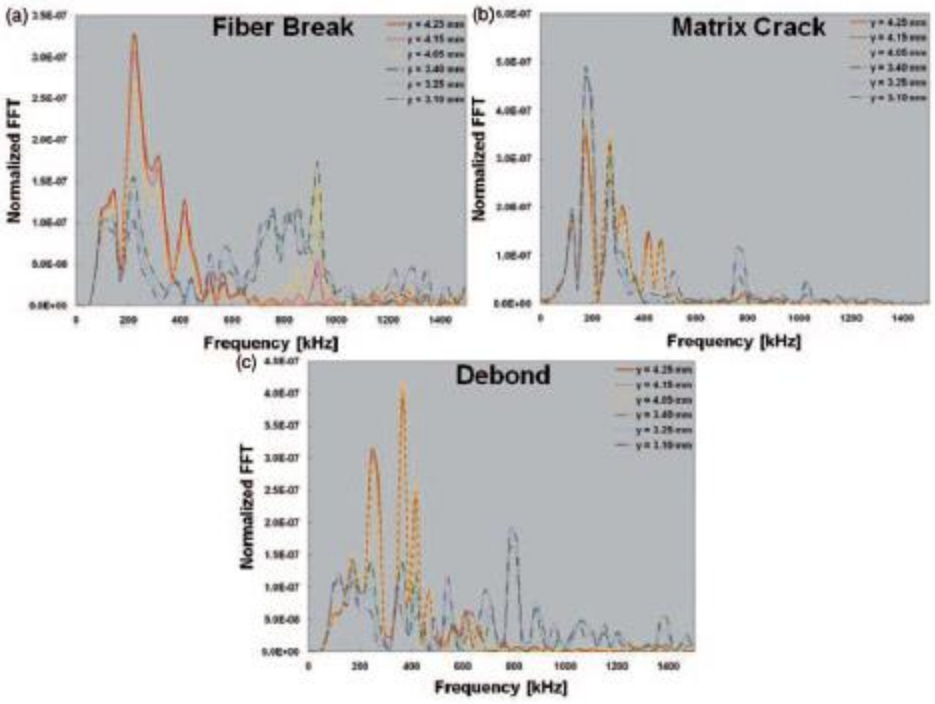

Figure 22: Experimental Waveforms, Burks, Frequency Domain

Source: (B. K. Burks 2013)

These events were shown to have large amounts of energy content between 100 and 300 kHz for every damage mechanism. These results in the time domain also show the impact of source depth, with obvious amplitude effect as the source moves further into the composite (y distance is from rod center). Post processing, a comparison of damage mechanisms was examined by analyzing their Peak Power (PP) (see Figure 23).

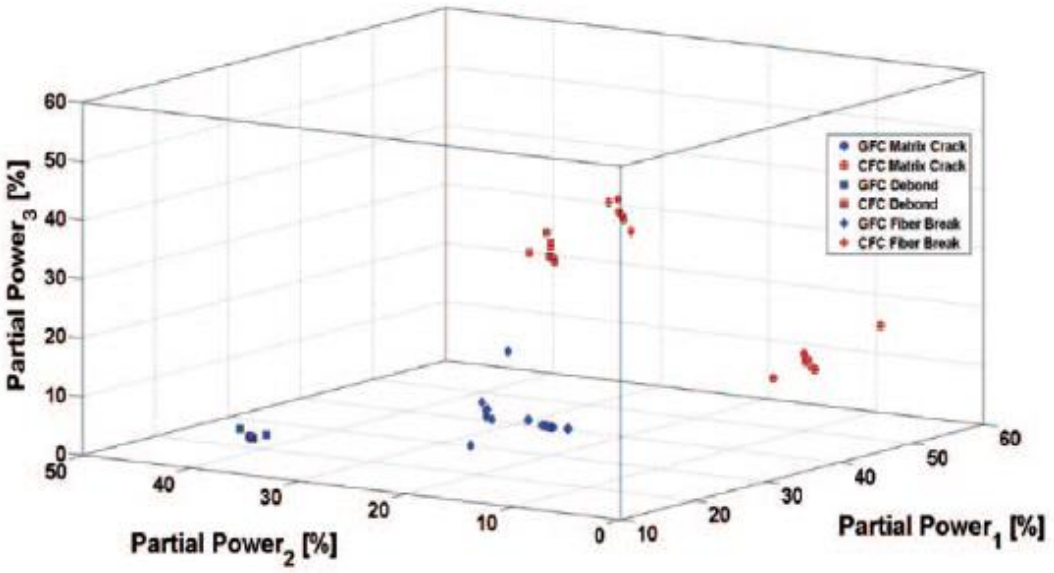

Figure 23: PP Comparison by Damage Mechanism and Fiber Type

Source: (B. K. Burks 2013)

Burks found that three-dimensional FEA modeling is capable of distinguishing between damage mechanisms in rod type geometry. These methods will be expanded upon for the purposes of this research.

2. METHODOLOGY

Since the primary experiment began off of the work of Megel et al, and the fixture was property of the University of Denver, it became the starting point for the experimental design. The previous fixture (see Figure 4) was designed for 4 point bend testing, however improvements could be made.

The most important design features for a 4 point bend test are the loading pins. Previous loading pins had loose tolerances on span width, allowing samples to move side to side and preventing reliable sample placement. This bend point thickness was modified by fabricating from aluminum blocks new loading pins, with ¼" dowel pins press fit into them. These loading pins were fixed to the base plate with an alternating dowel pin and threaded holes, allowing pins to be press fit into it, and it to be bolted into the loading pins through the base plate (see Figure 24).

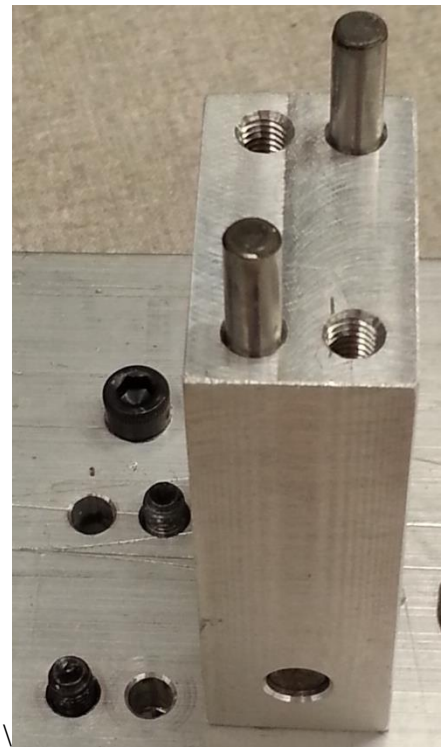

Figure 24: Loading Pins

The fixture also relies on separating top and bottom pieces, with the top piece containing the load pins, and the bottom piece acting as a sturdy base. The base has 2 guide pins which ensure alignment with the top piece via two bearings. Previous bearings were sleeve bearings and previous guide pins were loose and bolted on. These were replaced with high quality, press fit ball bearings and high quality steel, threaded guide pins. These guide pins were threaded into a newly fabricated aluminum base plate. The new base plate was ½" rather than the previous ¼", but with identical dimensions to comply with ASTM standards for 4 point bend tests. These new pieces proved to provide much more evenly distributed load with little to no frictional resistance.

Load was placed on a weight centering pin which attaches to the top fixture piece. Previous loads were applied approximately by adding 1 and 2lb weights. This method was found to be too approximate and cumbersome, so the weight centering pin was still utilized, but a single steel block was machined to load and used; this lead to more accurate loading and an easier test setup process.

Previous acid tank design involved an acrylic tank, which was found along with the fixture, but promptly broke during initial testing. This tank was critical to introducing acid to the samples while not putting additional notable stresses. Initial redesigns involved slotting an acrylic tank and sealing the slots from the outside with silicon. While this kept acid from leaking during testing, it allowed acid into the walls, which proved to cause damage not intended by breaking composites at the tank/sample interface. This design was ultimately replaced by a two part acrylic tank which could be sealed in two phases, first with the top open under the specimen lip and second up the sides and on top of the specimen. This proved to keep acid out of the points where the sample touched the acrylic.

Sensor attachment was placed on the ends of samples via superglue, but this was determined too high risk for the sensor damage and it was believed that increased sensitivity could be achieved by placing sensor faces parallel to fiber direction on the tension side between the loading pins. In order to determine appropriate gain for these particular sensors, gain was increased until ambient electronic noise caused triggering, then gain was backed off 6dB. This lead to an eventual gain of + 72dB, which by most

accounts of MAE, is considered quite sensitive, however, for the test of attempting to capture individual fiber breaks or small matrix cracks such sensitivity was necessary.

Along with this new placement, new sensor holders were designed for more repeatable placement and pressure. Rubber banding a backer plate to sensors was experimented with, but ultimately discarded for rapid prototype (RP) sensor holders which slid onto the samples (see Figure 25). All other aspects of the fixture were left as previous design dictated. A complete Solidworks assembly of the new fixture was created for visual representation (see Figure 26).

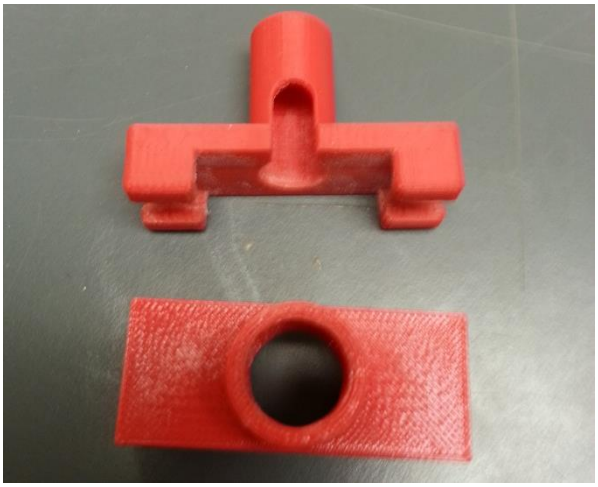

Figure 25: Sensor holders

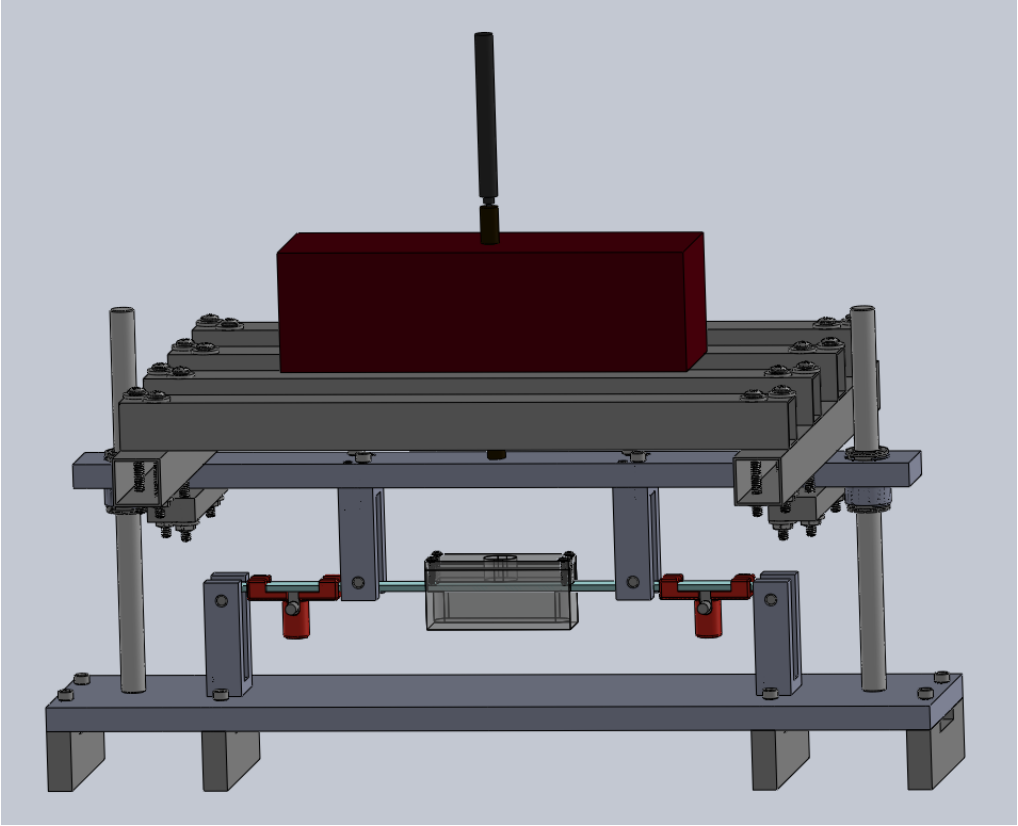

Figure 26: New Fixture Design

Implementation of safety procedures was important for the longevity of the test and protection of the tester. This involved proper personal protective equipment (PPE) and procedures for handling spills.

The following equipment was used: Noxious fume mask, goggles, chemical resistant gloves, chemical resistant jump suit, funnel, High Density Polyethylene (HDPE) squeeze bottle, washing bin, and Sodium Bicarbonate. The safety equipment was used during any portion of the test where acid was present. The funnel and squeeze bottle were used to easily add acid to the tank after loading. The test was done in this order to prevent a violent shaking of acid which could occur if acid was added before loading. Sodium

Bicarbonate was used any time a spill occurred and also to neutralize used materials before they were rinsed and stored for the next test. A mask was worn at all times for redundancy, as the tank was designed with only a small opening to prevent noxious fumes from propagating far from the sample.

This procedure was adhered to for every test, and met University standards for hazardous materials.

2.1 Materials Tested

The following seven PMCs were tested, which were classified by weight percent fibers:

Glasforms	Epoxy E-glass
1A	Vinylester Epoxy ECR-glass 1, 75% glass
3A	Vinylester Epoxy E-glass 1, 75% glass
4B	Vinylester Epoxy ECR-glass 2, 80% Glass
5	Polyester E-glass 1,
9	Epoxy E-glass 1,
11	Proprietary Material ECR-glass 2

The MPS composites were made by pultrusion and supplied to the project by MacLean Power Systems.

Glasforms samples were available from University of Denver. Each specimen was machined to 3.2 mm thick, 12.7 mm wide and 304.8 mm long. (Megel 2001) Each sample had one width-length face not machined, with this face being put in tension during the experiment. Samples were then incased in an acrylic, two piece case on a 3 inch section of the sample in the center. This case was sealed from above and below with silicone to ensure an acid proof boundary on the gauge section. In addition, the machined surfaces within the acrylic case were coated with petroleum jelly to prevent acid attacks on those particular surfaces.

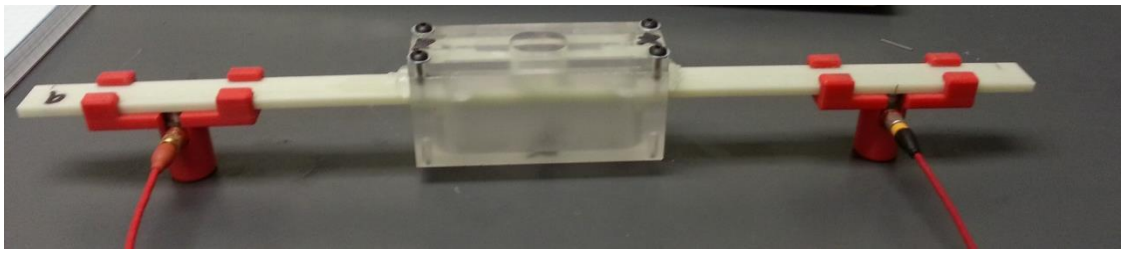

Figure 27: Prepped Sample

Sensors chosen for this test were Mistras CM-204S/R 90 degree broadband sensors. These sensors have adequate frequency response for composite materials monitoring, approximately 100kHz to 1500kHz.Custom sensor holders were designed and printed out of ABS plastic using a 3-D printer. Each holder has a spring behind the sensor and lips to mount the sensor. Each sensor face was coated with couplant to acoustically couple the MAE transducer to the test specimen surface, and slid into position halfway in-between the inner and outer load pins on each side of the sample. The sensor face was placed on the tension side (see Figure 27). The tension side was chosen over the compression side due to cracks only expanding in tension. Choosing this placement instead of perpendicular to fiber direction at the ends of the samples allows for more consistent signal acquisition due to less attenuation. These sensor holders ensured consistent sensor placement as well as equal and consistent pressure on the sensors.

2.2 Testing Procedure

After the tank was affixed and the sensors were in place, a pencil lead break was done on each width-thickness side of the sample to ensure the sensors were working and coupled properly. (ASTM Standard E2374-10 5.1) This test was done with the same acquisition settings as the full test and was saved for post-test analysis if necessary to determine proper coupling and sensor settings.

After the pencil lead break was completed, the sample was loaded to 83.97N (Megel 2001) and the LVDT set. This load generated an axial stress along the fibers of 134 MPa which corresponds to 26.7kN applied to a 16 mm diameter composite insulator in-service. Pencil lead breaks were again performed to ensure that loading had not caused a decoupling of the sensors to the sample. At this point Personal Protective Equipment (PPE) was donned and acid was added to the tank until the sample was submerged. For the majority of tests the acid used was 0.063N Nitric acid. (Megel 2001) For one test 1N Nitric acid was used to explore the effect of acid strength on results.

Upon completion of adding acid, the data acquisition was initiated on WaveExplorer and acoustic monitoring began.

Figure 28: Running test

2.3 Post-Test Procedure

After completion of the test, sensors were removed, the tank cleaned, and the sample was cut, cleaned and prepped for microscopy. Surface characterization of the specimens (matrix and fibers) was analyzed using a JEOL model JSM 5800 LV Scanning Electron Microscope (SEM) and an optical Olympus BX51M microscope. All the specimens were previously prepared and mounted using conventional procedures for electron and optical microscope observations. All microscopy, including procedure, results and images were done by Dr. Euripides Solis-Ramos.

2.3.1 Surface Characterization

To verify stress corrosion cracking of the fibers and their susceptibility to the corresponding testing condition, morphological surface characterization of the samples were conducted by microscopy techniques before and after of each test. The analysis of microscopic images is allowed to present and discuss a reasonable comparison of the degree of degradation of the composites and particularly of stress corrosion cracking on the fibers. Since this characterization falls under separate research conducted by Dr. Euripides Solis-Ramos, only pre and post-test images are shown to illuminate surface damage from SCC.

2.3.2 Signal Processing

For signal processing, the waveforms recorded by WaveExplorer were individually exported, along with event vs. time data and parametric data. These signals were then processed by a custom Matlab code. Electromagnetic interference (EMI) is inevitable when making MAE measurements at such high gains. These signals were determined to

be signals whose peak amplitude occurs simultaneously on each sensor, as well as having any observable mechanical dispersion. EMI signals were isolated, and ignored.

Pre-trigger data should be very flat, indicating that the sensors are on, but not displacing until the damage mechanism wave hits. When pre-trigger energy (PTE) is loud, it can increase the amplitude of signals, causing false triggers of events (see Figure 29). The level of acceptable PTE was determined to be $> 0.2V^2\mu s$.

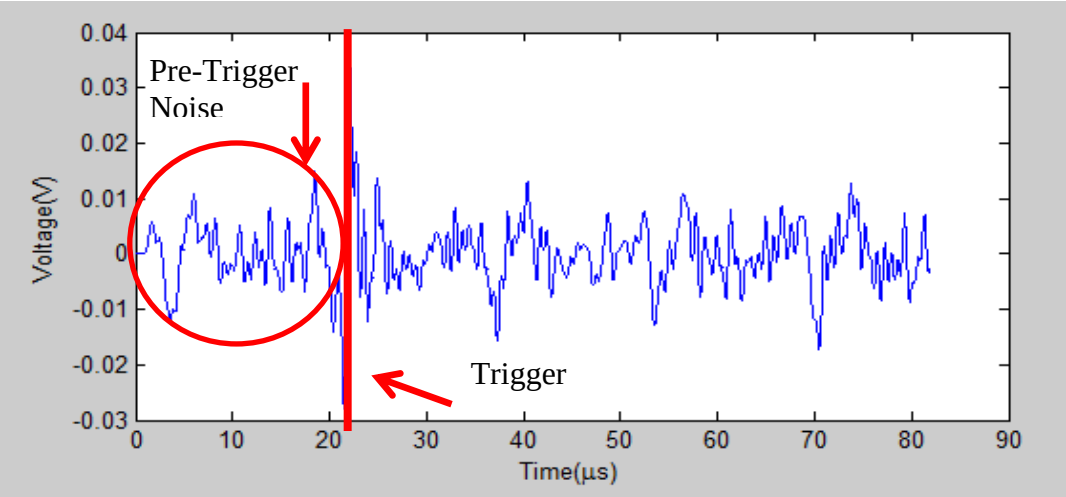

Figure 29:PTE

Each signal was passed through a high pass 4 pole Butterworth filter of 100 kHz and a low pass 14 pole Chebyshev filter of 1500 kHz. These filters were established by doing a pole and filter study to determine how to properly filter out signals greater than 1500kHz. Initially a Butterworth filter with 4 poles was attempted for both high and low pass. High pass filter was accurately cutting frequencies below 100kHz but the low pass was not. As a test, an impulse signal was used on poles on the high pass were increased to determine effectiveness at cutting frequencies over 1500kHz (see Figure 30). When it

became apparent that the number of poles was not effective enough, a Chebyshev filter was tested in the same manner (see Figure 31).

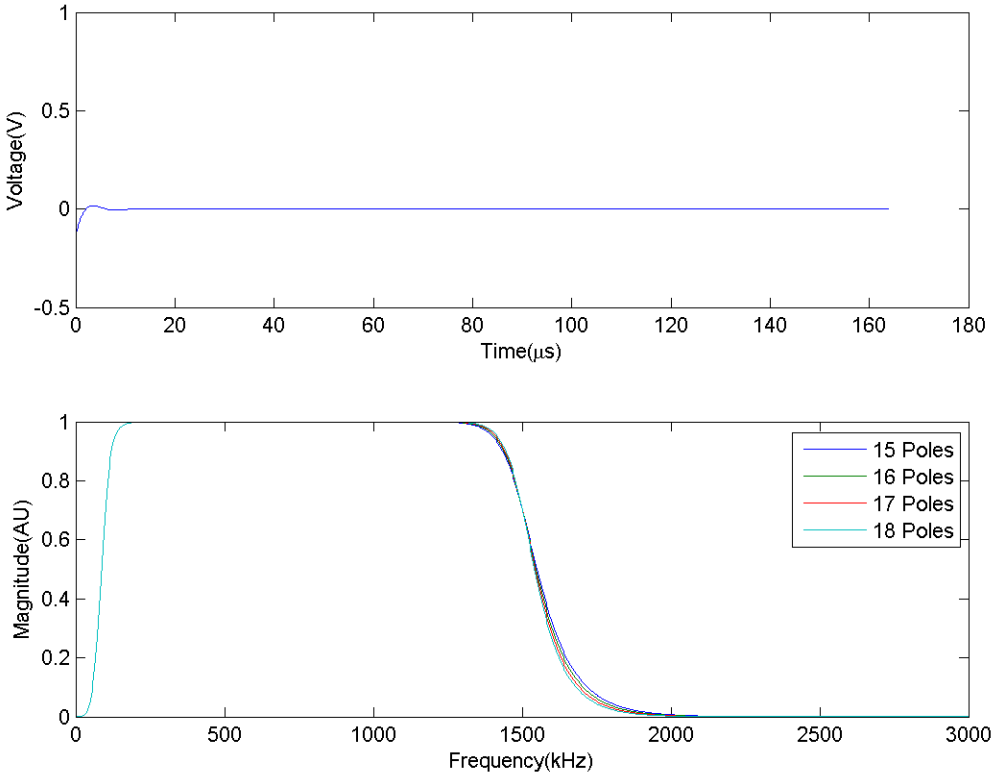

Figure 30: Butterworth HP Filter Test Signal, Pole Study

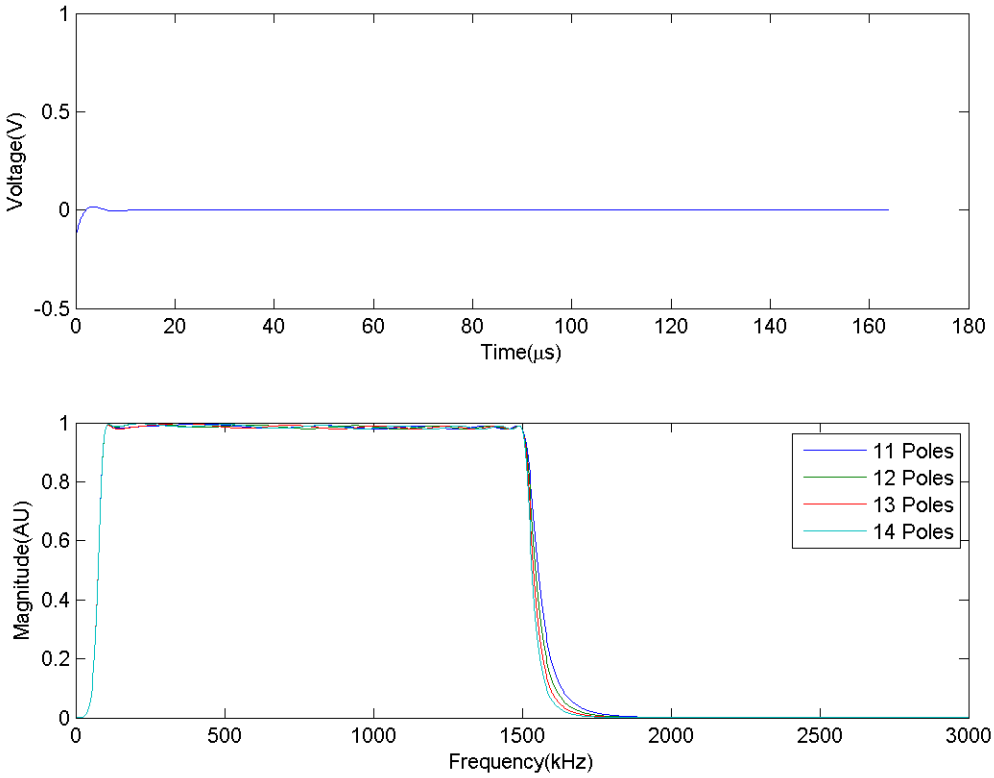

Figure 31: Chebyshev HP Filter Test Signal, Pole Study

This new filter had adequate high range frequency cut off, so a test signal was used to determine effect on the time and frequency domain. The signal showed significant improvement in both cut off frequency filtering (see Figure 32) but also in the cleaning of errant noise in the signals (see Figure 33 and Figure 34).

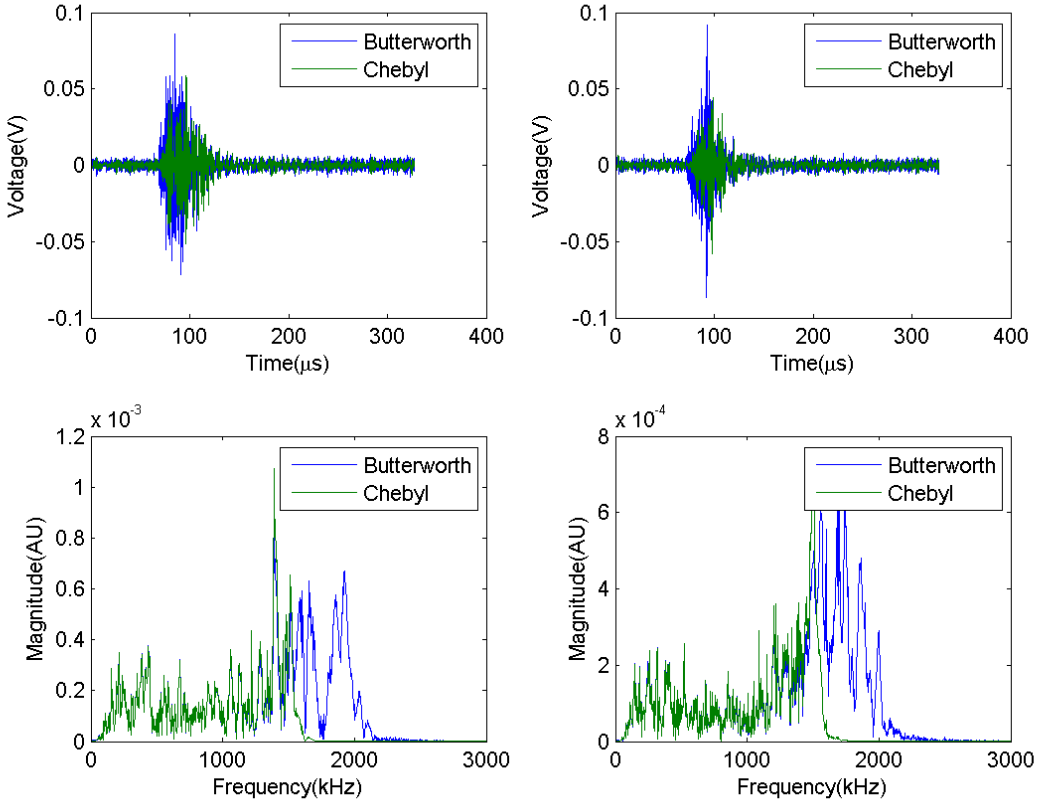

Figure 32: Filtering Test Comparison, Time and Frequency Domain

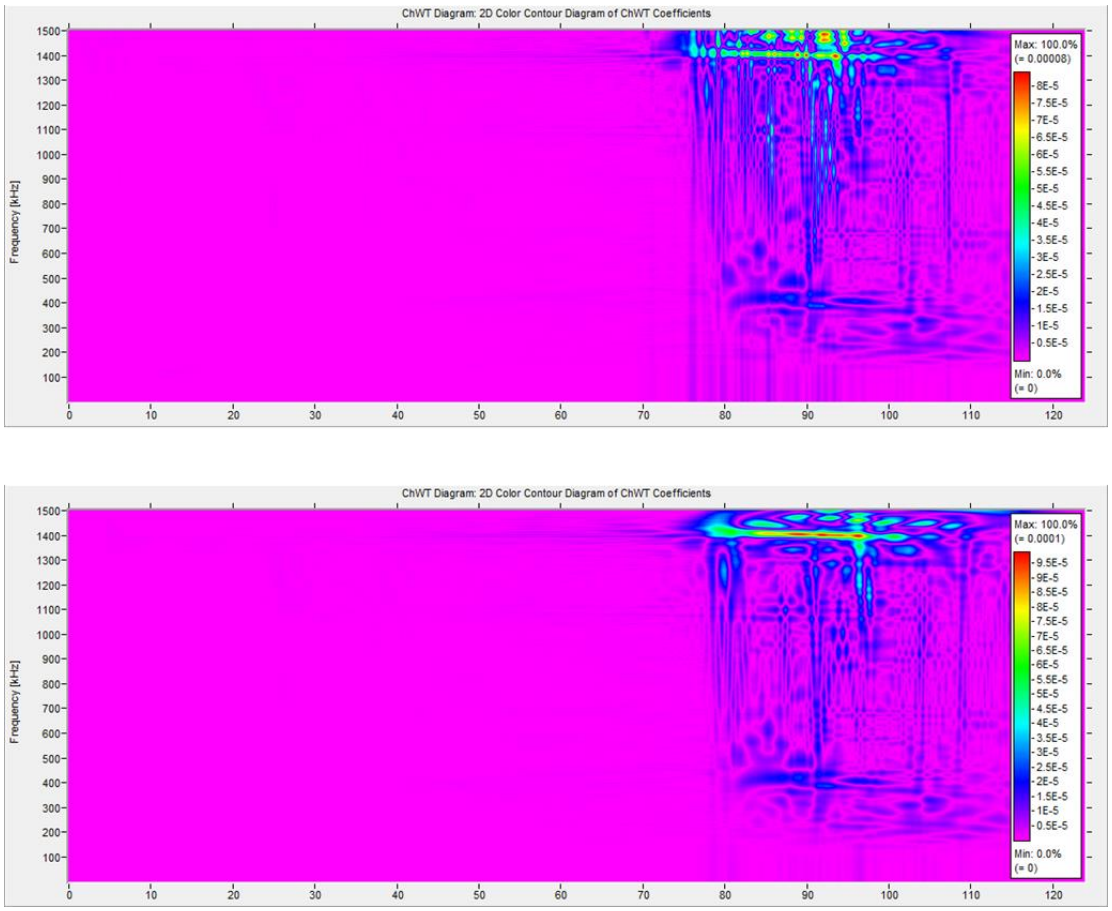

Figure 33: Butterworth HP Filtering, CWD

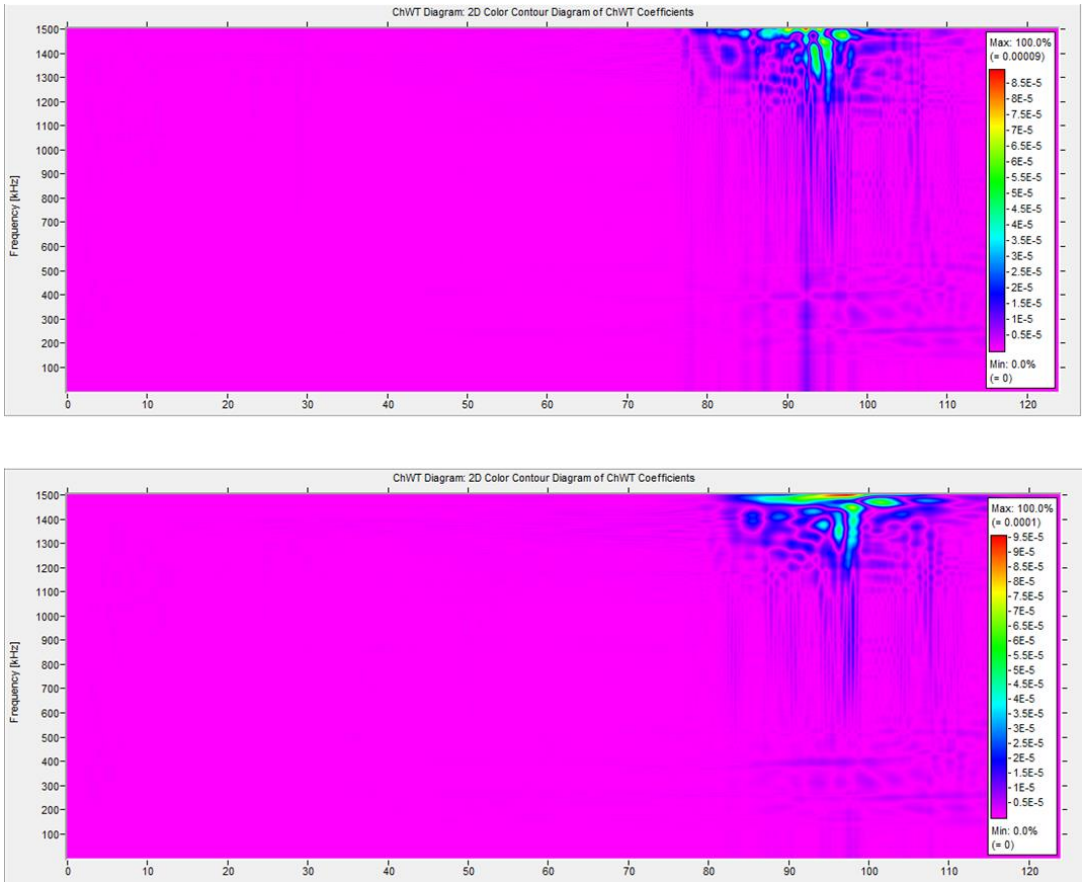

Figure 34: Chebyshev Filtering, CWD

After filtering the data, the spectral content of the waveforms was evaluated in the frequency domain via a Fast Fourier Transform (FFT). This data was paired with the signal in the time domain and saved in an image as well as a comparison between both channels in the frequency domain.

Calculations were also done on the data to determine the PP and the weighted peak frequency (WPF) for each signal (equations 1 and 2). WPF determines the scaled centroid of a spectrum, while PP determines the area under the spectrum curve for a given frequency range divided by the total area under the spectrum curve. These metrics

provide a means of showing the natural clustering of different source mechanisms in the frequency domain when wave propagation effects are taken into account. PP had bounds of 500, 0, 1500, and 700 kHz for f1, f2, f3, and f4 respectively. This data was compiled for each test and graphed (see Figure 35).

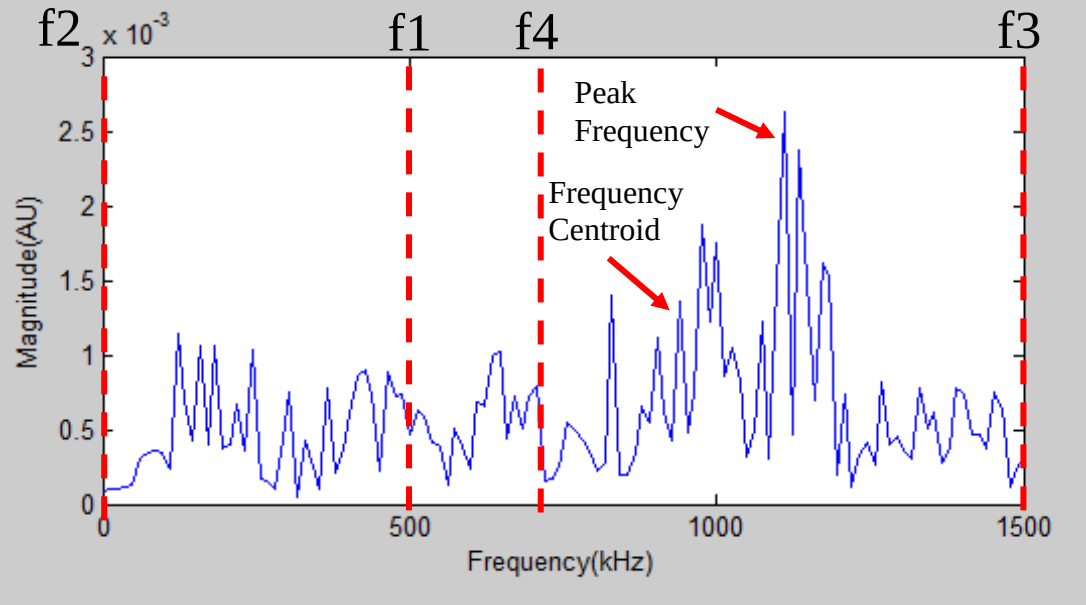

Figure 35: PP and WPF Example

$$\boldsymbol{WPF} = \sqrt{\boldsymbol{f_{max}} \cdot \boldsymbol{f_{centroid}}} \quad (1)$$

f_{max} = Frequency position of the maximum amplitude of the spectrum

$$f_{centroid} = \frac{\int \boldsymbol{f} \cdot \widehat{\boldsymbol{U}}(\boldsymbol{f})\boldsymbol{df}}{\int \widehat{\boldsymbol{U}}(\boldsymbol{f})\boldsymbol{df}}$$

$U(t)$ = Waveform in the Time domain

$\widehat{U}(f)$ = Fast Fourier − Transformation of U(t)

f = Frequency

$$\boldsymbol{PP} = \frac{\int_{f_1}^{f_4} \widehat{\boldsymbol{U}}^2(\boldsymbol{f})\boldsymbol{df}}{\int_{f_2}^{f_3} \widehat{\boldsymbol{U}}^2(\boldsymbol{f})\boldsymbol{df}} \quad (2)$$

2.3.3 Source Location

In order to link potential signal clustering with damage mechanisms, a technique had to be used to locate the experimental signals with a source location. This technique would show that the mechanism claimed by PP vs. WPF plots is, in fact, the damage observed by microscopy.

Typical source location for MAE events requires at least 3 sensors to triangulate the signal in 3D and uses only peak amplitudes. This methodology usually involves taking the peak amplitude of signals in the time domain and using that arrival time to determine the source location as sensors are placed at varying distance from the source mechanism. This is usually done by setting an amplitude threshold and using the time when the wave crosses this threshold for both sensors. The difference in this time was the arrival time. This was determined to be inferior to frequency based location due to the ability to isolate said frequency so that attenuation of higher frequency waves in larger plates could be negated. (Ziola 1991)

For this experiment, only 2 sensors were used, which requires a linear source location methodology. Since the sensors are placed on the tension surface, expected damage is also expected on the tension surface, and sample width is small relative to length, this assumption should be valid.

CWDs also have the ability to show strong modal differences. CWDs show the signal in the time domain, with amplitude vs. time, as well as a secondary plot which shows the frequency domain, with frequency vs time and amplitude color coded. This, along with dispersion curves, shows clear modal content. Since different damage

mechanisms are believed to have different modal wave makeup, these CWDs can be used in combination with PP vs. WPF data to differentiate between different signal types (or equivalently source mechanisms) (see Figure 11).

In order to obtain accurate source locations and wave content, a methodology of obtaining wave speed at peak frequencies rather than amplitudes, and analyzing CWDs was used. (M. Hamstad 2014) In order to obtain group velocities, PLBs were done on a glass fiber composite specimen with sensors at known distances of 6" and 9". These pencil lead breaks were then transformed and their CWDs examined. In these CWDs the peak amplitude in frequency was observed for both channels. Since this frequency is representative of a specific part of the wave, arrival at both sensors is staggered based on their distance. This frequency was used to determine an arrival time for each sensor, and with distances being known, a wave velocity was calculated. Experimental data was then examined in the same manner, to determine peak frequencies for both channels, and with a known velocity, used to determine source distance from sensor location. (M. A. Hamstad 2012)

2.4 Modeling

Modeling was used to link MAE signals with damage mechanisms. The model simulates the composite samples by entering in material properties and MAE data for unidirectional composites. The composite sample was built in HyperMesh, and meshed with all hexahedral elements. The model requires a very fine mesh, with 20 linear elements per shortest wavelength for a converged solution (M. A. Hamstad 1994). The high end of the observed frequencies is 1500 kHz with group velocities at approximately 2mm/μs. For this case elements have to be <=100 μm to capture desired data (see Figure 36 -Figure 38).

Figure 36: Mesh

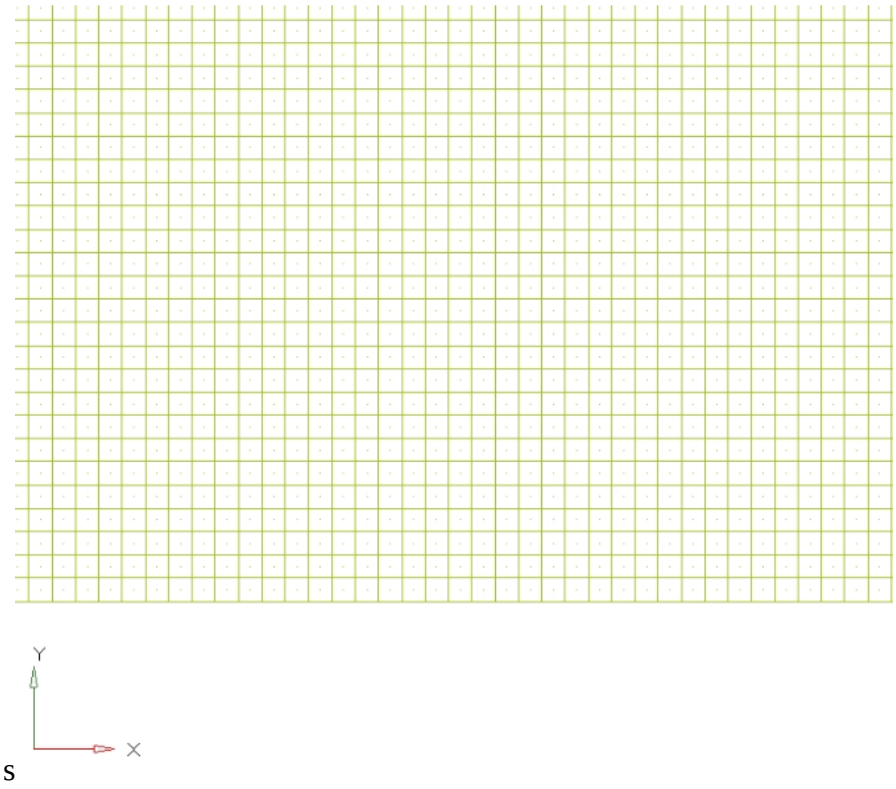

Figure 37: Mesh, close up

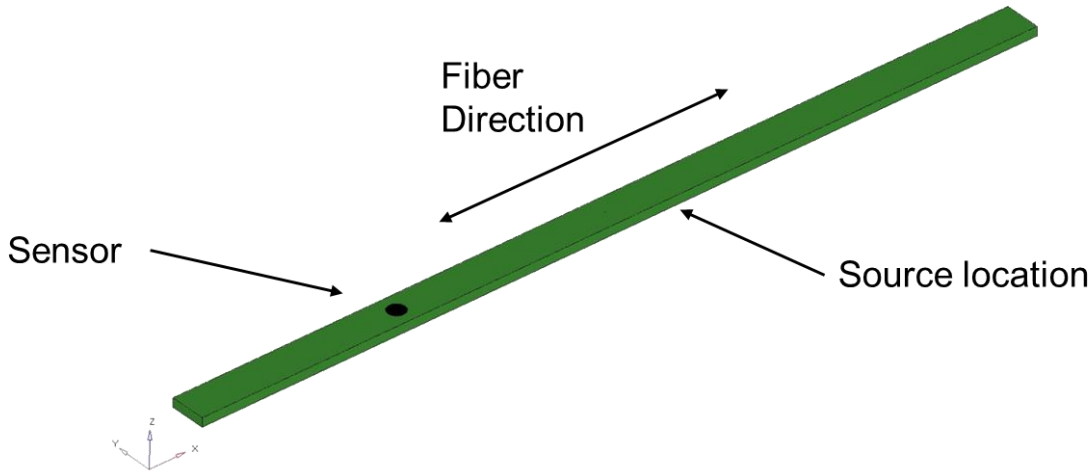

Figure 38: Model setup

Damage/fracture mechanics shows that energy release is preferential in unidirectional composites, where fiber fracture results in an energy release in the fiber direction, matrix splitting releases energy perpendicular to the fiber direction and debonding is a combination of the two. For the purposes of this model, this information was used to apply loads in the directions of preferential energy release based on the damage mechanism; source aligned with fibers for a fiber break, and source transverse to the fibers for matrix splitting (see Figure 39).

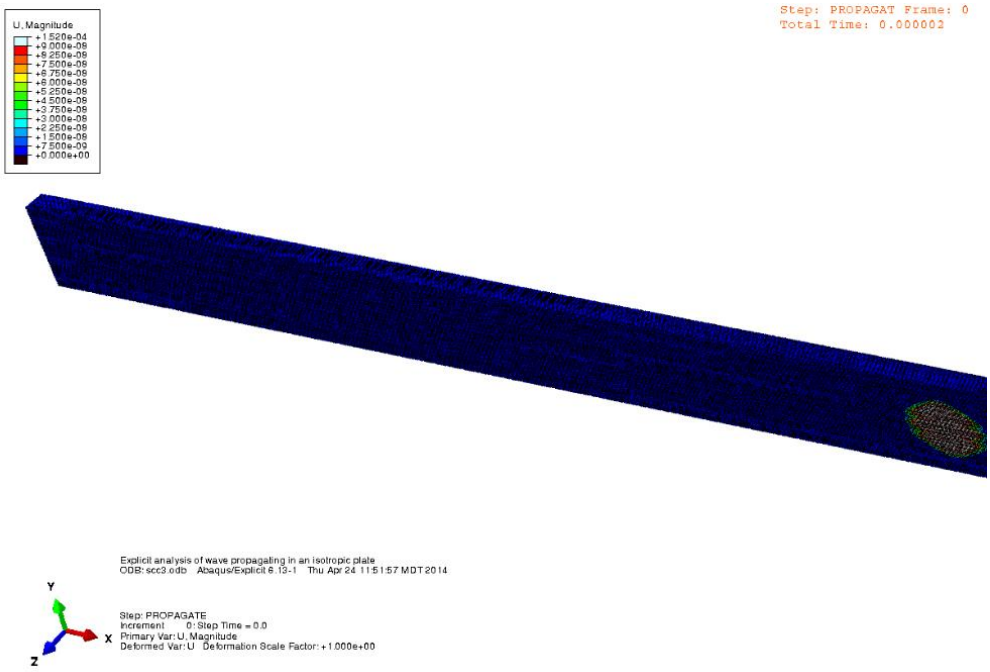

Figure 39: Matrix Crack Simulation Animation Snapshot

Simulations are run as an explicit model with dynamic loading to excite the source mechanism, and then stepped forward in time to account for stress wave propagation. The aperture effect matters in this case, and is taken into account by numerically integrating the displacement or velocity at all nodes in the sensor region of the model.

An example signal for a matrix crack shows the amplitude wash out of the signal and a visualization of the sensor area shows how a single node velocity will not capture the full, realistic signal as the sensor face experimentally will (see Figure 40 and Figure 41).

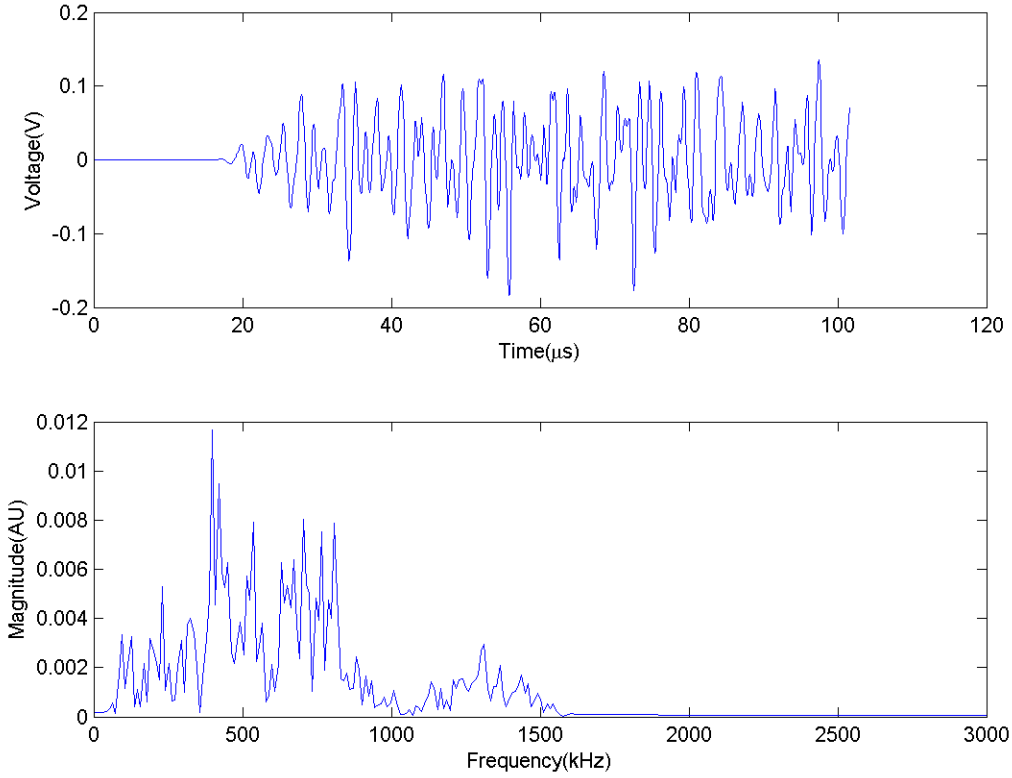

Figure 40: Waveform, Matrix Crack, 1550ns Rise Time, Sensor Node

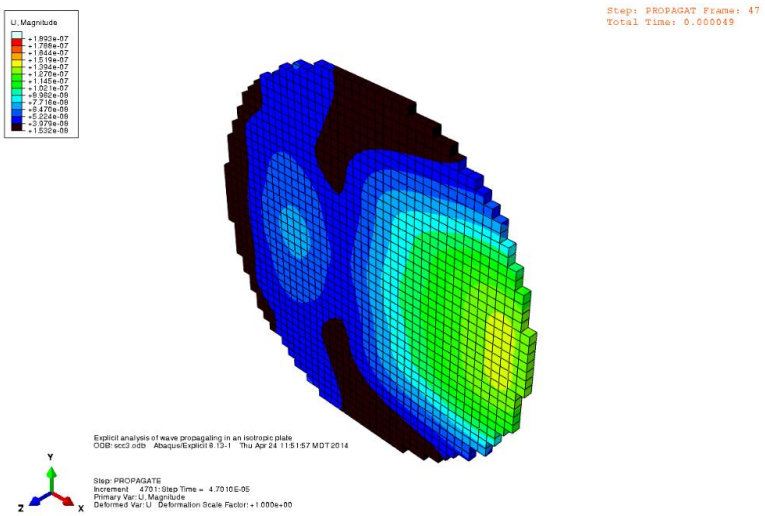

Figure 41: Sensor Face, Matrix Crack, 1550ns Rise Time

In order to simulate fiber breaks and matrix cracks properly, rise times must be calculated. In this work, the rise time is defined as the total time taken for the excitation of a given damage mechanism. This rise time is effected by material properties and total size of the crack. For fiber breaks, crack length was determined to be the fiber diameter, and for matrix cracking the length was taken as an average of observed length based on material from microscopy.

Calculations were done using two methods, which calculate the Rayleigh wave speed, the theoretical upper limit at which a propagation crack may run. (B. Burks 2013) The most precise method is done by calculating longitudinal and shear wave velocities, C_L and C_S, using the stiffness matrix for a given material, resulting in Rayleigh Wave Speed, C_R (equation 3). (Gilson 2008) The approximate result can be obtained by calculatingV_R, which gives the knockdown percentage used to multiply shear wave velocity by to solve for C_R (equation 4). (Pichugin 2006)

$$\left(\frac{C_R}{C_S}\right)^2 * \left\{\frac{{C_R}^6}{{C_S}^6} - \frac{8{C_R}^4}{{C_S}^4} + {C_R}^2\left(\frac{24}{{C_S}^2} - \frac{16}{{C_L}^2}\right) - 16\left(1 - \frac{{C_S}^2}{{C_L}^2}\right)\right\} = 0 \quad (3)$$

$$C_L = \sqrt{\frac{C_{11}}{\rho}}$$

$$C_S = \sqrt{\frac{C_{44}}{\rho}}$$

$$V_r = \frac{0.87+1.12v}{1+v} \quad (4)$$

v = Poisson's Ratio

These calculations were based on the well determined published values for each matrix material (see Table 1), and yielded maximum Rise Times for each event type (see Table 2).

Table 1: Matrix Material Properties

Material	Young's Modulus (GPa)	Poisson's Ratio	Density (g/cm^3)
Epoxy	1.500	0.350	1.250
Vinyl Ester	2.675	0.358	1.495
Polyester	1.000	0.370	1.700

Table 2: Rise Time

Material	Calculated Rayleigh Wave Speed (km/s)	Crack Length (μm)	Rise Time (ns)
Glass Fiber	2.80-3.10	12.50	2.0-4.0
Epoxy	0.62	14.82	23.79
Vinyl Ester	0.76	21.83	28.73
Polyester	0.43	20.05	46.13

These Rise Times represent the fastest possible wave speed, a speed that is not reasonable for practical application. It should also be noted that fiber break theoretical rise times are an order of magnitude faster than for matrix cracking. This script used has a rise time range of 0.1μs – 2μs for the fiber break, and 1-2μs for matrix cracking, values determined to be adequately larger than calculated rise times as were observed experimentally by others. (Gorman, Modal AE Analysis of Fracture and Failure in Composite Materials, And the Quality and Life of High Pressure Composite Pressure Vessels 2011) These conditions have different amplitude cards, which were created by running a Matlab script to represent rise times used.

The wave content of the simulated signal were processed in the same manner as the experimental signals were, by taking it to the frequency domain and examining the spectral content. This data gives much insight into where each mechanism falls on the spectrum, thus allowing for a linking of MAE data to particular damage mechanisms. This data was then compared to SEM imaging to confirm the results.

Since true rise times are more range based estimates rather than known certainties, this model is meant to be forward predictive while still operating within the reasonable ranges calculated numerically and postulated by previous MAE work. Results from this model will give a more accurate Rise Time range for the specific materials used.

This model was also run with variance in source location (0.15”closer and further away source from sensor location). This was done by changing the location of the source to alternate node sets. Additionally the model was run for varying material properties, with the variables being fiber type, matrix material and volume fiber fraction. For the purposes of this model, fibers used were E-glass and ECR. Matrix material was Epoxy and the proprietary material. Volume fiber fraction was 60% and 70%. Both of these model types were run individually, with only a single variable for each set to determine dependency of the model to those characteristics. This was done for both the matrix crack and fiber break simulations.

3. RESULTS

Presented are all results from SCC testing, 3 Point bend testing, Microscopy, and Modeling.

3.1 Results from SCC Testing

3.1.1 Events vs. Time

Event vs. time data was exported directly from the WaveExplorer software that notes the time in the test when each event happened and logs this for the duration of the test. Results for the Glasform's data are shown in Figure 42.

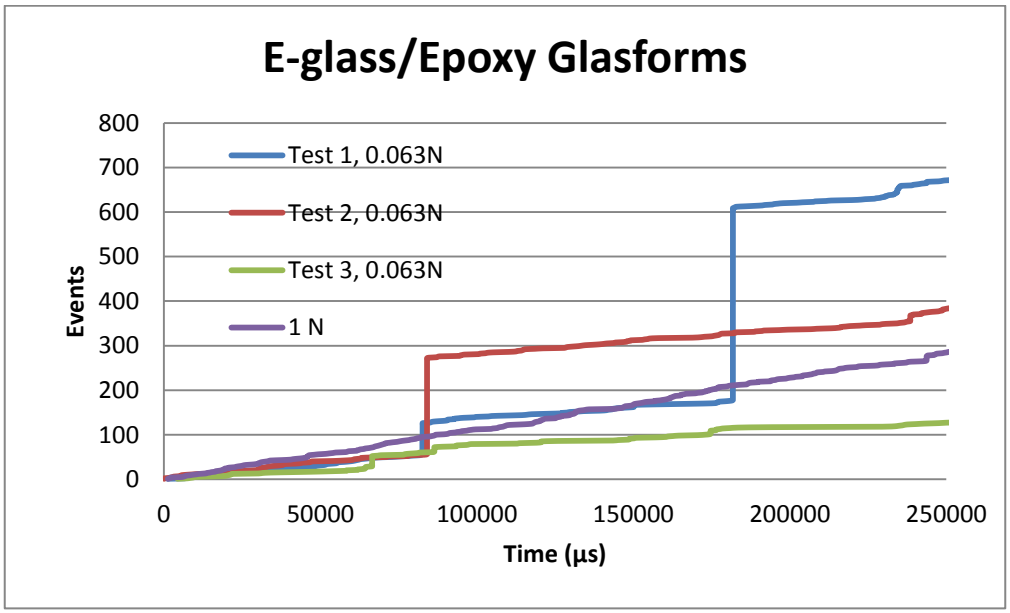

Figure 42: Glasforms Events vs. Time curves

Tests 1, 2, and 3 have event counts of 672, 446 and 132 respectively while the 1N test had an event total of 290. This data includes EMI data, which had to be filtered out using Matlab. Total event total after filtering can be seen in Table 3, filtering techniques can be seen in section 2.3.2.

Events vs. time for MPS samples can be seen in Figure 43 and Figure 44. Tests on E-glass samples #3A(2), #5(3), and #9(2) had event totals of (12, 93), (442, 40, 92), and (27, 32) respectively before filtering out EMI. Tests on ECR samples #1A, #4B and #11 had totals of 1220, 8831, and 3868 respectively before filtering out EMI. Due to time constraints, #4B and #11 had only 1000 signals each processed and the totals were extrapolated for the full set. This data contains mostly non-event signals as it was determined post-test that cables were damaged. Adjusted totals can be seen in Table 3 for all of these tests. Sample 11 was filtered twice, once with the previously mentioned EMI filter, and again by filtering out signals whose PTE exceeded a value of $0.2\frac{V^2}{\mu s}$, indicating a false trigger. Only a forward modeling finite element approach along with accurate source location and microscopy observations at these locations can confirm what these events relate to.

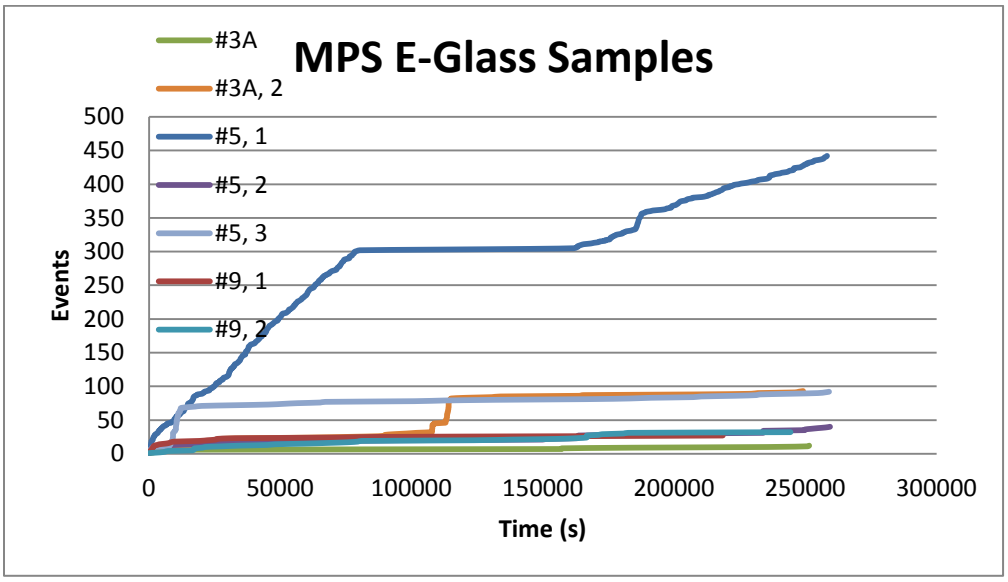

Figure 43: MPS specimens Events vs. Time behavior

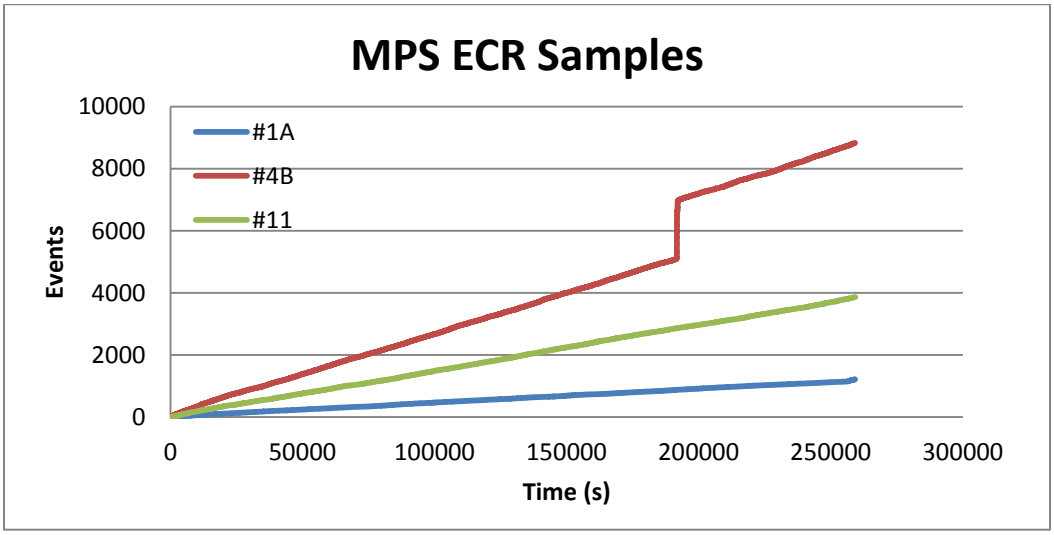

Figure 44: MPS ECR specimens Events vs. Time behavior

Table 3: Events vs. Time Counts

Sample Manufacturer	Sample type	Acid Type	Event Total
MPS	ECR-1/Vinylester	0.063N Nitric	920
MPS	E-Glass/Vinylester(#3A)	0.063N Nitric	11
MPS	E-Glass/Vinylester(#3A) 2	0.063N Nitric	80
MPS	ECR-2/Vinylester (#4B)	0.063N Nitric	5026*
MPS	E-Glass/Polyester (#5)	0.063N Nitric	437
MPS	E-Glass/Polyester (#5) 2	0.063N Nitric	35
MPS	E-Glass/Polyester (#5) 3	0.063N Nitric	77
MPS	E-Glass/Epoxy (#9)	0.063N Nitric	27
MPS	E-Glass/Epoxy (#9) 2	0.063N Nitric	29
MPS	ECR/Proprietary (#11) 1	0.063N Nitric	590*
Glassforms	E-Glass/Epoxy 1	0.063N Nitric	597
Glassforms	E-Glass/Epoxy 2	0.063N Nitric	219
Glassforms	E-Glass/Epoxy 3	0.063N Nitric	110
Glassforms	E-Glass/Epoxy	1N Nitric	201

***- Extrapolated data for entire set from 1000 signals**

The much higher event count for ECR composites was unexpected, as ECR fibers are resistant to SCC. This data set also had a much higher frequency of EMI signals than other samples. The reason for very "noisy" tests is thought to be largely related to degraded/antiquated equipment and limited facilities for MAE work. The noisy environment, which was encountered after moving the test prior to MPS testing, does not lend itself to relevant event vs. time data.

Post testing it was hypothesized that equipment from another experiment, mainly hot plates used to maintain a certain temperature on electronic switches, caused large amounts of EMI. While this kind of large error in event number is not helpful to data sorting, it does not eliminate signal analysis all together.

3.1.2 Wave Velocity

In order to properly source locate, a wave velocity had to be calculated for the composites. PLBs were conducted as described in 2.3.2 using flexural mode as the dominant mode. The CWDs resulted in arrival times of 102.04µs and 131.16µs respectively for Ch1 and Ch2 at 288kHz for 152.4 mm and 228.6 mm (see Figure 45and Figure 46). Using the difference in known distance and arrival times, a velocity of 2616.76m/s was calculated. This number is reasonable with published data. (Giordano 1998)

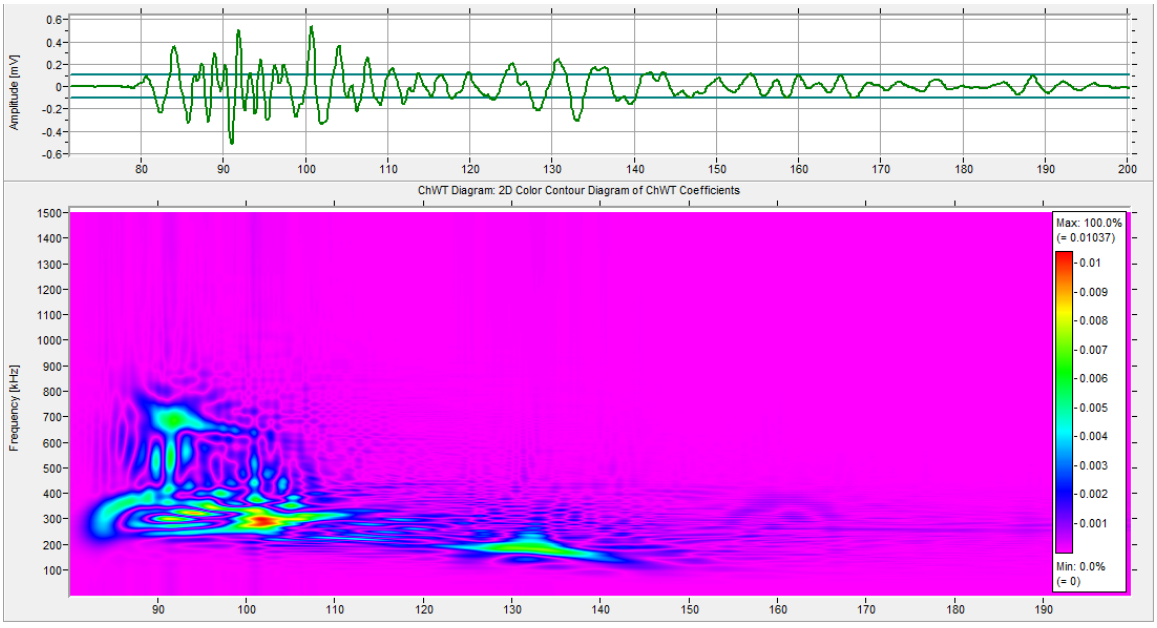

Figure 45: Source Location PLB CWD, Ch1

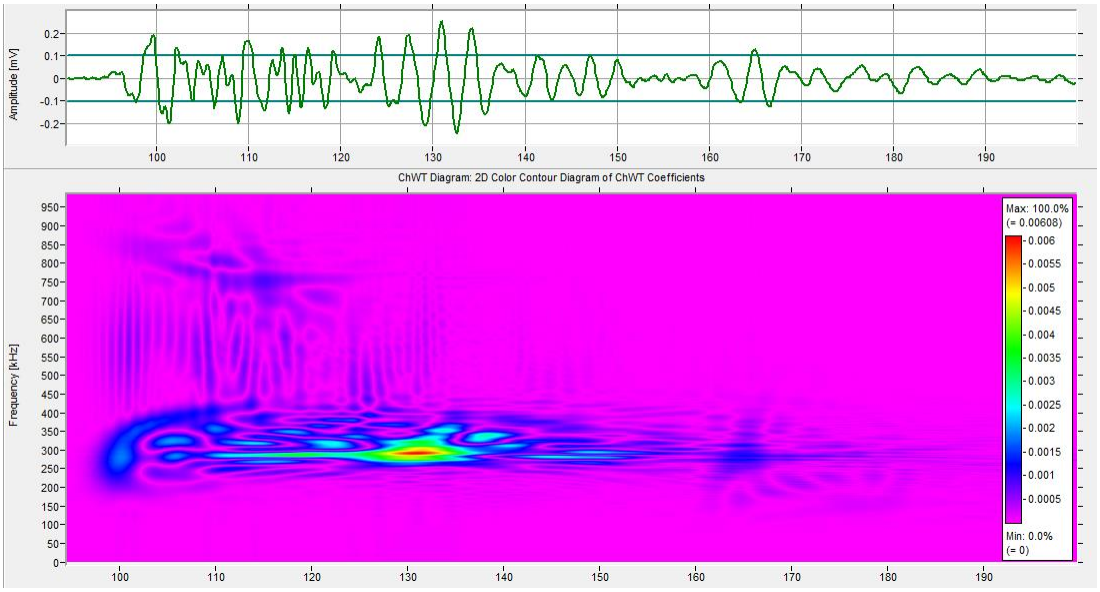

Figure 46: Source Location PLB CWD, Ch2

3.1.3 PP vs. WPF

The primary goal in using MAE on SCC tests was to attempt to classify damage mechanisms by type. Since event vs. time data has shown it is unable to do this, efforts were moved to analyzing the spectral content of waveforms which facilitates the natural clustering of source mechanisms to gain a better understanding of the SCC process. To accomplish this objective, WPF and PP were utilized. The methodology for creating these plots is discussed in 2.3.2.

Clustering for these plots would indicate a repeated event type, giving a range of PP and WPF for which a particular event occurs. The E-Glass/Epoxy composites show very good examples of this clustering (see Figure 47 - Figure 49).

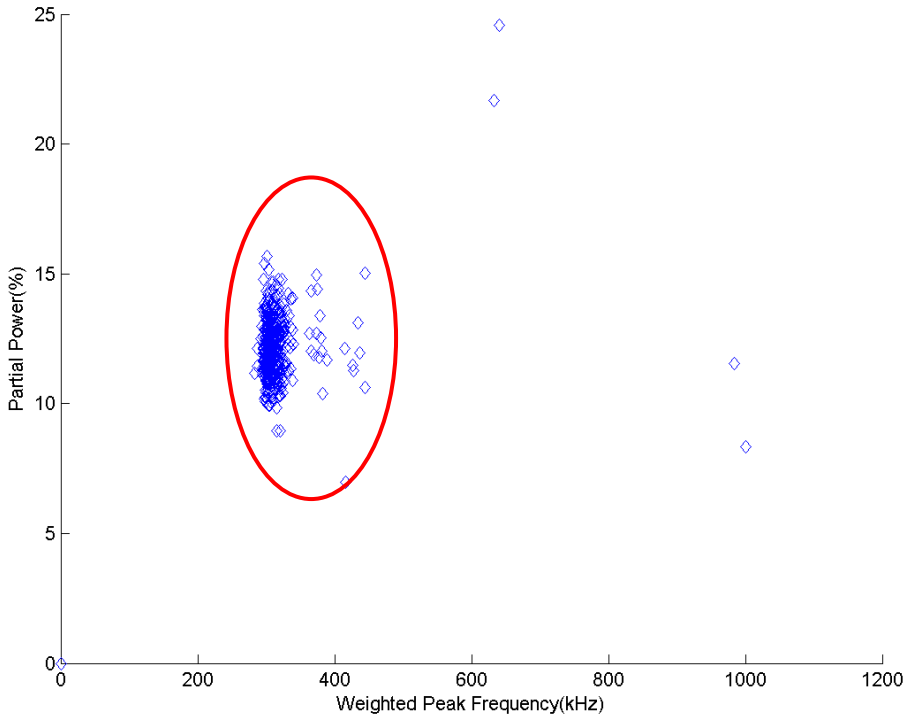

Figure 47: Eglass Epoxy 6/18/13, Ch1

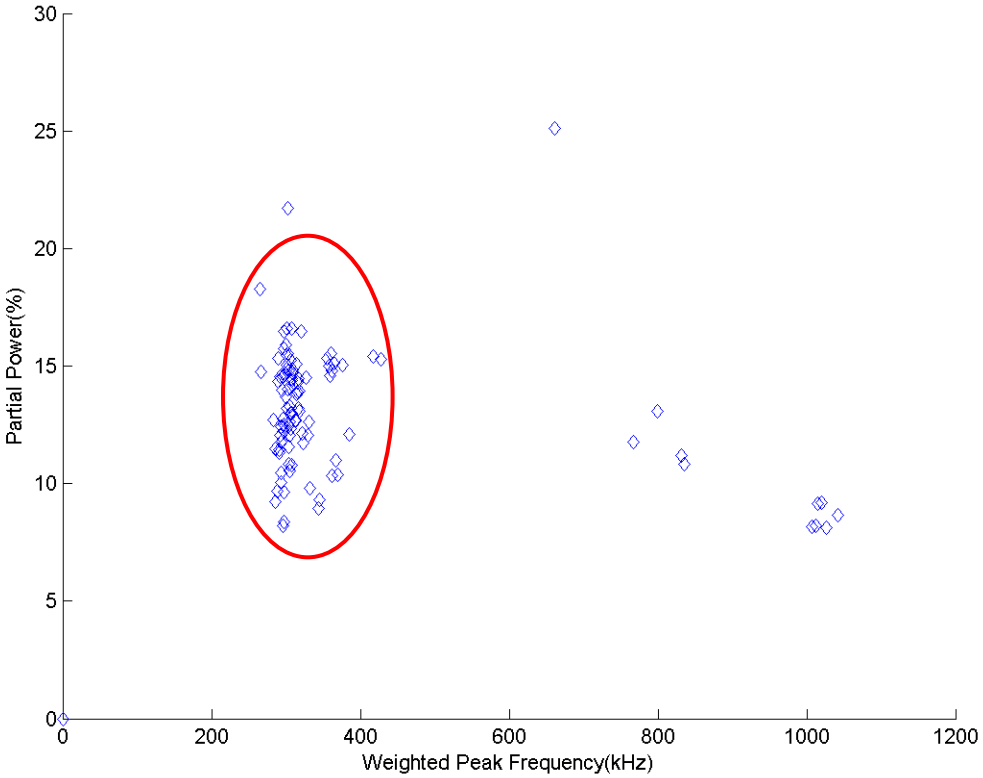

Figure 48: Eglass Epoxy 6/24/13, Ch2

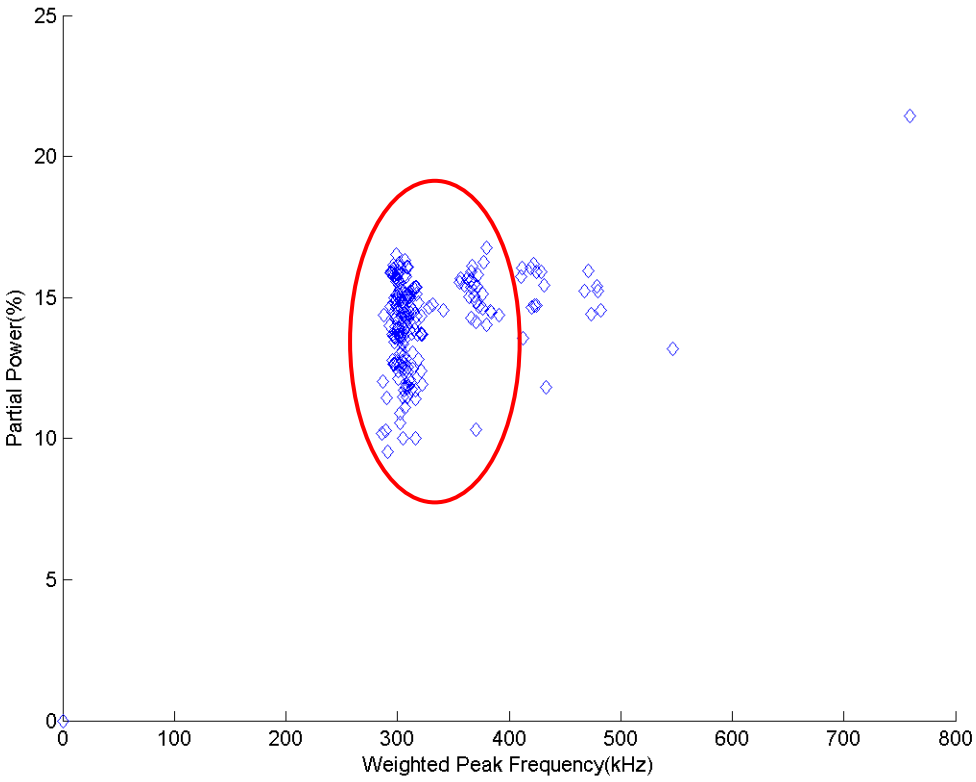

Figure 49: Eglass Epoxy 7/2/13, 1N, Ch2

Results do show strong clustering between 300kHz-400kHz for each of the shown SCC tests. Interestingly, only the 1N test shows any significant clustering outside of this range, which was expected to have at least two clusters (one for fiber breakage, and one for matrix cracking). After this was observed, CWDs for each test were observed and representative ones shown, which all indicate strong flexural modes and are shown in the same order as the PP vs. WPF figures (see Figure 50-Figure 52).

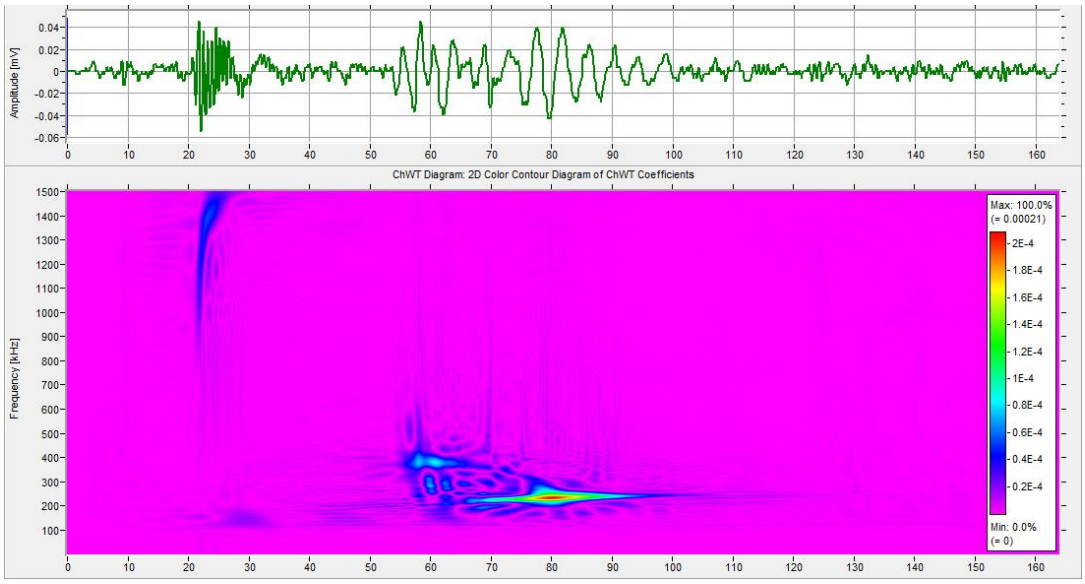

Figure 50: Eglass Epoxy 6/18/13 CWD, Ch1 Waveform #312

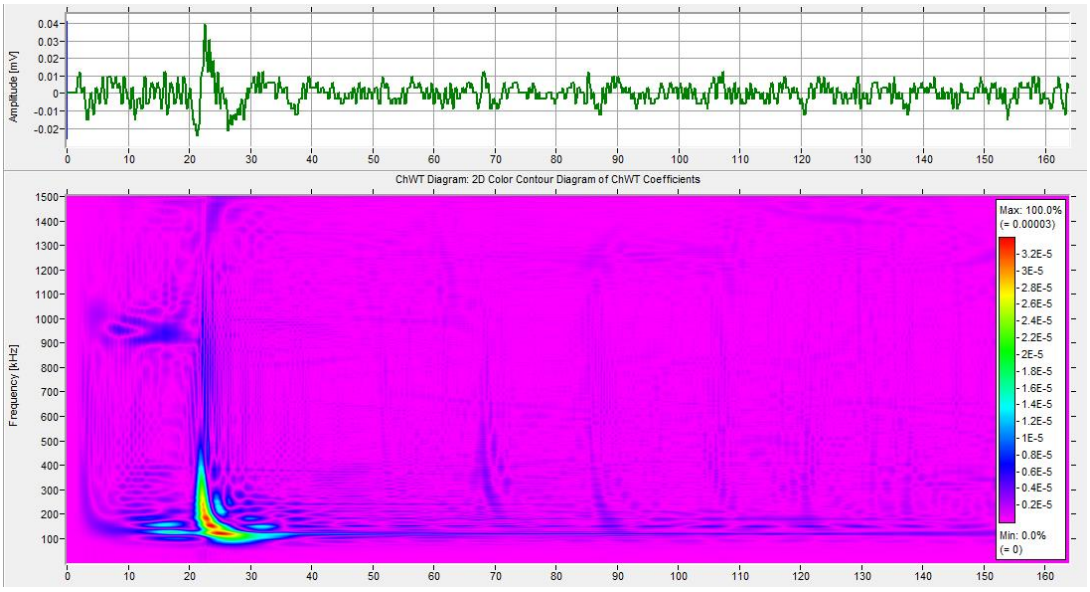

Figure 51: Eglass Epoxy 6/24/13 CWD, Ch2 Waveform #29

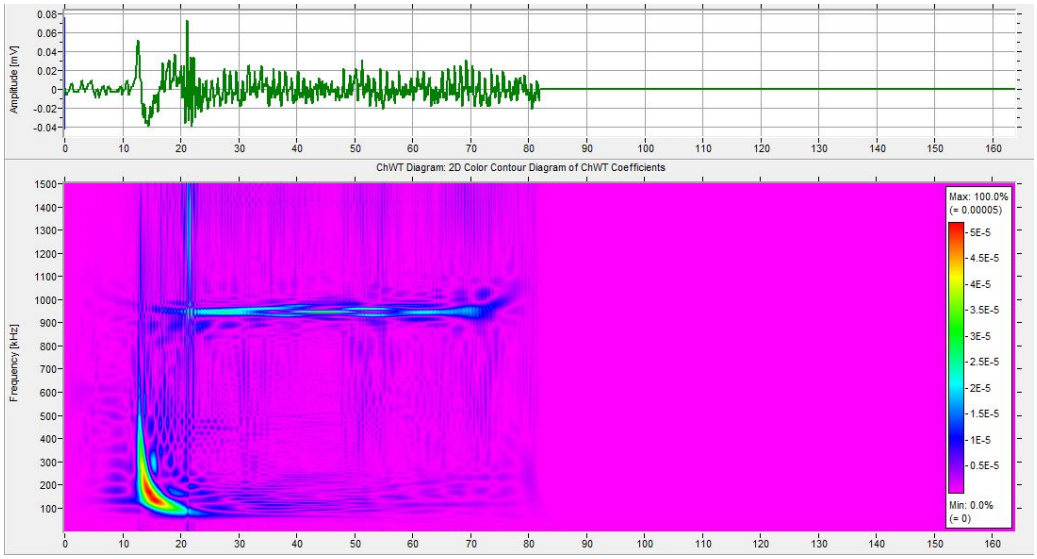

Figure 52: Eglass Epoxy 7/2/13 CWD, 1N, Ch2 Waveform #274

3.2 3 Point Bend Testing

Upon the completion of SCC testing, observing the experimental WPF vs. PP frequency, only one cluster was observed. It was unclear whether this cluster was matrix cracking or fiber breaking, so in an effort to gain more insight, a 3 point test was done. A smaller 5" sample was used due to test design, with sensors being placed 1 inch from each end (see Figure 53). This test was done with fiber orientation parallel to loading pins to facilitate primarily matrix cracking (see Figure 54).

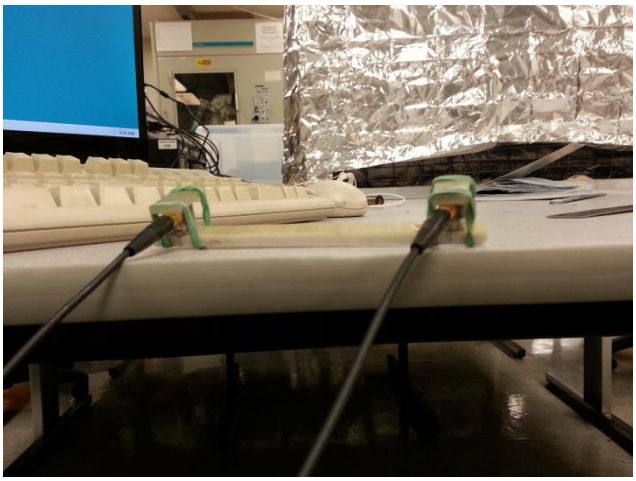

Figure 53: 3 Point Sensor Set-up

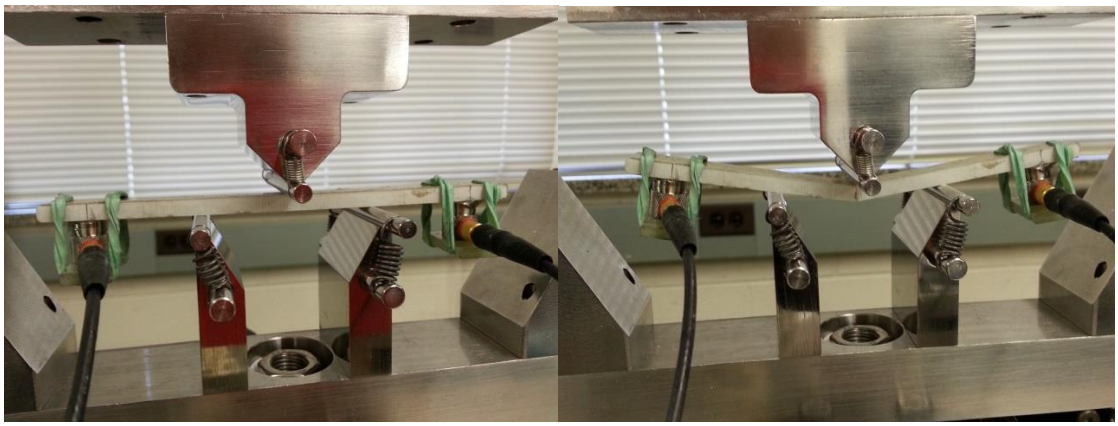

Figure 54: 3 Point Bend Test

This test was performed using the same software and settings as the SCC test, with the only difference being the gain was decreased to +52dB. This was done due to the expected energy of the events being large, sustained cracks, rather than the slow forming individual ones during SCC tests. The post processing of the signals was completed and the PP vs WPF analyzed and the largest, most identifiable cluster circled (see Figure 55).

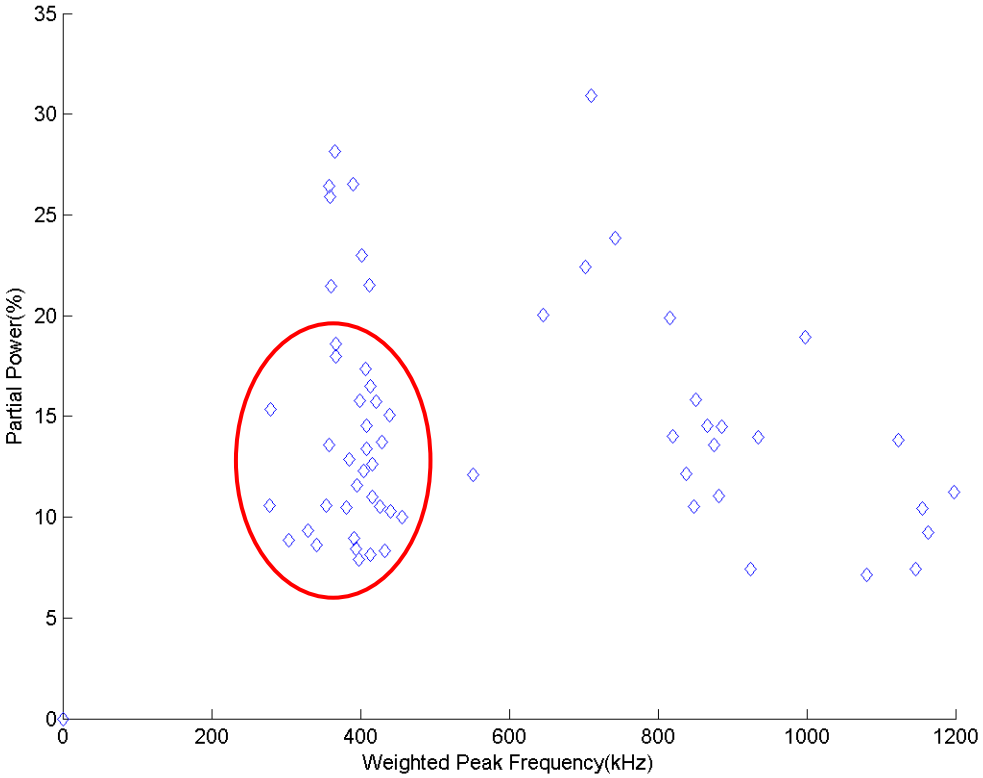

Figure 55: PP vs. WPF, 3 Point Bend

The circled data cluster represents the majority of the signals from the 3 point bend test. This signal cluster ranges from 270kHz to 483kHz WPF and 6.07% - 19.16% PP. Examining the CWDs of a few representative waves shows strong flexural mode (see Figure 56 and Figure 57). This cluster location and CWD mode analysis both confirm with results from SCC testing, indicating observed signals were indeed matrix cracking. Source location at one of the peak amplitude frequencies, in this case 203kHz, confirms that the source was in fact in the central section of the sample. Arrival times for this example were 103.48 and 100.84 μs respectively, yielding a difference in arrival time

of less than 5mm (sample was not perfectly centered, but other arrivals times confirmed this was the location of the damage from the load pin). It should be noted that this test involved fibers 90° off axis from the SCC tests, which does have an effect on the propagation of damage mechanisms through the composite to the sensors.

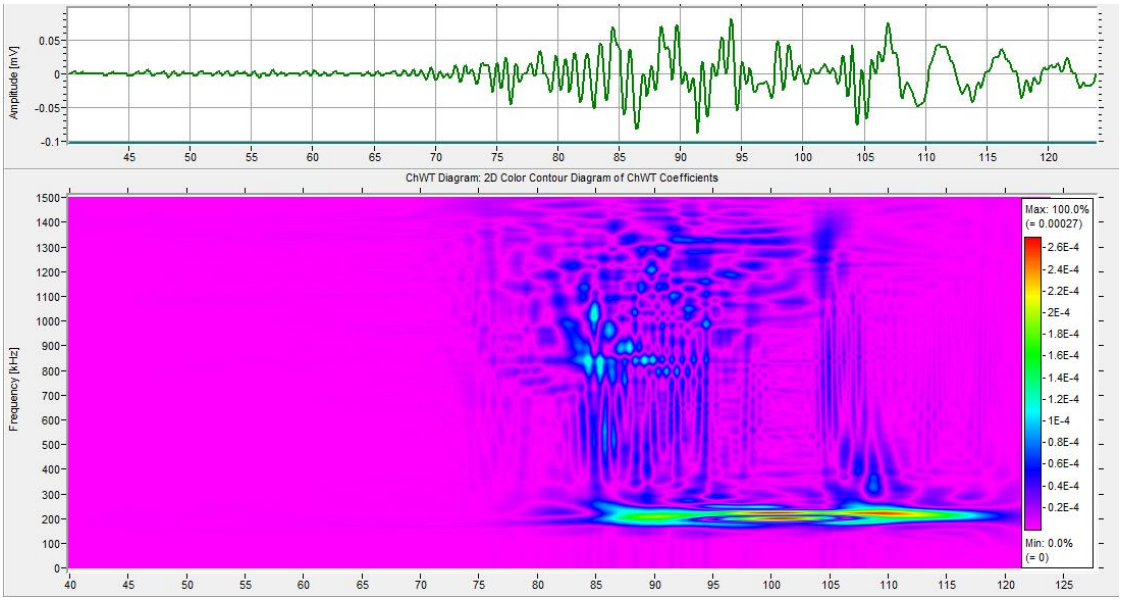

Figure 56: Representative Waveform CWD, Waveform #8 Ch1

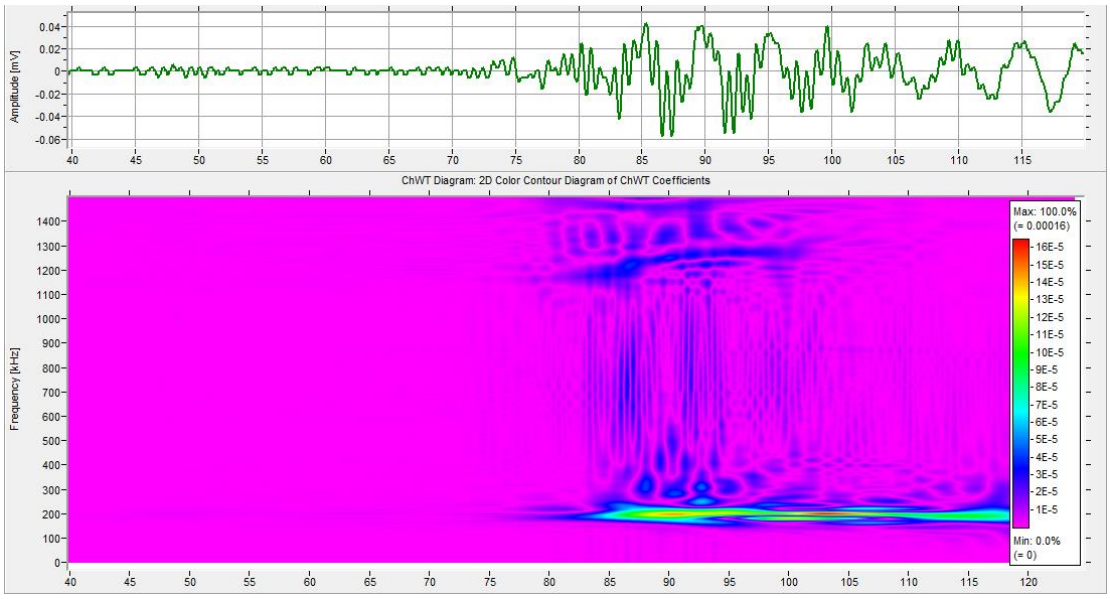

Figure 57: Representative Waveform CWD, Waveform #8 Ch2

3.3 Modeling Results

The intent of the forward predictive model was to simulate fiber breaks and matrix cracks as well as the effect of source location and material properties. The setup and explanation for this model can be seen in 2.4.

Modal acoustic emission has been discussed previously, with the primary modes for this research having been flexural and extensional mode. These modes have different propagation speeds as extensional propagates fastest in the down the length of the composite while the flexural arrives slightly later (see Figure 58 and Figure 59). As well as having different speeds, strong reflections off of width edges and specimen end are noted (see Figure 60).

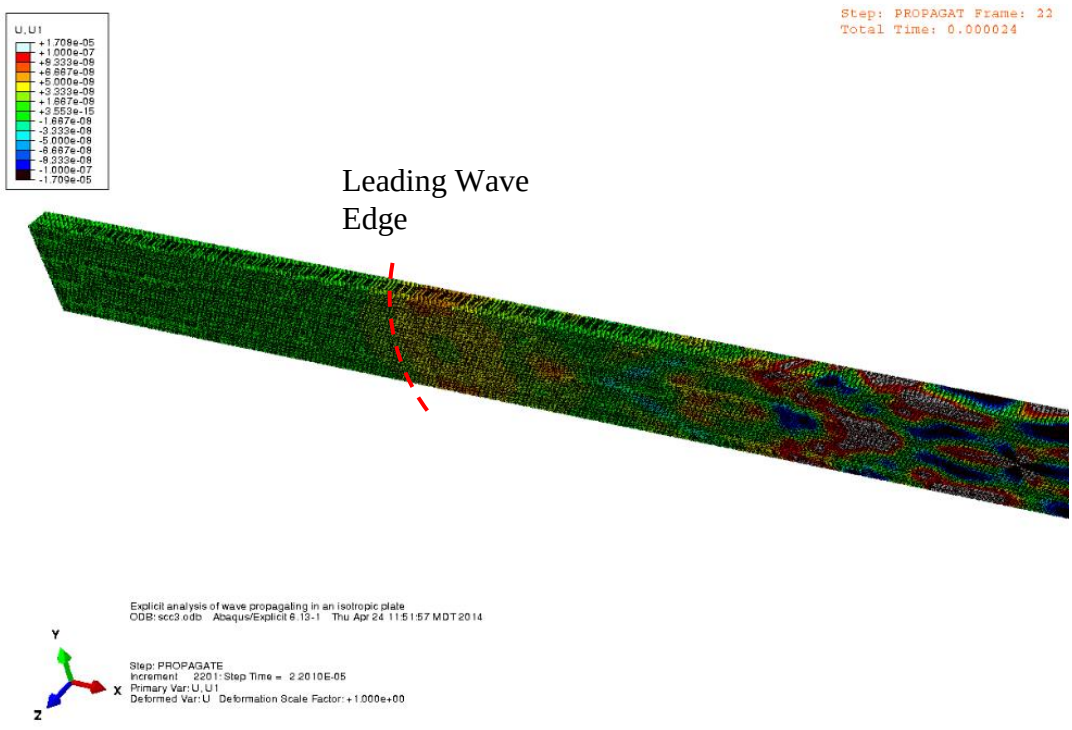

Figure 58: Waveform Animation, Matrix Crack, Extensional Mode

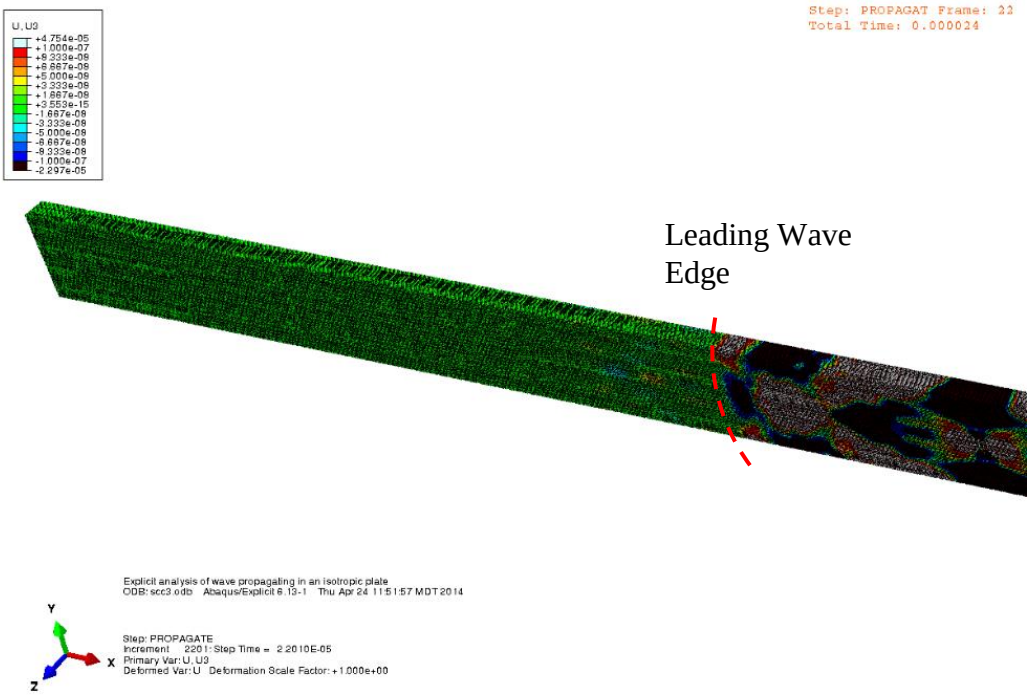

Figure 59: Waveform Animation, Matrix Crack, Flexural Mode

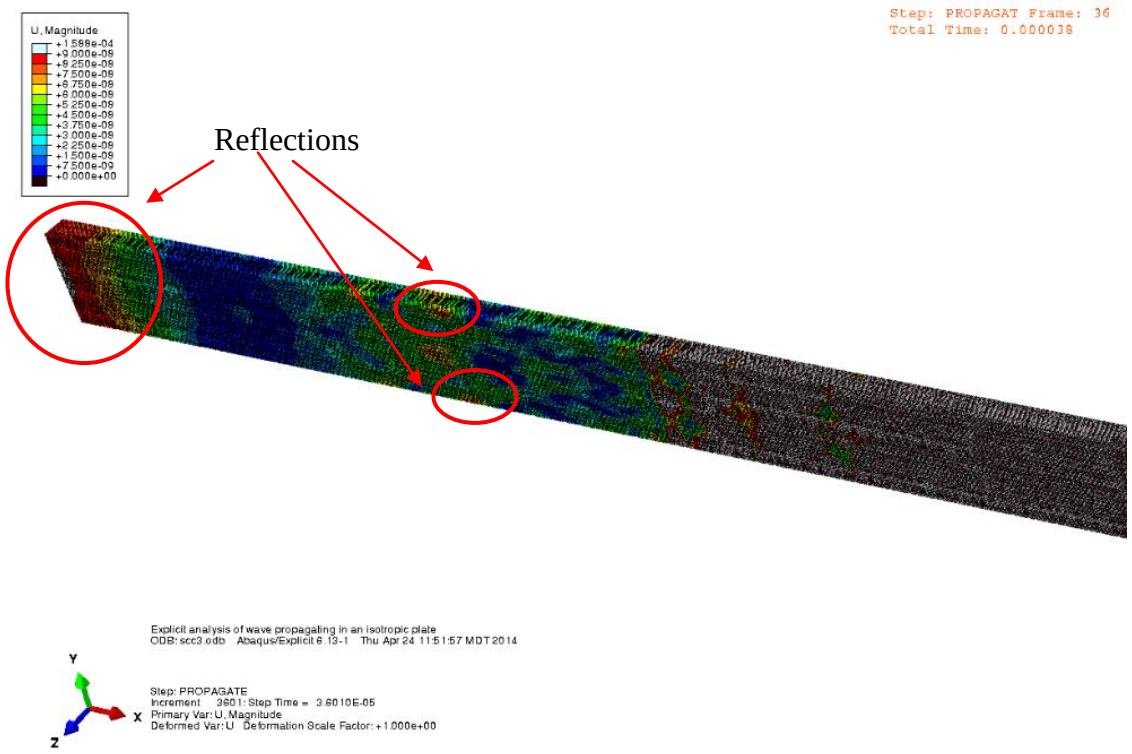

Figure 60: Waveform Animation, Matrix Crack, Reflections

3.3.1 Rise Time

Rise time was the primary variable in question, and thus the most resources were devoted towards its completeness. For Fiber breaks, this Rise Time was varied between 0.1μs – 2μs. This signal was post processed in the same manner as the other waveforms through the Matlab code and the PP vs. WPF examined (see Figure 61).

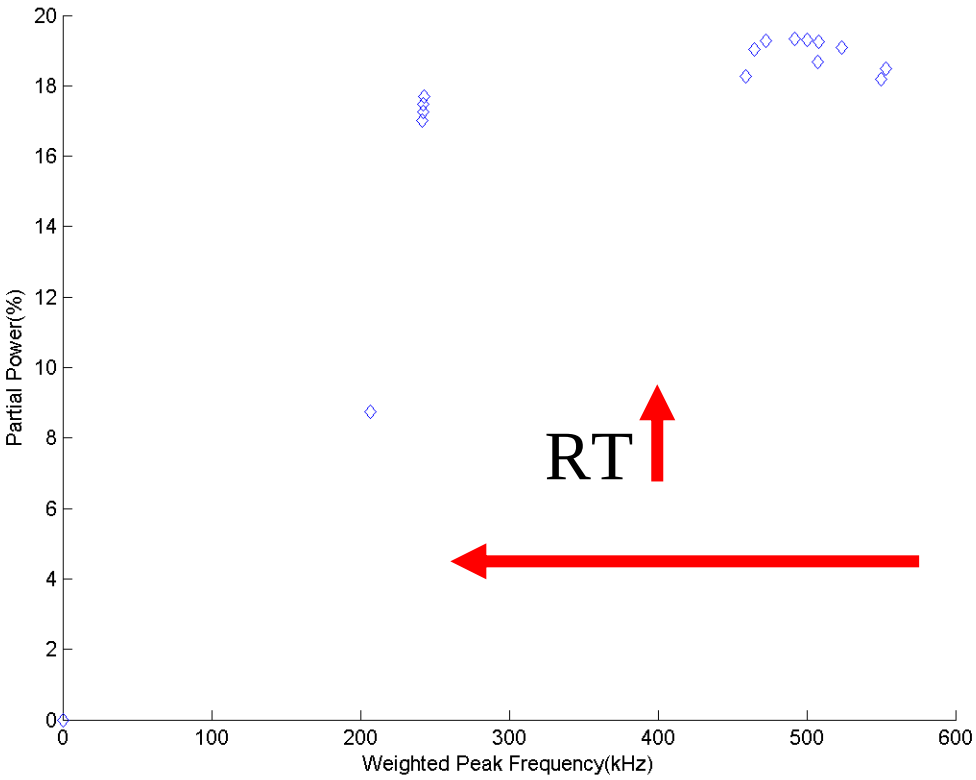

Figure 61: PP vs. WPF, Fiber Break Model

The trend immerged that as Rise Time increased, WPF decreased, until at one point, it decreases drastically. In order to understand why there was a drastic decrease, the waveforms were examined in the time and frequency domain (see Figure 62 and Figure 63). Each contains two dominant frequency peaks which greatly affect the WPF of the figures, which have identifying arrows in Figure 63. As RT increases, the amplitude of the second peak decreased until at 1325ns it has equal magnitude as the first point. Subsequently, higher RT waves have a second peak of increasingly smaller amplitude. This is the point at which the WPF significantly drops off as is seen in Figure

61. These combined factors lead to a reasonable RT between 800-1000ns with a resulting WPF of 459 kHz-500 kHz and a PP of 18.26%-19.3% for a simulated fiber break. Longer RT than 1000ns were run, but were considered unrealistically long.

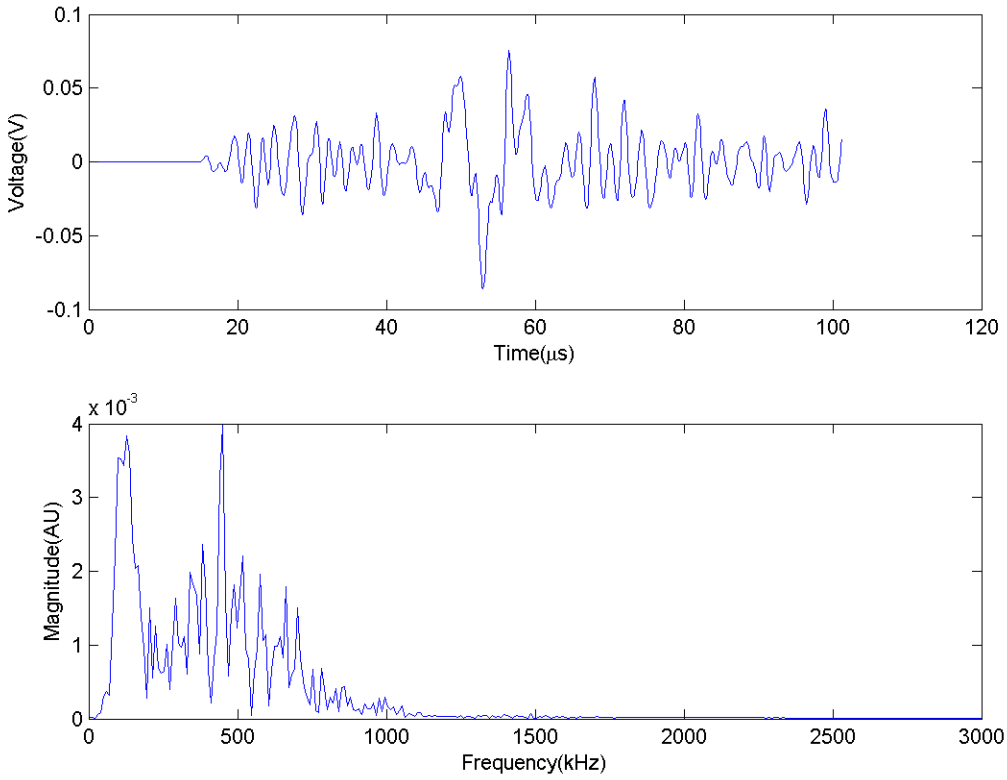

Figure 62: Waveform, 1250 ns RT, Fiber Break

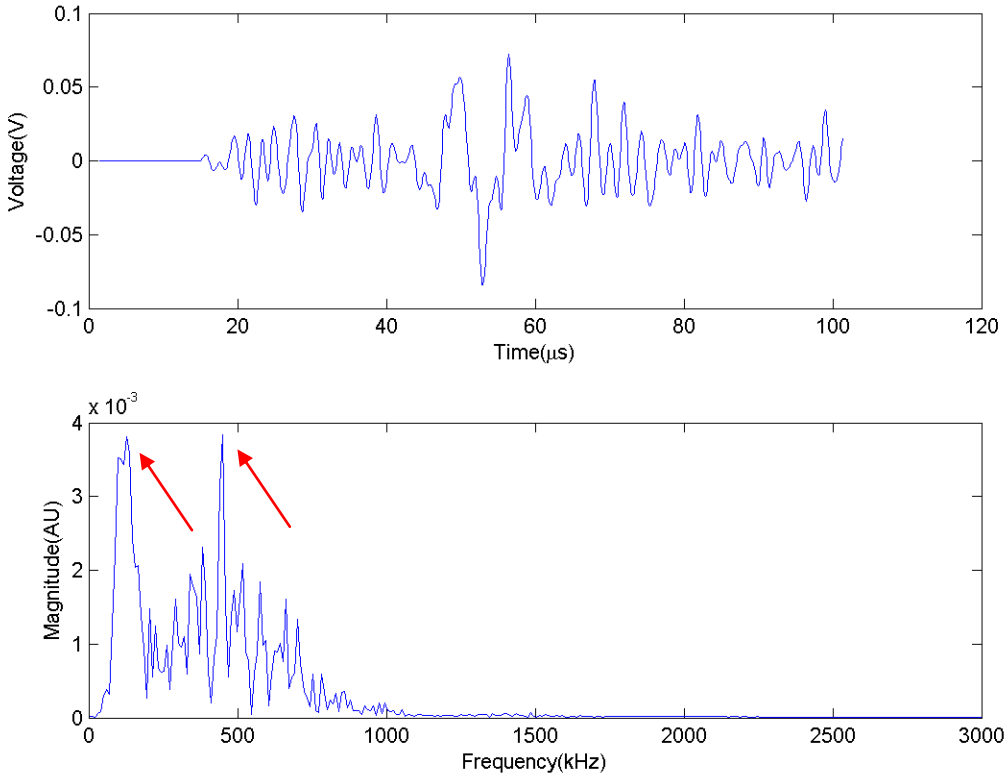

Figure 63: Waveform, 1325 ns RT, Fiber Break

The matrix crack simulation was similarly processed and the WPF vs. PP examined (see Figure 64).

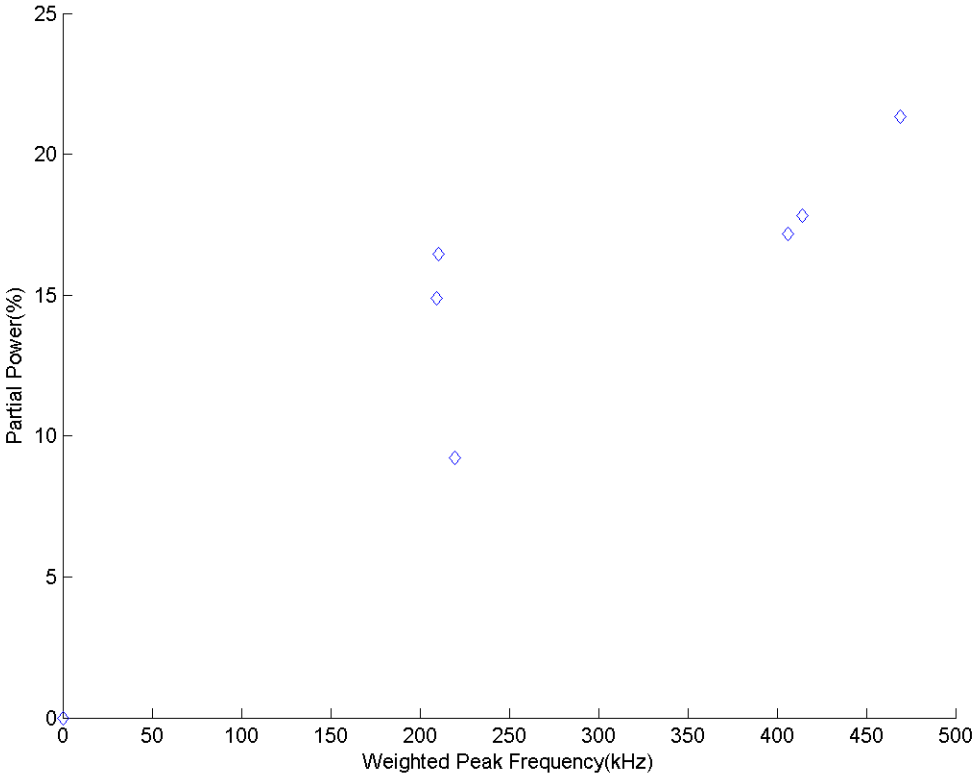

Figure 64: PP vs. WPF, Matrix Cracking Model

Similarly this model experienced the same drop-off and for the same reasons, with the 3rd frequency peak becoming less than or equal to the first frequency peak (see Figure 65).

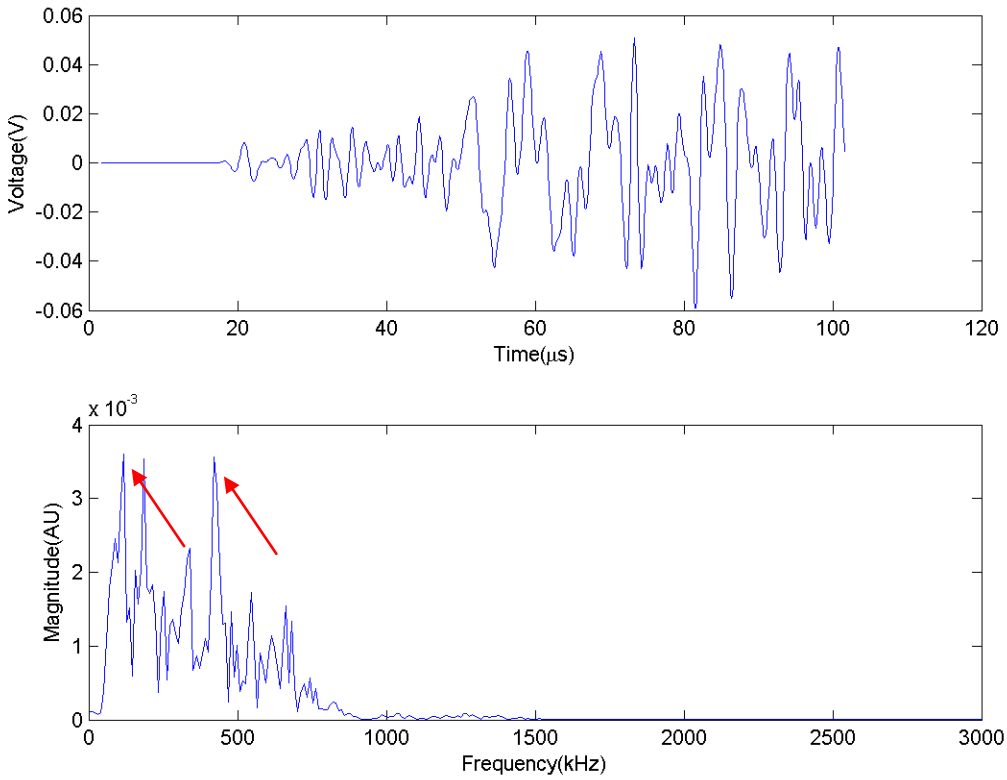

Figure 65: Waveform, 1600 ns RT, Matrix Crack

These combined factors lead to a reasonable RT between 1500-1550ns with a resulting WPF of 406kHz-469kHz and a PP of 17.17%-21.35%. 1000ns was included but was deemed too fast to be realistic.

This data was graphed on top of the 3 point test data to show convergence of the model to experimental results with the same red circle superimposed to show clustering (see Figure 66). Note that fiber break simulation does not have a cluster. This result was expected as 3 point bending orientation should be primarily matrix cracking.

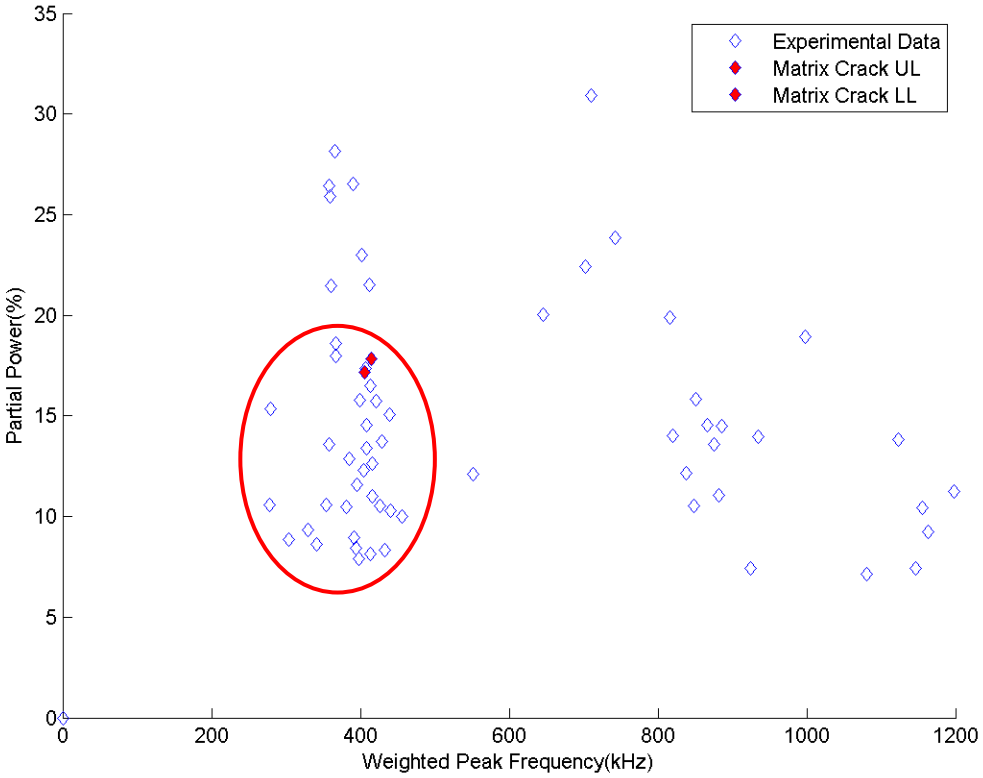

Figure 66: PP vs. WPF Overlay, 3 Point Test and Model

3.3.2 Signal Distance

After adequate rise times were established, effect of signal distance could be quantified. This was done by changing the node set where the force was being applied on the model rather than moving the sensor location. For this distance, the source was left centered from width wise, while lengthwise distance was adjusted to be plus/minus 3.81mm from its original length centered position. The source was again left on the surface of the sample, as that is where the majority of events are expected to occur experimentally. PP vs. WPF is again examined, with the original, centered value left for comparison (see Figure 67 and Figure 68).

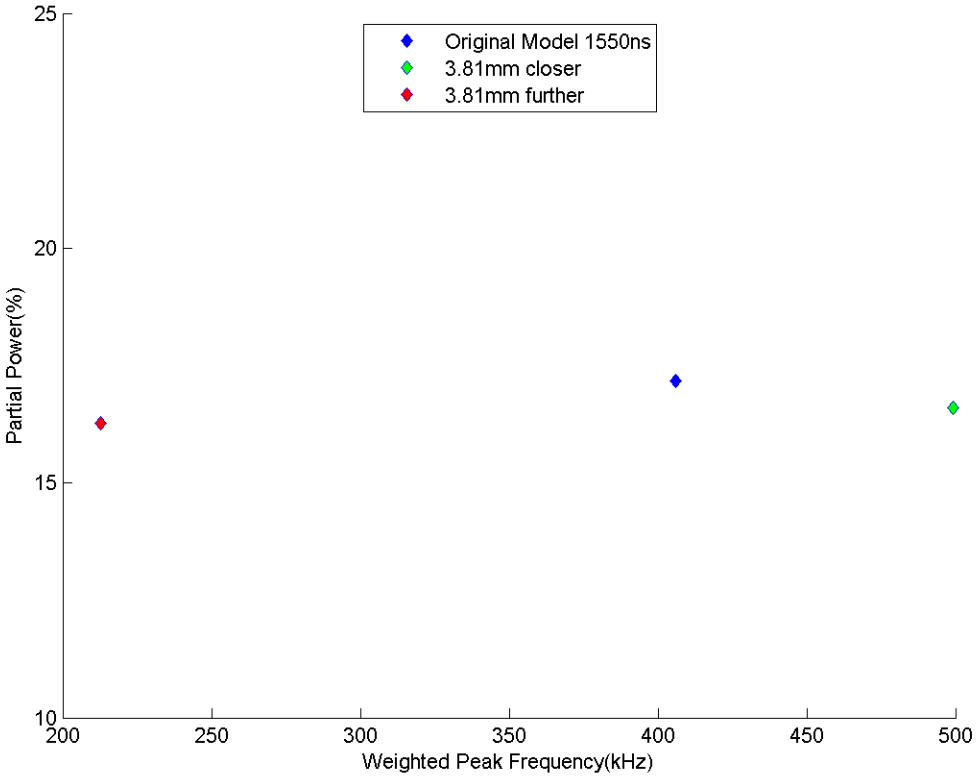

Figure 67: Distance Study, Matrix Crack, 1550ns RT

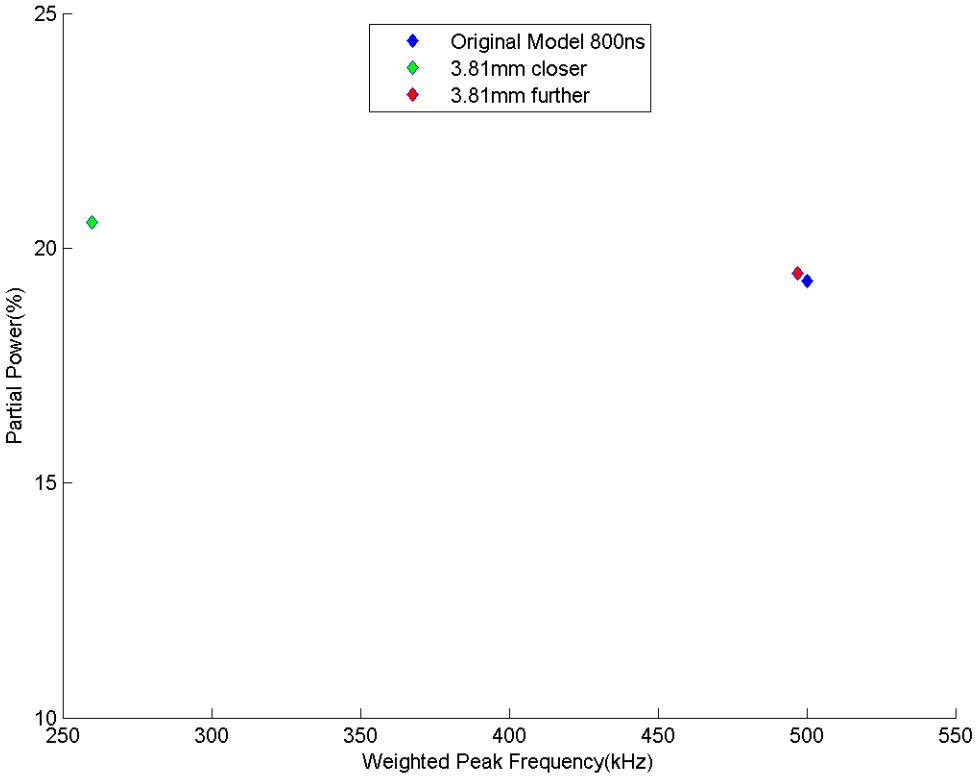

Figure 68: Distance Study, Fiber Break, 800ns RT

Results for both fiber break and matrix crack were expected, as changing their location had large effects for a closer fiber break, and a further away matrix crack. It was thought that the specific rise time chosen might have an effect, so alternate rise times within the acceptable range were tested and the PP vs. WPF again examined (see Figure 69 and Figure 70).

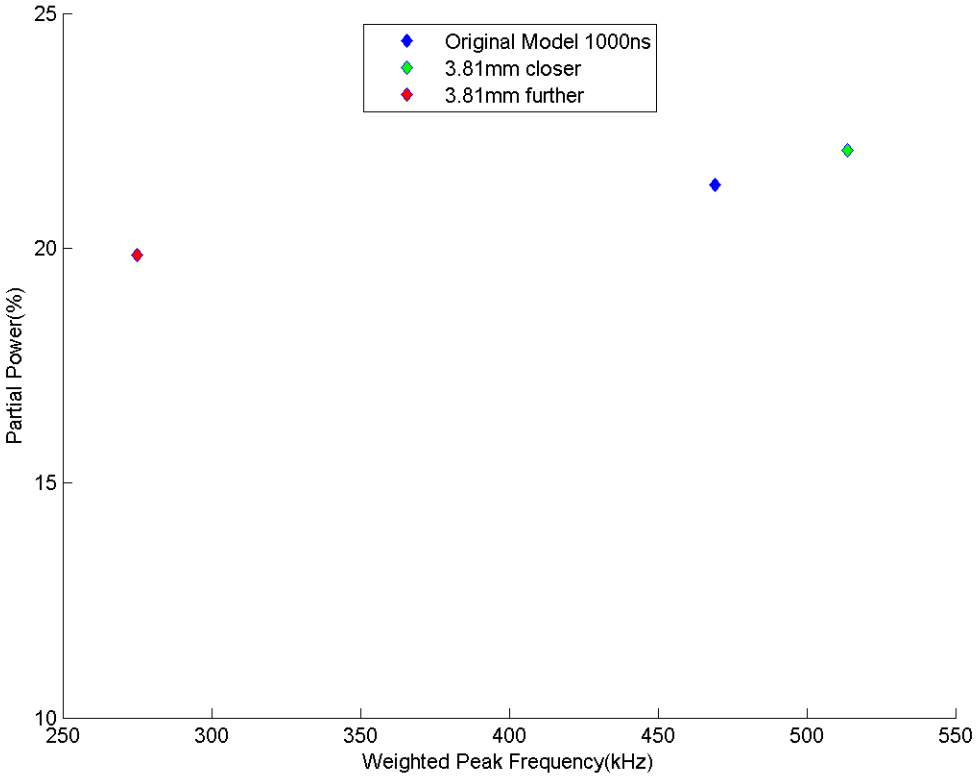

Figure 69: Distance Study, Matrix Crack, 1000ns RT

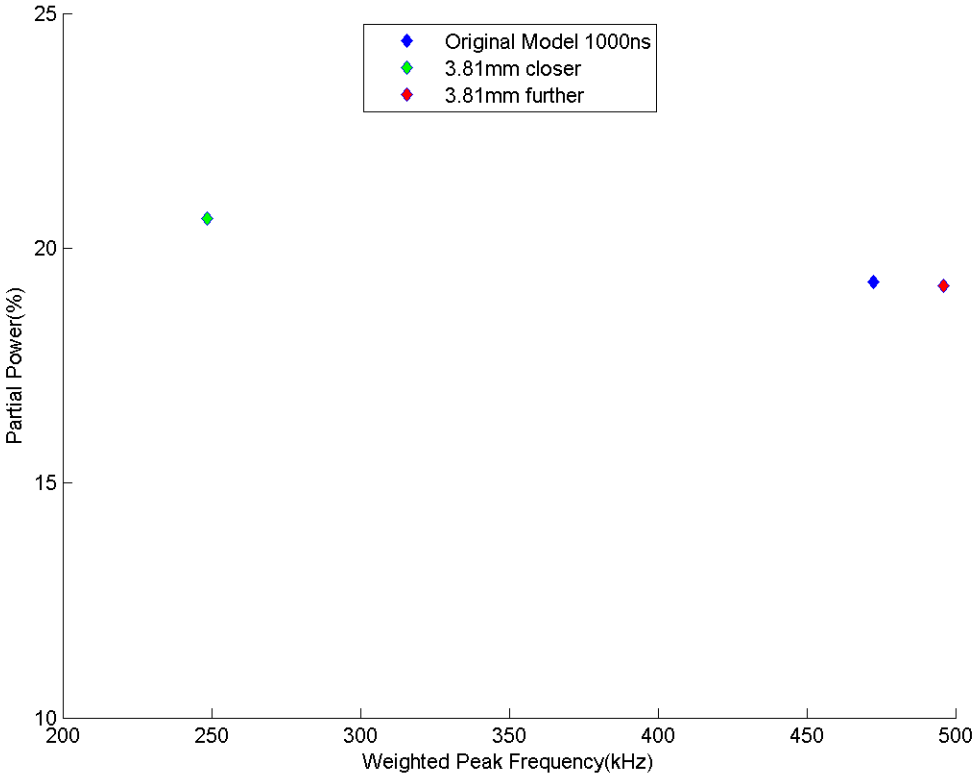

Figure 70: Distance Study, Fiber Break, 1000ns RT

The trend remained the same for both damage mechanisms so the waveforms were examined (see Figure 71 and Figure 72).

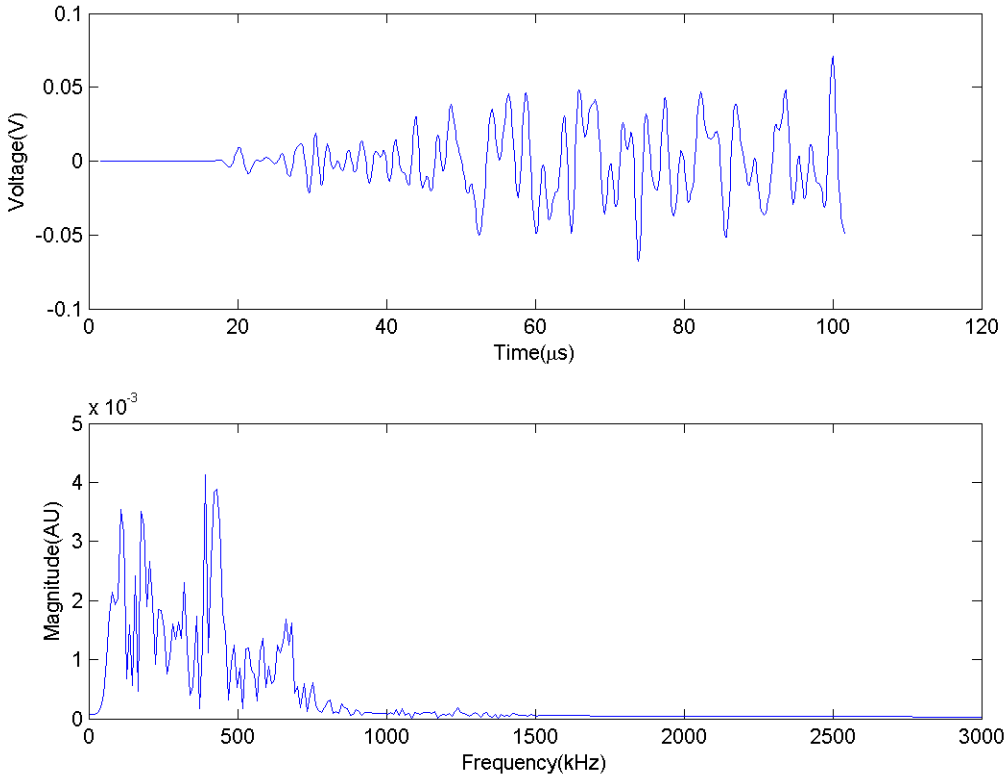

Figure 71: Waveform, Distance Study, Matrix Crack, 1550ns RT, Closer

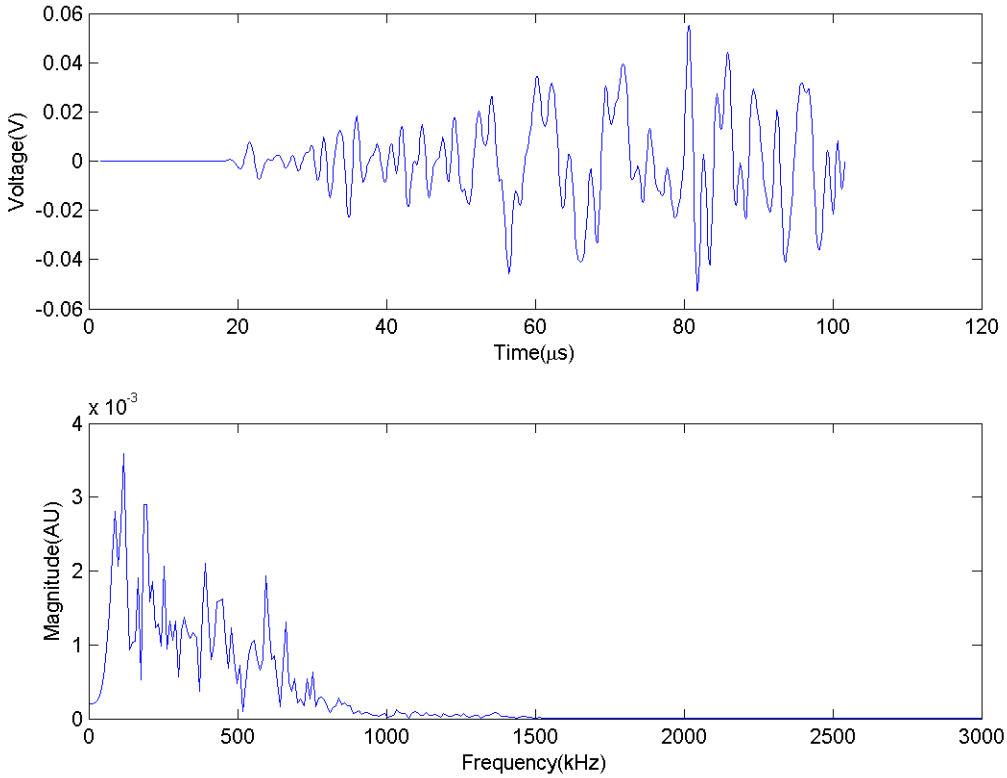

Figure 72: Waveform, Distance Study, Matrix Crack, 1550ns RT, Further

This change in difference fundamentally changed both the shape of the wave in the time domain by increasing the peak at approximately 80μs and a peak amplitude in the frequency domain at approximately 400kHz for the further signal. This is expected as distance should decrease the amplitude in the time domain slightly due to attenuation and reflections off of sides will create changes in the received wave based on constructive and destructive in. The model is strongly affected by the reflections of the waves off of the narrow width of the generated surface waves, an issue which does affect experimental results, as can be seen by the clusters ranges as well as comparing signals from ch1 with

ch2. This same issue was seen in the fiber break models, but with the peak amplitude being a lesser frequency peak and the time domain signal having different shape.

3.3.3 Material Properties

Model variable dependence was again tested, but with the variable being material properties. The method for doing this can be seen in 2.4. Fiber break shows, as expected, that a change in material properties affects PP and WPF as the material constants of the propagation medium is important in determining wave content (see Figure 73)

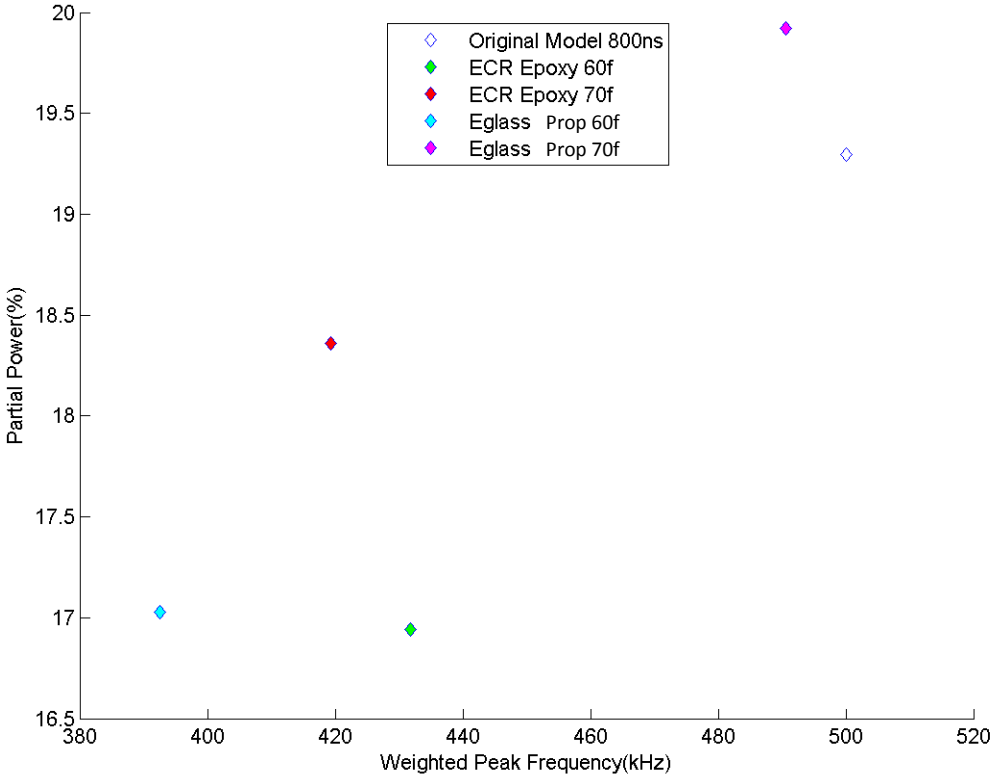

Figure 73: Material Study, Fiber Break, 800ns RT

Waveforms were investigated for these types to examine how shape changed with material properties, beginning with volume fiber fraction. (see Figure 74 and Figure 75).

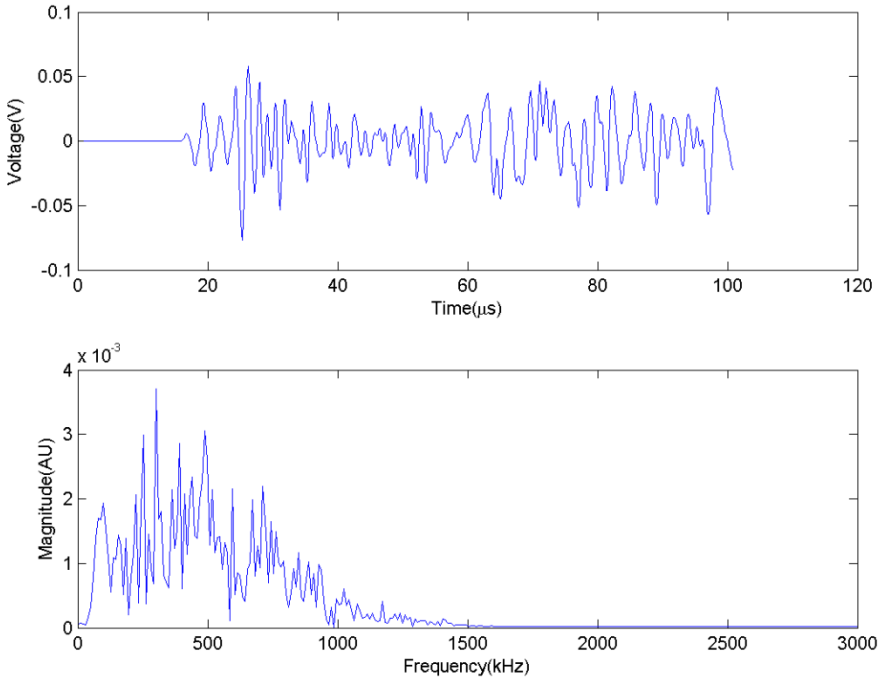

Figure 74: ECR Epoxy, 60f, Fiber Break

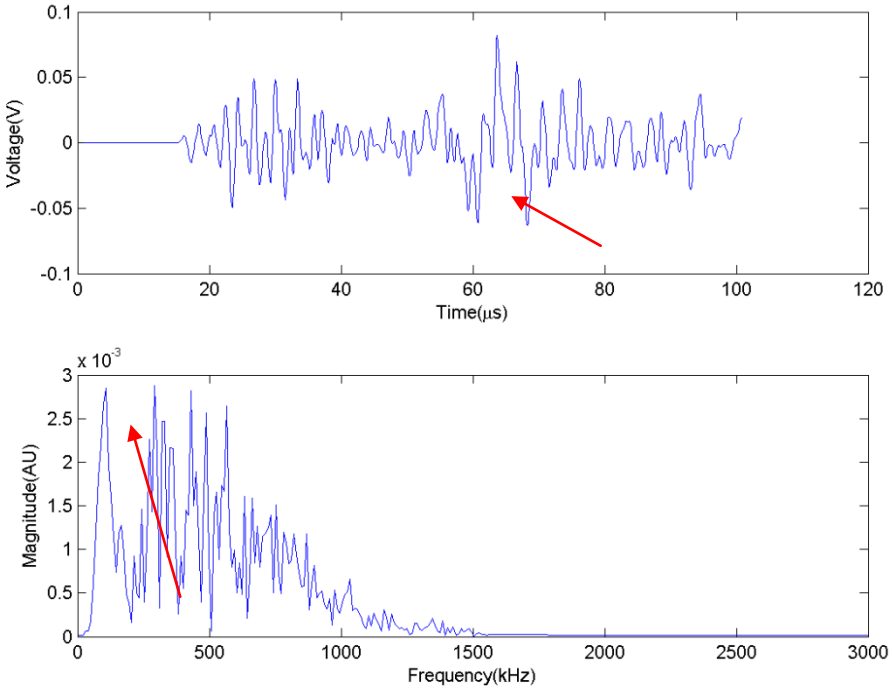

Figure 75: ECR Epoxy, 70f, Fiber Break

PP between 60% and 70% f shows a change from 16.94% to 18.36% while WPF changed from 431.7 kHz to 419.3 kHz. Changes can be seen in both the time and frequency domain, with amplitudes both increasing at values around 65μs in the time domain and 100 kHz in the frequency domain. Shape remains largely unchanged other than those two amplitude changes. When compared to the E-glass model, a large portion of the time domain is different between the 40μs-60μs range (see Figure 76). This appears to have impact only on the lowest amplitude peak, reducing that peaks amplitude. One of the largest reasons for this could be a result of Leaky Lamb Waves, which show a loss of flexural mode in solids by mode being absorbed into liquids when there is a

solid/liquid interaction at damage mechanisms. (B. H. Burks, The Impact of Solid-Fluid Interaction on Transient Stress Wave Propagation due to Acoustic Emissions in Multi-Layer Plate Structures 2014)

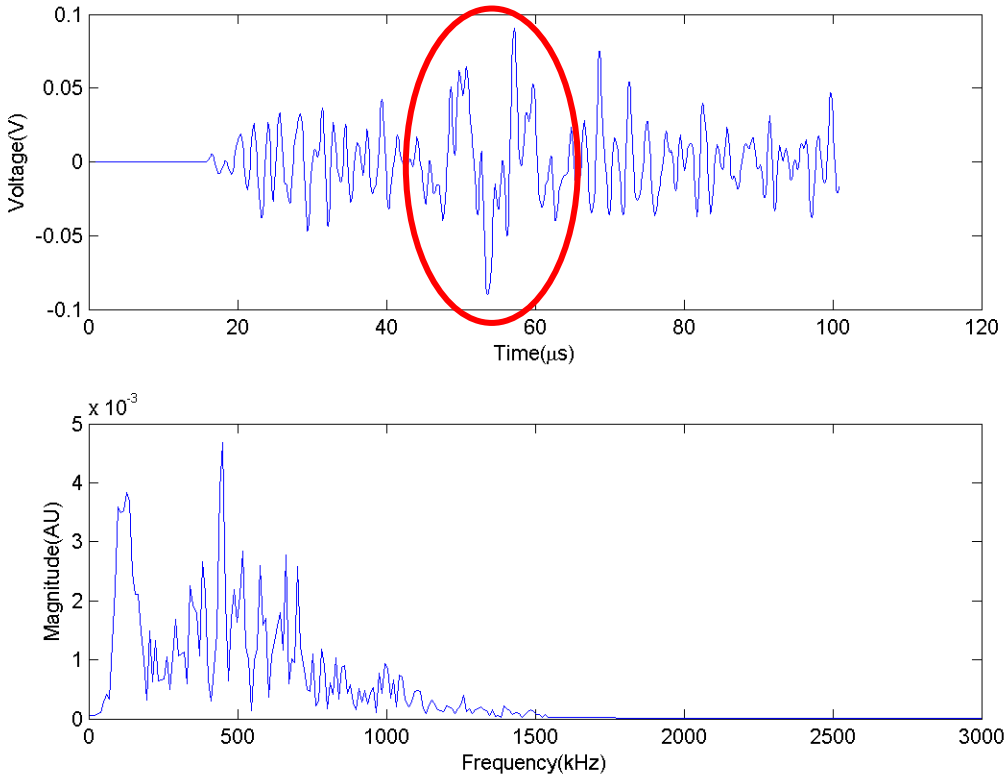

Figure 76: Fiber Break, 800ns RT

This shape is completely different, but for this range of data only. It should be noted observed impact on frequency domain is several larger amplitude "spikes" between 250 kHz and 500 kHz. This effectively lowers the WPF. A similar effect can also be seen when matrix material is changed (see Figure 77).

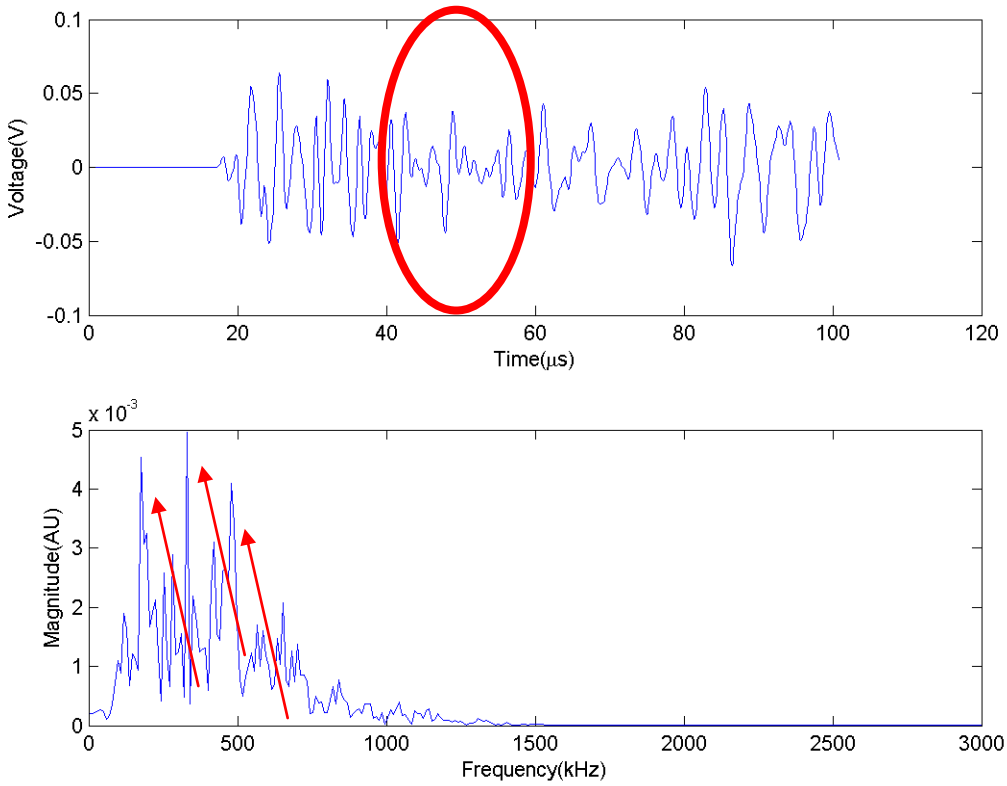

Figure 77: E-glass Proprietary Material, 60f, Fiber Break

Arrows indicate where peak amplitudes in the frequency domain differ from volume fiber fraction in the E-glass PU samples. The peaks shown contributed to the strong WPF difference between models, which was a PP of 17.03%-19.92% and 392.5 kHz-490.6 kHz for 60%f and 70%f respectively.

In addition to fiber breaks, matrix cracks were also examined. Using the same criteria, a rise time of 1500ns was used and the same material properties changed (see Figure 78).

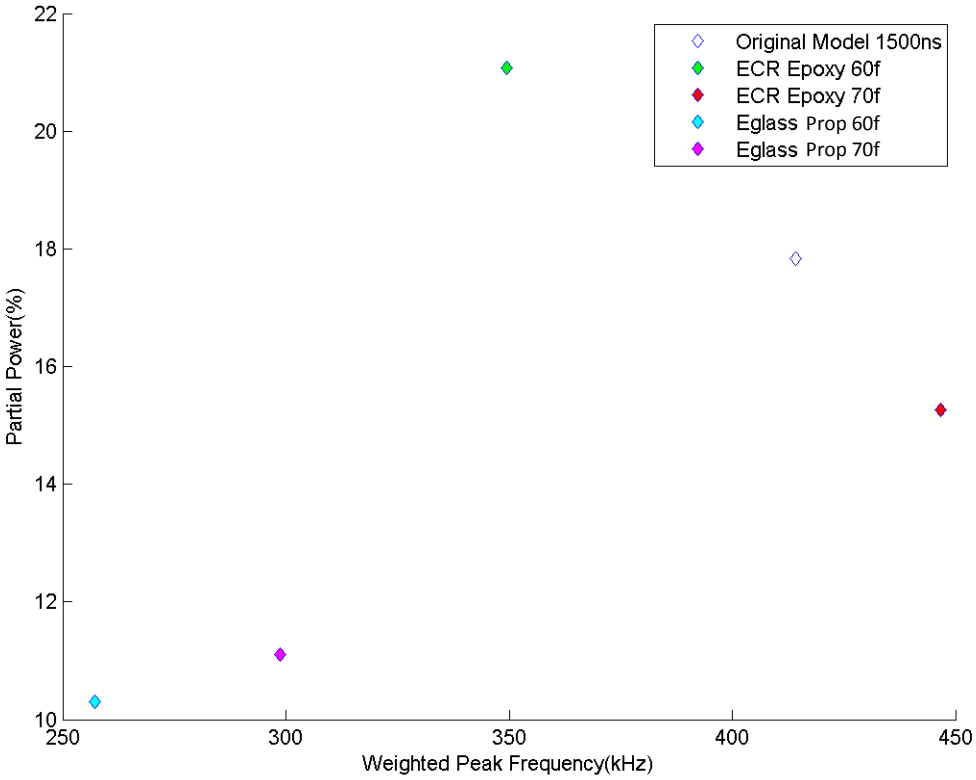

Figure 78: Material Study, Matrix Crack, 1500ns RT

Similar trends can be noticed in the large discrepancies between similar materials, but with a large gap between ECR fiber types rather than PU matrix materials.

Waveforms are examined to understand key differences (see Figure 79 and Figure 80)

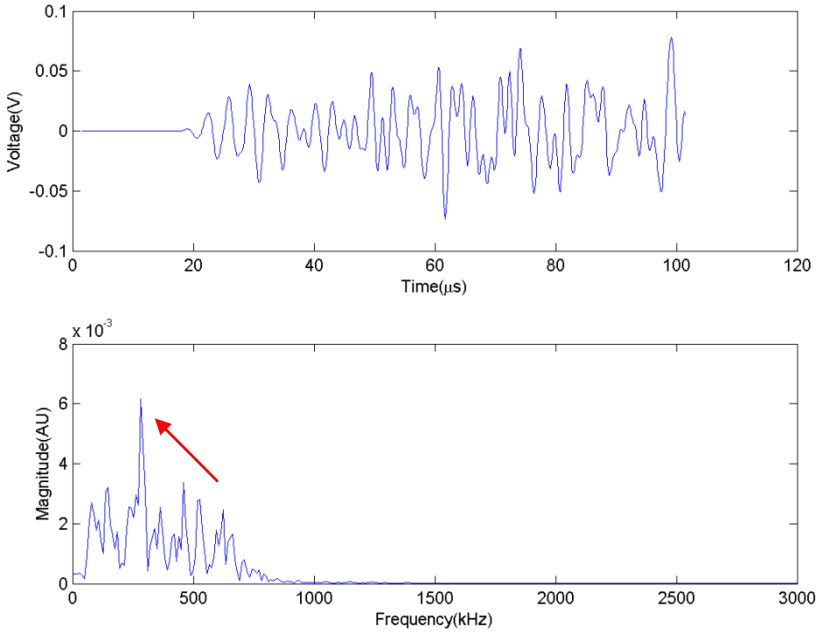

Figure 79: ECR Epoxy, 60f, Matrix Crack

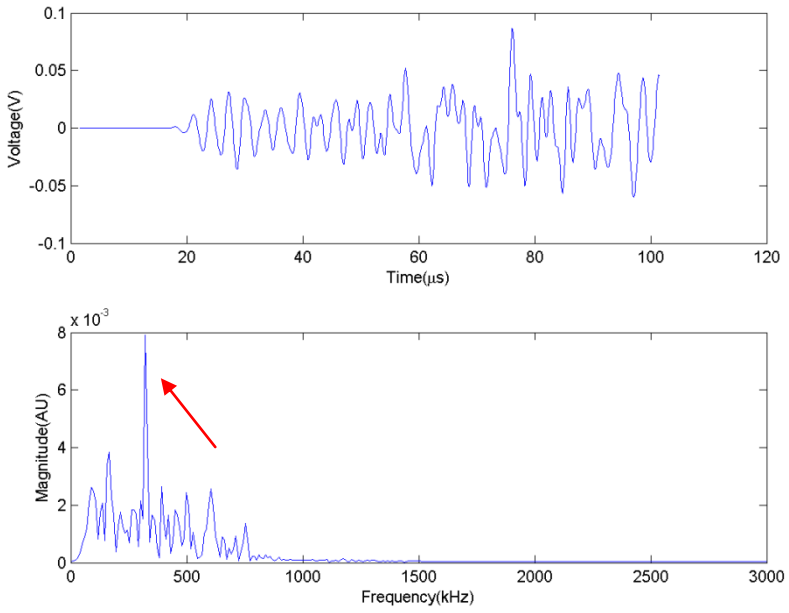

Figure 80: ECR Epoxy, 70f, Matrix Crack

The largest difference between these two simulations is the dominating peak in each frequency domain. The peak from the 60f model is 0.0062 in amplitude and located at 283kHz while the 70f model peaks with an amplitude of 0.0079 at 322kHz. The increased amplitude and greater frequency push the 70f simulation WPF almost 100kHz higher.

When comparing the ECR fiber to the E-glass fiber model, the time domain looks very similar in shape and amplitude, however, when the frequency domain is examined, differences in dominating amplitudes can be observed (see Figure 81).

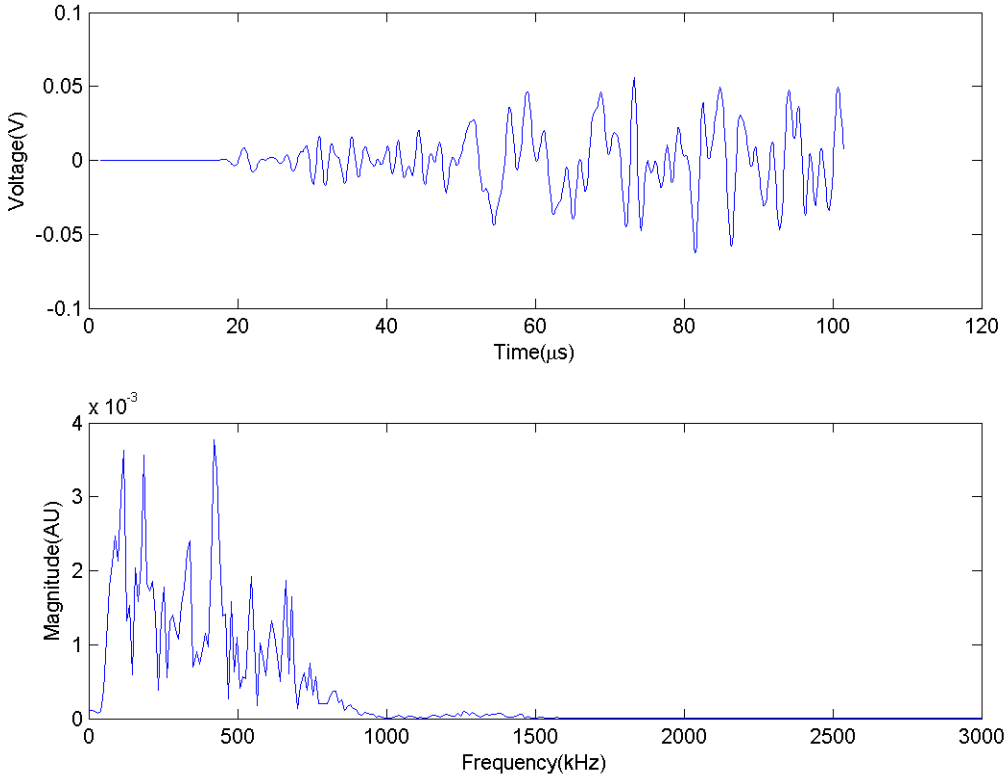

Figure 81: Matrix Crack, 1500ns RT

The same peak in the frequency domain that was highlighted in Figure 80 is completely missing in the original simulation, leading to a lesser WPF.

Examining the difference between matrix materials leads to the largest difference in WPF and PP for any of the simulations involving material properties (see Figure 82).

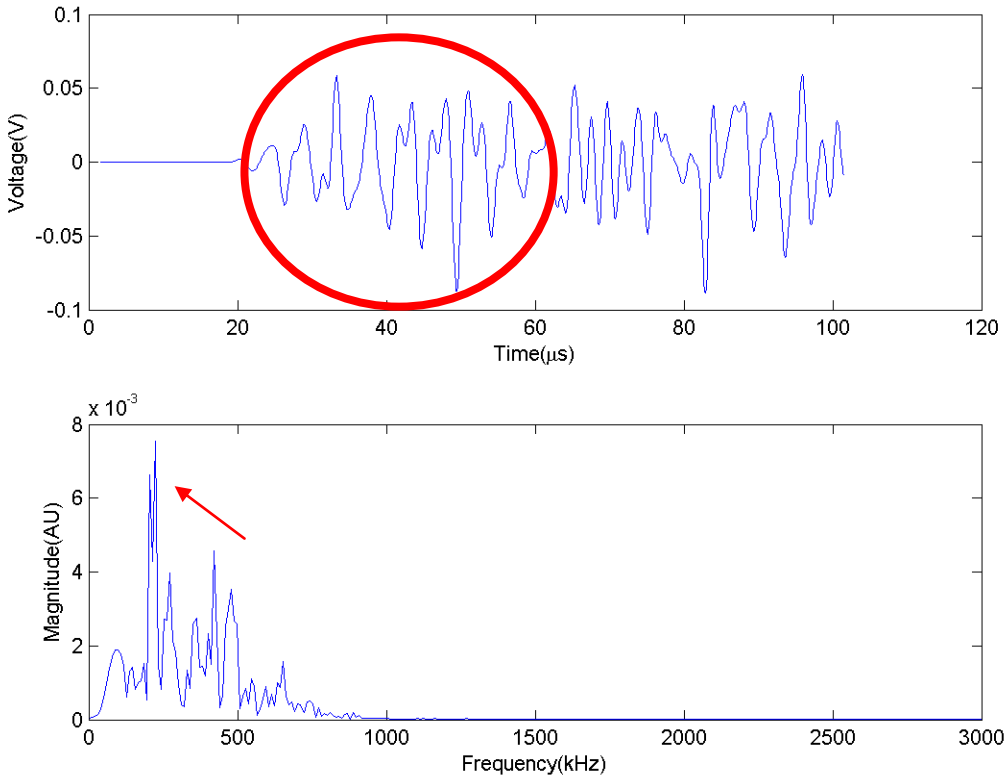

Figure 82: E-glass Proprietary Material, 70f, Matrix Crack

For this simulation differences can be seen in both the frequency and time domain. The signal between 20μs and 60μs has similar shape, but larger amplitude while the frequency has a large, lower frequency peak. These differences lead to a largely decreased WPF.

3.4 Microscopy

E-glass fiber reinforced composite materials had been very well documented and discussed from different perspectives. (H. Li 2011) (R. B. Jones 2004) (R. S. Jones 2010) However, for the new variants of ECR-glass fiber (corrosion resistant), it difficult to evaluate their susceptibility to failure when they are subjected to combined conditions such as stress and acidic environments. Stress corrosion cracking can involve many mechanisms, such as the type of composite, exterior surface quality, fiber size, matrix fracture, fiber-matrix debonding, type of mechanical loading, etc. These effects, alone or in combination, are often difficult to analyze. The main factor responsible for the stress corrosion cracking in the composite materials appears to be the glass fiber rather than the matrix, as the resin appears to play a protective role by protecting the fibers from the corrosive environment.

The purpose of this morphological surface characterization was to describe if the initial status of their surfaces, particularly the exposed fibers, played a determinant role in their susceptibility to stress corrosion cracking. Figure 83 through Figure 86 show representative microstructures (same magnification) of surfaces of the eight composites evaluated and Figure 87through Figure 90 show differences observed from SCC testing.

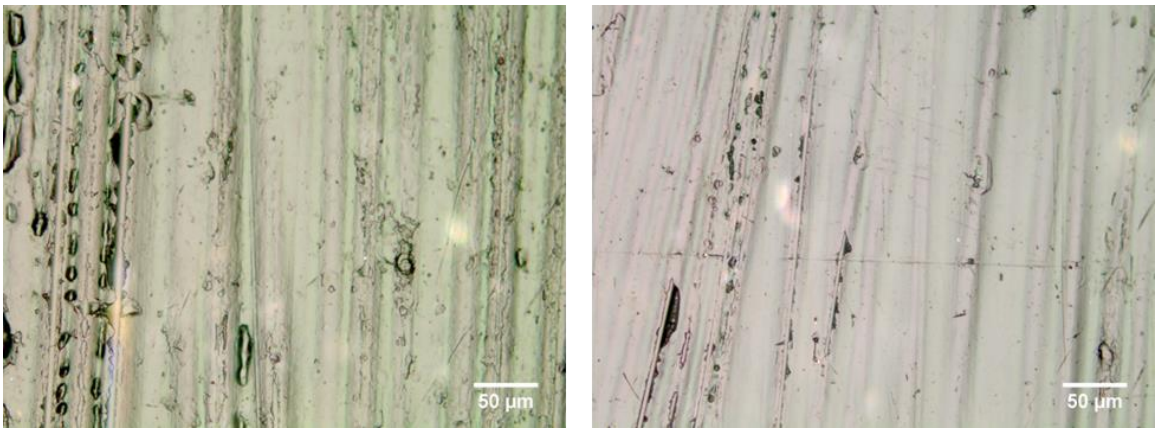

Figure 83: Vinylester, ECR-glass 1 and E-glass 1, As Received

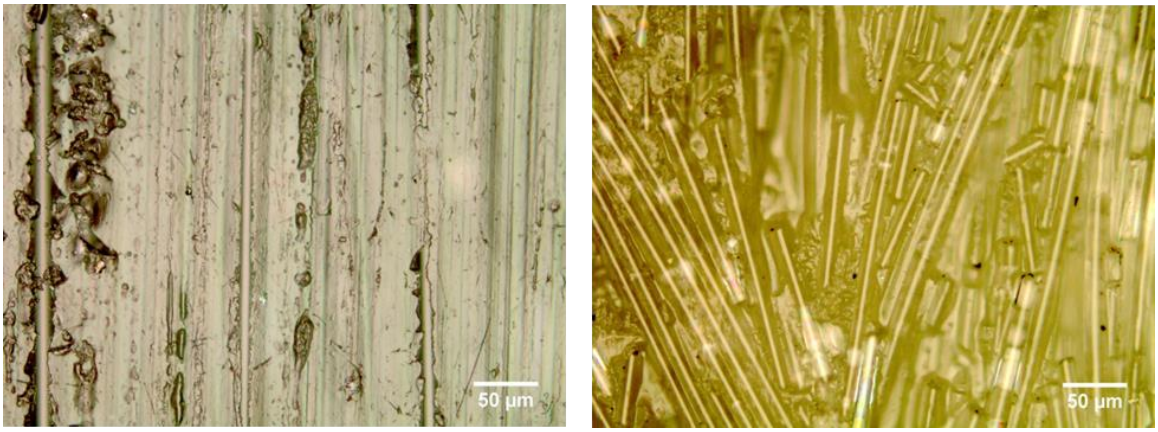

Figure 84: Vinylester ECR Glass-2, Polyester E-glass 1, As Received

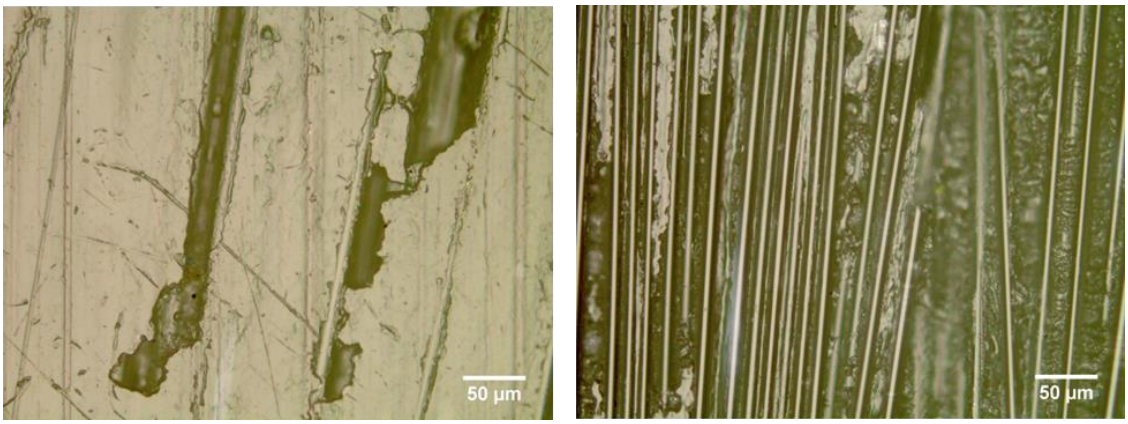

Figure 85: Polyester ECR-glass 2, Epoxy E-glass 1, As Received

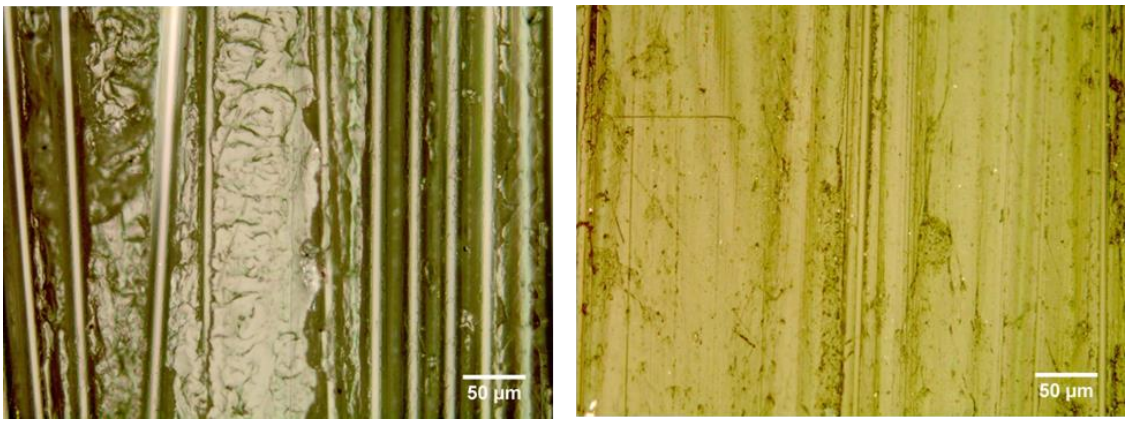

Figure 86: Epoxy ECR-glass 2, Proprietary material ECR-glass 2, As Received

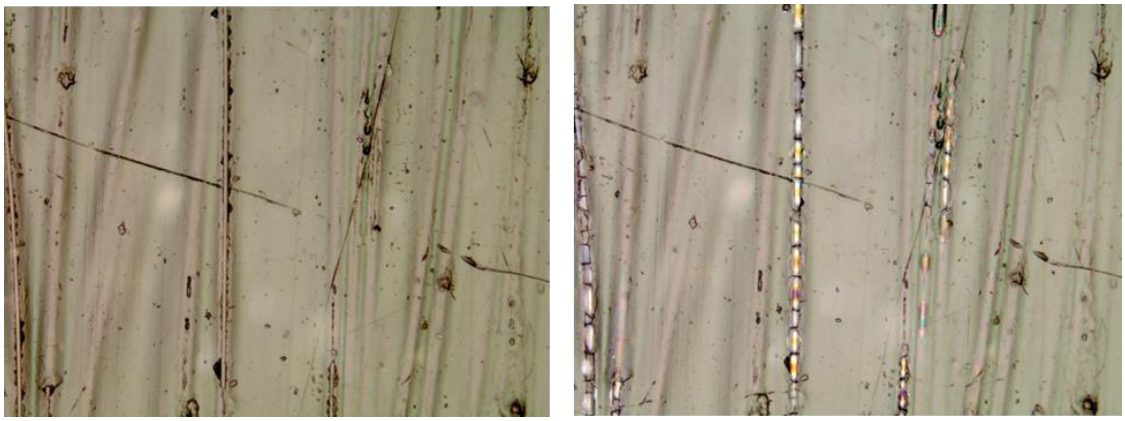

Figure 87: (3A) Vinylester E-glass 1, Before and After, 1N

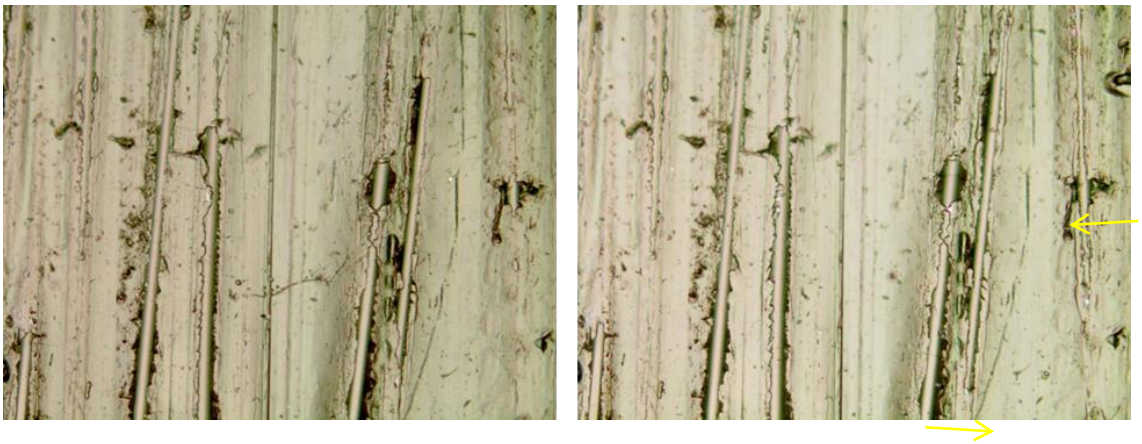

Figure 88: (4b) Vinylester E-glass 2, Before and After, 1N

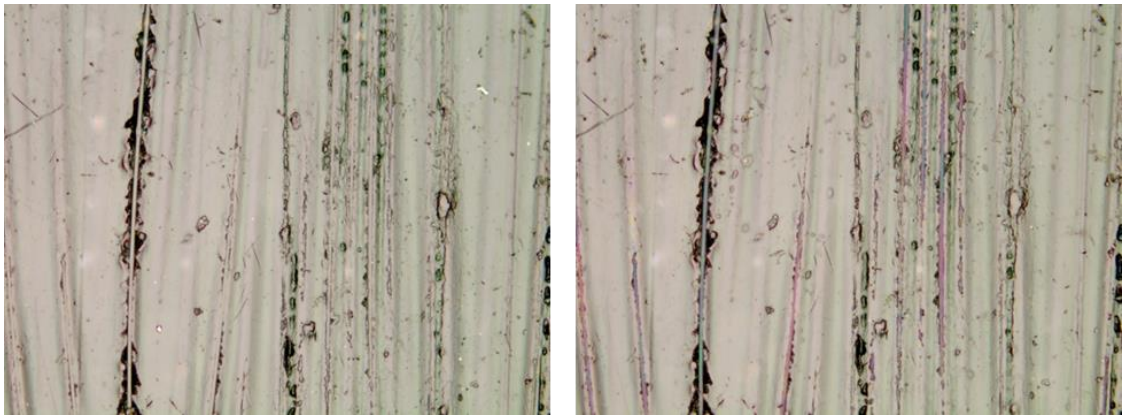

Figure 89: (3A) Vinylester E-glass 1, Before and After, 0.063N

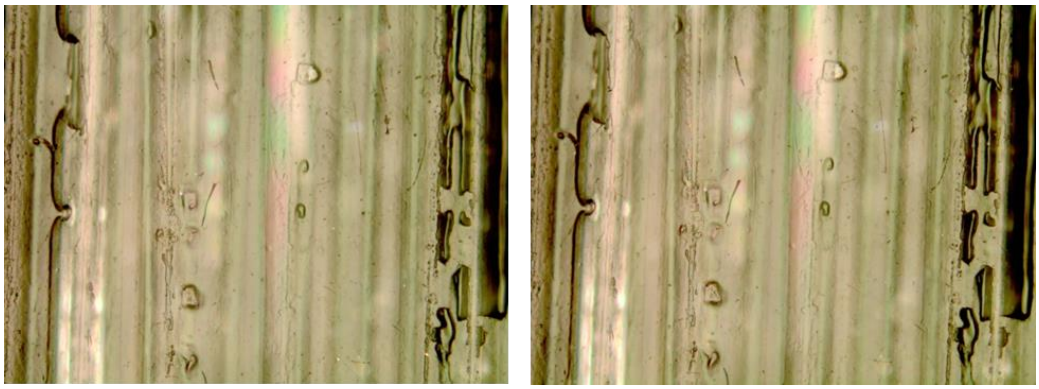

Figure 90: (6) Polyester ECR-glass 2, Before and After, 0.063N

4. DISCUSSION

Presented are details concerning the more interesting results. Comparison between SCC results and all other methodologies will be highlighted.

4.1 SCC Testing

SCC testing consisted of all of the data retrieved from the 4-point bend test and resulting post processing.

4.1.1 Events vs. Time

The results presented in this work show clear implications with respect to the AE monitoring of SCC. It was noted early in experimentation that the original method of using event vs. time data to glean a quantitative sense of how resistant a material was to SCC was not going to be practical. While normally this kind of data would be greatly useful for determining the number of events that occur in a test and at what point they happened, the test type and equipment hindered that. In addition this type of data does not increase understanding of damage mechanism type or effect on material strength with events vs. time data.

SCC is an emerging field, and being such, does not have well defined and established methodologies for monitoring damage. Normally, events vs time would be able to show a great deal about rate of damage accumulation, however, the noise associated with this test and break down in equipment hampered this, leaving it only useful for a small handful of data. This meant that the method could not be applied to all

the accumulated data, and thus was not included as a useful methodology for the purposes of this experiment.

4.1.2 Modal Acoustic Emission

MAE is most commonly used on pressure vessels for cyclic loading at loads, much higher and cycles, longer test duration, and significantly larger samples than tests run for this experiment. While this seems somewhat insignificant, the impacts were substantial.

Increased loading means increased energy release at events. This means sensitivity of the sensors does not require pushing the limits of them. For SCC, loading rates are relatively small and comparable to in-service loading conditions whereas for composite vessels they are testing failure by creep or load. The nature of SCC means that the fibers and matrix are cracking at lower loads due to the corrosion, meaning strain energy is not nearly as high upon damage. This decreased strain energy release means that sensitivity of the sensors has to be high enough to monitor for such events, increasing the number of noise events significantly. While tests were devised to improve upon the work of Megel et al, specifically in duration, increased noise proved a hindrance in tests of these lengths. In addition, most pressure vessel event types are multiple fibers, where SCC tends to be individual damage events rather than groups. These kinds of differences help explain why 3-point tests experienced very few erroneous signals compared to SCC tests.

Preparation impacted both the signal analysis as well and ability to isolate damage mechanisms. Since the experiment was designed in the vein of previous similar tests,

sample size was already set and optimized. This sample size was not a given cast size from the supplier, so samples had to be machined. While great lengths were taken to protect these machined sides from additional mechanical and chemical damage, damage was inevitable. Any machined surface, no matter how precisely is more susceptible to damage from defect and stress concentrations. This is important for the purposes of this test because only two sensors were used. Having only two sensors means location of the damage mechanism is linear, so having damage on the top surfaces would still register not only as an event, but also as one possibly on the side where monitoring was desired. This complicates ranking composites even further, but does not necessarily interfere with classification as the mechanism is slightly different. Also, this was hopefully not as prevalent as desired damage since the largest machined face was solely in compression, where matrix cracking cannot occur and fiber breaks are less likely due to loading conditions.

Sample sizes were quite small for standard MAE work. Since propagation length is much larger than width and depth, geometry comes into play when it comes to signal shape. Reflections of the wave off of the sides can change the shape of the wave before they reach the sensors. Sensors were placed significantly closer than in previous tests, making this less prevalent, but geometry eliminates the possibility of proximity so close that interference is eliminated. The new location does greatly decrease the amount of signal cancelation associated with end placed sensors. Previous sensor setup was centered on the smallest dimension, causing top to bottom signals to have large degrees of wave manipulation from sample geometry.

The combination of all of these factors does make analysis significantly harder, but not impossible. Robust methods of analysis should prove useful for tests of all types and more than likely would be strengthened with changes to the mentioned difficulties.

PP vs. WPF methods used showed strong clustering; however, clustering was isolated largely to a single cluster. Observed microscopy and historical data shows more than one event type.

Clustering for each SCC test was consistently in the same range, a WPF of 300 kHz-400 kHz and a PP from 7%-17%. While this range could probably be tightened with more rigorous filtering, clustering remained strong through tests shown. This method of analysis is not rigorously proven, so the wave content was also observed to give a more complete picture. Cluster data all exhibited strong flexural modes, which matrix cracking has historically been linked to. (Sause, Simulation of Lamb Wave Excitation for Different Elastic Properties and Acoustic Emission Source Geometries 2010) (B. H. Burks, The Impact of Solid-Fluid Interaction on Transient Stress Wave Propagation due to Acoustic Emissions in Multi-Layer Plate Structures 2014) The same clustering range in addition to the same wave content was strong evidence that observed and locatable events were matrix cracking. While this identification of one damage mechanism was tremendous, it was not the totality of desired results. Fiber breaks were not clearly identifiable in cluster, or in wave content by classical definition. Microscopy confirmed that there were fiber breaks, but they were not registering on the sensors. In addition, since wave content was not confirmation enough for a single mechanism, 3-point bend testing was added to ensure that clustering and content were a match.

4.2 3-Point Bend Test

3-Point bend testing was done to supplement SCC data, and to confirm the clustering from SCC tests was indeed matrix cracking. This test proved to have another cluster in the same ranges as the SCC testing. This cluster was the majority of the signals from the bend test, which should be comprised of mostly matrix cracking. This was ensured by fiber direction and knowledge of the stress state applied to the specimen relative to the anisotropic strength of the material. Damage mechanisms have been theorized this way in the past, with experimenters forcing damage mechanisms and determining them using various testing methods. (Huguet 2002) This by itself should be considered inadequate to make such assumptions, but in combination with SCC PP vs. WPF clustering as well as wave content, sufficient evidence to make such a claim exists.

One key significant note should be mentioned, with the orientation of the composite for the 3-point test, comes a slight change in wave propagation. 3-point wave propagation goes through perpendicular fibers to reach the sensor surface, whereas SCC tests have a 90° fiber offset. This can potentially change the wave shape and frequency response. For the purposes of this test, it still overlapped within the same cluster, but perhaps there could be a slight difference in signals between tests.

4.3 Model

The purpose of using a model to compliment data was done for forward predictive purposes. Despite many studies involving MAE and composites, projected Rise times are still largely theoretical and approximate. The primary and initial purpose of the model was to achieve a more narrow range for Rise times. This was done by using approximate material properties of the composite and importing them into a model. This model takes into account the varying rate of propagation in composites, a very non trivial detail, and the understanding of preferential energy release by mechanism. While this model is sophisticated in those methods, it still has limitations which are important to note.

Rise times of appropriate ranges were plugged into the model, and their PP vs WPF observed to compare to experimental data. For matrix cracking, this range was clearly defined by the combination of SCC and 3-point bend data. While running Rise times in these ranges did yield a PP and WPF within the range of SCC clusters, several implications should be understood. While the model has sophisticated wave propagation, force application and accurate material properties associated with it, it does not in fact have clear boundaries separating “fibers” from “matrix”. While this might be deemed as simplistic, waveforms are on the order of magnitude that they are not affected by this property for glass fibers. It has been defined as orthotropic, which is a more accurate characterization of material properties, but the wave would propagate differently with unavoidable differences in an experimental composite layup (imperfections, voids, fiber misalignment etc.). This change could have slight effects on the tight range predictions given for Rise times.

Distance study proved to show the importance of combining methodologies for classification of damage mechanisms. Distance of a damage mechanism from source does have an effect on the WPF due to geometric restrictions causing increased reflections. This has the potential to muddy clustering WPF data; however, it can be avoided with larger sample sizes or multiple sensors. As this experiment was conducted without either of those controls, attention has to be paid not only to clustering data, but also to time domain, frequency domain, and CWD analysis of signals. Geometry, as was mentioned earlier, can have a large effect on the waves' reflections on boundaries before reaching the sensors. The small dimensioning of this sample leads to complications in the WPF, and this is exacerbated in the model simulations.

The primary difference between the damage mechanisms modeled and their real world results is the simplification of their energy release. Experimentally, they are not 2 dimensional as the crack and the break start from the highest tension face and go to the depth of the medium being damaged. While the model properly orients the energy releases by mechanism, the force is being applied on the surface, but is a body force. This method does yield very usable results, but it is a limitation none the less. This orientation was used, mostly due to computational limitations for doing thickness out of plane forces as an even finer mesh would be required. In order to supplement this limitation, a 2d model would need to be made with damage mechanisms having depth to handle the thickness out-of-plane damage.

A materials study showed some limitations in having a homogenous model with composite properties applied to directions vs. experimentally flawed, real world

composites. In the fiber break, it was noted that only axial stiffness and density properties affected the WPF. The change for a given mechanism is more strongly affected by matrix material than is the case experimentally. Also, the change in PU for fiber fraction is more pronounced since the PU is so pliable and the fibers are not. Experimentally, fiber properties would be much more important to wave content than matrix material for a fiber break. The same material study for matrix cracked proved to support this theory when changing the fiber type kept values near original values. Since the matrix energy release is perpendicular to fiber direction, the matrix properties would affect WPF much more strongly for this model. This was also observed, as well as fiber fraction affecting density for all models contributing to a change in all WPFs.

4.4 Comparison Between Tests

At the onset of this research, it was desired to show the damage mechanisms detectable by MAE. While an event type was isolated through PP vs. WPF, Modal Waveform analysis, and 3-point bend test data, fiber breaks were still not determined experimentally. It is possible that some fiber breaks were seen by equipment, but numbers were not large enough to classify fully and show the trend. Hypothesis for this reason is related to the nature of the events.

It has been shown that fiber breaks largely cause in-plane deformation, while matrix cracking largely results in out-of-plane deformation. This could explain why fiber breaks were not recorded by MAE and matrix cracks were. Sensors were placed on the intended damage face, meaning out of plane waves would be more likely to register on the sensor in this orientation. Fiber breaks could pass right over the sensor without enough energy to start triggering. It should be noted that during tension tests, which data was ultimately discarded, showed the ability to sense fiber breaks when they were in great numbers.

Despite the drawback in only showing a single cluster identity type, the analysis for that mechanism was quite thorough. The method has proven to work across multiple samples and multiple test types. This test has shown PP, WPF and Rise time values for the e-glass polymer matrix composites tested, as well as developed a forward predictive model for future experiments.

4.5 Evaluation of Shortcomings

One of the hardest things to overcome from this research was the rapid breakdown in equipment. After the method had been refined, only a few tests were carried out before noise and false triggering began to interfere with data collection. This coincided with a change in labs, however it was believed to also be a strong result of degrading equipment. Used equipment was a decade and a half old, and proved not to be durable enough to complete this research as intended. In addition, the age of the software proved to make for very inefficient testing. As false signaling increased, problems were encountered with filtering and storage. The computer only had 0.97 GB of memory, which would quickly fill up during a three day test, and would cause an overflow error, losing all data for that test. In addition, if data was of a size able to be used, the software version required signals to be pulled off individually, by cycling through signals one by one and exporting them. More current versions allow for all signals to be pulled off at once, which would streamline the process of post processing back to being automated through Matlab. Also no USB port exists on this computer so signals had to be blocked to under 500, taken on a zip disk to a computer with both a zip drive and a USB, and then taken from USB to computer to be post processed. This hurdle was more time consuming than prohibitive.

Despite these difficulties, enough data was collected to prove the methodology being used. This was supplemented with additional tests due to lack of data, but proved to be adequate enough. Since an additional purpose was to be able to rank composites for their SCC resistance, this proved to be impossible using MAE methodology given the

equipment failure. The only way to properly do this is by using microscopy for this experiment; however, future implementation of this methodology could be used to do this very task with improved equipment and facilities.

5. CONCLUSION

1. Events vs. Time data proved to be irrelevant for more modern techniques, and were not used as a determining method.

2. MAE showed several differences from traditional pressure vessel testing worth noting:
    - Decreased loading for SCC tests limited energy release from events. These single events were harder to monitor for than group events typical of pressure vessel testing.
    - Sample size was set and required machining. Both affect data by affecting modes through reflection and events through stress concentrations and surface damage.

3. PP vs. WPF plots showed strong clustering for both 3 point tests and SCC testing in the same range, a WPF of 300kHz-400kHz and a PP from 7%-17%.

4. Clustering signals were analyzed further using MAE methods and showed to be strongly flexural.

5. Combination of both MAE methods, PP vs. WPF plots, expected damage mechanism for 3 point test, and historical data showed that observed signals were matrix cracking.

6. Fiber Breaks were not observable using MAE methods for SCC tests, despite microscopy confirming events taking place. This is thought to be largely due to fiber breaks being in plane events rather than out of plane, making them harder to register given sensor placement.

7. FEA modeling proved to be useful in predicting previous research range of Rise Times
    - Matrix Crack simulation falls within experimental ranges for WPF and PP.
    - Model material study showed impact of material properties as well as density has an effect on wave content.
    - Sample size within the model makes changes in source distance effect modal content of waves.

8. Evidence between all testing clearly showed methodology to work for matrix cracking and identified reasonable Rise Times, MAE modes, WPF, and PP of those events.

6. SUGGESTIONS FOR FUTURE RESEARCH

1. 4 Sensors, 2 on damage face and two on sample ends to more fully encapsulate data.

2. Change in sample dimensions to eliminate modal reflection issue and eliminate the need for machining surfaces.

3. Update AE equipment to eliminate computer size and signal export issue.

4. Update AE labs for less EMI interference.

5. Include different acid types and strengths. Sulfuric, nitric, hydrochloric, from low to high molarity.

6. Create an SCC standard test (acid type and strength, load, methodology etc).

7. Create a more sophisticated model to account for additional damage mechanisms (fiber matrix debonding, broken fiber vibration) and a thickness out of plane 2d damage model.

REFERENCES

Barre, S., Benzeggagh, M. "On the use of Acoustic Emission to Investigate Damage Mechanism in Glass-Fibre-Reinforced Polypropylene." *Computer Science Technology*, 1994: 288-294.

Breckenridge, F., Proctor, T., Hsu, N., Fick, S., Eitzen, D. "Transient Sources for Acoustic Emission Work." *JSNDI*, 1990: 20-37.

Burks, B., interview by J. Kosak. *Rise Times* (2013).

Burks, B., Hamstad, M. "On the Anisotropic Attenuation Behavior of the Flexure Mode of Carbon Fiber Composites." *ICCM19.* Montreal, Canada, 2013.

Burks, B., Hamstad, M. "The Impact of Solid-Fluid Interaction on Transient Stress Wave Propagation due to Acoustic Emissions in Multi-Layer Plate Structures." 2014.

Burks, B., Kumosa, M. "A Modal Acoustic Emission Signal Classification Scheme Derived from Finite Element Simulation." *International Journal of Damage Mechanics*, 2013: 1-20.

Ely, T., Hill, E. "Longitudinal Splitting and Fibre Breakage Characterisation in Graphite/Epoxy Using Acoustic Emission Data." *Materials Evaluation*, 1995: 288-94.

Gary, J., Hamstad, M. A. "On the Far-field Structure of Waves Generated by a Pencil Lead Break on a Thin Plate." *Acoustic Emission*, 1994: 157-170.

Gilson, D. R. "An Investigation of Surface Acoustic Waves." Lab Report, 2008.

Giordano, M., Calabro, A., Esposito, C., D'Amore, A., Nicolais, L. "An Acoustic-Emission Characterization of the Failure Modes in Polymer-Composite Materials." *Composites Science and Technology*, 1998: 1923-1928.

Gorman, M. "Modal AE Analysis of Fracture and Failure in Composite Materials, And the Quality and Life of High Pressure Composite Pressure Vessels." *Journal of Acoustic Emission*, 2011: 1-28.

Gorman, M. "Plate Wave Acoustic Emission." *Journal of Acoustic Emission Volume 90*, 1991: 358-364.

Gorur, R.S., Orbeck, T. "Surface Dielectric Behavior of Polymeric Insulation under HV Outdoor Conditions." *IEEE Transactions on Electrical Insulation*, 1991: 1064-1071.

H. Li, P. Gu, J. Watson, J. Meng. "Acid Corrosion Resistance and Mechanism of E-Glass Fibers - Boron Factor." *Journal of Materials Science*, 2012.

Hamstad, M. A., Gary, J. "On the Far-field Structure of Waves Generated by a Pencil Lead Break on a Thin Plate." *Acoustic Emission*, 1994: 157-170.

Hamstad, M. "On Characterization and Location of Acoustic Emission Sources in Real Size Composite Structures- A Waveform Study." *Journal of Acoustic Emission*, 1995: 31-41.

Hamstad, Marvin A. "A Waveform-Based Study of AE Wave Propagation by Use of Eight Wide-band Sensors on a Composite Pressure Vessel." *30th European Conference on Acoustic Emission TEsting & 7th International Conference on Acoustic Emission.* Granada, Spain, 2012.

Hamstad, Marvin, interview by Jon Kosak. *AE Source Location* (February 22, 2014).

Huang, M. "Using Acoustic Emission in Fatigue and Fracture Materials Research." November 1998. http://www.tms.org/pubs/journals/jom/9811/huang/huang-9811.html (accessed 2014).

Huguet, S. "Use of Acoustic Emission to Identify Damage Modes in Glass Fibre." *Composites Science and Technology*, 2002: 1433-1444.

Hull, D., Clyne, T. *An Introduction to Composite Materials.* Cambridge University Press, 1996.

Jones, R., Betz, D. *Journal of Material Science 39*, 2004: 5633-5637.

Jones, R., Stewart, J. *Journal of Non-Crystalline Solids 356*, 2010: 2433-2436.

Jones, W.D. "More Heat, Less Sag." *IEEE Spectrum*, June 2006.

Kumosa, L., Armentrout, D., Kumosa, M. "An Evaluation of the Critical Conditions for the Initiation of Stress Corrosion Cracking in Unidirectional E-glass/Polymer Composites." *Composites Science & Technology*, 2001: 615-623.

Kumosa, M., Kumosa, L., Armentrout, D. "Failure Analyses of Nonceramic Insulators Part 1: Brittle Fracture Characteristics." *Electrical Insulation Magazine*, May/June 2005: 14-27.

Kumosa, M.,Armentrout, D., Burks, B., Hoffman, J., Kumosa, L., Middleton, J., Predecki, P. "Polymer Matrix Composites in High Voltage Transmission Line Applications." *18th International Conference on Composite Materials.* JeJu, 2011.

L. Kumosa, M. Kumosa, D. Armentrout. "Resistance to Stress Corrosion Cracking of Unidirectional Glass/Polymer Composites Based on Low and High Seed ECR-glass Fibers for High VOltage Composite INsulator Applications." *Composites*, 2003: 1-15.

Li, H. *Journal of Petroleum Science and Engineering 78*, 2011: 371-375.

Li, H., Gu, P., Watson, J., Meng, J. "Acid Corrosion Resistance and Mechanism of E-Glass Fibers - Boron Factor." *Journal of Materials Science*, 2012.

Lih, S., Mal, A. "On the Accuracy of Approximate Plate Theories for Wave Field Calculations in Composite Laminates." *Wave Motion 21*, 1995: 17-34.

Megel, M., Kumosa, L., Ely, T., Armentrout, D., Kumosa, M. "Initiation of stress-corrosion cracking in unidirectional glass/polymer composite materials." *Composites Science and Technology*, 2001: 231-246.

Miller, R., Hill, E., Moore, P. *Volume 6: Acoustic Emission Testing.* American Society for Nondestructive Testing, 2005.

Nayfeh, A. "The General Problem of Elastic Wave Propagation in Multilayered Anisotropic Media." *Journal of Acoustic Society of America*, 1991: 1521-1531.

Noble, B., Harris, S. J., Owen, M. J. "Stress Corrosion Cracking of GRP pultruded rods in acid enfrionments." *Journal of Materials Science 18*, 1983: 1244-1254.

Pichugin, A. V. "Approximation of the Rayleigh Wave Speed." Sheffield, UK: University of Sheffield, 2006.

Prosser, W. H., Jackson, K.E., Kellas, S., Smith, B.T., McKeon, J., Friedman, A. "Advanced, Waveform Based Acoustic Emission Detection of Matrix Cracking in Composites." *Materials Evaluation*, 1995: 1052-1058.

Prosser, W., Hamstad, M., Gary, J., O'Gallagher, A. "Finite Element and Plate Theory Modeling of Acoustic Emission Waveforms." *Journal of Nondestructive Evaluation*, 1999: 83-90.

Qiu, Q., Kumosa, M. "Corrosion of E-Glass Fibers in Acidic Environments." *Composites Science and Technology*, 1997: 497-507.

Rusmee, P. *High Strength Composites.* 2005. http://www.mech.utah.edu/~rusmeeha/labNotes/composites.html (accessed 2014).

Sause, M. "Acoustic Emission Signal Propagation in Damaged Composite Structures." *Journal of Acoustic Emission Volume 31*, 2013: 1-18.

Sause, M. "Simulation of Lamb Wave Excitation for Different Elastic Properties and Acoustic Emission Source Geometries." 2010: 1-13.

Schmuck, F., Tourreil, C. "Brittle Fractures of Composite Insulators an Investigation of their Occurrence and Failure Mechanisms and a Risk Assessment." CIGRE WG, 2003.

Schneider, H. M., Hall, J. F., Karady, G., Rendowden, J. "Nonceramic Insulators for Transmission Lines." *IEEE Transactions on Power Delivery*, October 1989: 2214-2221.

Sharma, K. "Polymeric Insulators." Technical Article, 2001.

Ziola, S., Gorman, M. "Source Location in Thin Plates using Cross-Correlation." *Journal of Acoustical Society America Vol 90*, 1991: 2551-2556.